JOURNAL OF MATHEMATICAL PHYSICS VOLUME 10, NUMBER 1 JANUARY 1969

High-Frequency Scattering by a Transparent Sphere. II. Theory of the Rainbow and the Glory

H. M. NUSSENZVEIG
Department of Physics and Astronomy, The University of Rochester, Rochester, New York

(Received 15 April 1968)

The treatment, initiated in Paper I [J. Math. Phys. **10**, 82 (1969)], of the high-frequency scattering of a scalar plane wave by a transparent sphere is continued. The main results here are an improved theory of the rainbow and a theory of the glory. The modified Watson transformation is applied to the third term of the Debye expansion of the scattering amplitude in terms of multiple reflections. Only the range $1 < N < \sqrt{2}$, where N is the refractive index, is considered. In the geometrical-optic approximation, this term is associated with rays transmitted after one internal reflection, and there are three angular regions, corresponding to one ray, two rays, or no ray (shadow) passing through each direction. Together with transition regions, this leads to six different angular domains. In the 1-ray and 2-ray regions, geometrical-optic terms are dominant. Correction terms corresponding to the 2nd-order WKB approximation are also evaluated. In the 0-ray region, the amplitude is dominated by complex rays and surface waves. The 1-ray/2-ray transition is a Fock-type region. The rainbow appears in the 2-ray/0-ray transition region. The extension of the method of steepest descents due to Chester, Friedman and Ursell is applied. The result is a uniform asymptotic expansion for the scattering amplitude. It reduces to Airy's theory in the lowest-order approximation, but its domain of validity is considerably greater, both with regard to size parameter and to angles. The glory is an example of strong "Regge-pole dominance" of the near-backward scattering amplitude. Van de Hulst's conjecture that surface waves are responsible for the glory is confirmed. However, besides surface waves taking two shortcuts through the sphere, higher-order terms in the Debye expansion must also be taken into account. By considering also the effect of higher-order surface-wave contributions, all the features observed in the glory (apart from the polarization) are explained. Resonance effects associated with nearly-closed paths of diffracted rays lead to large, rapid, quasiperiodic intensity fluctuations. The same effects are responsible for the ripple in the total cross-section. Similar fluctuations appear in any direction, but their amplitude increases with the scattering angle, becoming a maximum near the backward direction, where they are dominant. They can also be interpreted as a collective effect due to many nearly-resonant partial waves in the edge domain. The dominant surface-wave contributions can also be summed to all orders for $N < 1$, leading to a renormalization of the propagation constants of surface waves.

1. INTRODUCTION

In Paper I of this work[1] the high-frequency asymptotic behavior of the scattering amplitude for a scalar plane wave incident on a transparent sphere was investigated, with the help of techniques developed in an earlier paper.[2] It was assumed that

$$\beta^{\frac{1}{3}} \gg 1, \quad |N-1|^{\frac{1}{2}}\beta^{\frac{1}{3}} \gg 1, \tag{1.1}$$

where $\beta = ka$, k is the wavenumber, a is the radius of the sphere, and N is the refractive index.

The Debye expansion of the scattering amplitude, in terms of an infinite series of multiple internal reflections, was employed. In Paper I, the first two terms of this series, corresponding to direct reflection from the surface and to direct transmission through the sphere, were evaluated. Both $N > 1$ and $N < 1$ were treated.

In the present paper, the third term of the Debye expansion is evaluated and the effect of higher-order terms is discussed. In many cases of practical importance, higher-order terms may be neglected, although their contributions have to be taken into account in the neighborhood of certain special directions, as will be seen later. Any such contribution may be evaluated, in principle, by methods similar to those developed here.

In contrast with the first two terms, it is not possible to give a uniform treatment of the third term, valid for all $N > 1$. As is shown in Sec. 2, there are five different ranges of the refractive index, each of them requiring a separate treatment. This subdivision arises already at the level of geometrical optics. It is due to the fact that, for different ranges of N, there are different subdivisions into angular regions, each angular region being characterized by the number of rays going through a given direction within that region. This number may vary between zero and three.

Here we shall be concerned mostly with the range

$$1 < N < \sqrt{2}, \tag{1.2}$$

[1] H. M. Nussenzveig, J. Math. Phys. **10**, 82 (1969) (preceding paper; referred to as I).
[2] H. M. Nussenzveig, Ann. Phys. (N.Y.) **34**, 23 (1965) (referred to as N).

because we have in mind the application to light scattering by water droplets, and the refractive index of water, $N = 1.33$, falls within this range. Although several interesting phenomena occur in other ranges, especially near the transition points, our attention in the present work is focused mainly on the range (1.2). In this range, according to geometrical optics, there are three different angular regions: a 0-ray (shadow) region near the forward direction, a 1-ray region near the backward direction, and a 2-ray region in between. Taking into account, also, the corresponding transition regions, we find a total of six different angular regions to be considered.

The structure of the third term differs from that of the previous ones in many respects. Physically, this difference is due to the fact that it contains two new features, associated with two very beautiful natural phenomena: the rainbow and the glory. They are contained, respectively, in the 2-ray/0-ray transition region and in the region near the backward direction.

The remaining four regions, which we call "normal," are discussed first (Sec. 3). In the 1-ray region, in addition to the geometrical-optic contribution, we find surface waves, excited at the 1-ray/2-ray shadow boundary, corresponding to diffracted rays that take two "shortcuts" across the sphere. The 1-ray/2-ray transition region corresponds to a normal (Fock-type) transition. In the 2-ray region, there are two real saddle points, corresponding to the two rays passing through each direction within this region. These saddle points become complex in the shadow (0-ray) region, and, due to their presence, the amplitude cannot be reduced to a pure residue series in this region.

The rainbow (Sec. 4) corresponds to a new type of light-shadow transition, associated with the confluence of a pair of geometrical rays (real saddle points) and their transformation into complex rays (saddle points). The corresponding mathematical problem is the asymptotic expansion of an integral having two saddle points that move towards (or away from) each other. This problem has only recently been solved by Chester, Friedman, and Ursell.[3,4] By applying their method, we find a uniform asymptotic expansion of the amplitude, valid throughout the rainbow region and matching smoothly with the results in neighboring regions. Airy's classical theory of the rainbow,[5] the best approximate treatment known so far, corresponds to the lowest-order approximation in this expansion. The assumptions upon which Airy's theory is based, are known to have only a very limited range of applicability; the present theory is valid over a considerably extended range.

The glory corresponds to a strong enhancement in near-backward scattering. A more complete description of this effect and of some of the attempts to explain it is given in Sec. 5. The order of magnitude of the intensity predicted by geometrical optics is far too small to account for the effect. It was conjectured by Van de Hulst (Ref. 6; Ref. 7, p. 373) that the glory is due to surface waves of the kind discussed in Sec. 3, that make two shortcuts across the sphere. However, no quantitative treatment of the problem has been given. The modified Watson transformation enables us to treat the neighborhood of the backward direction and to evaluate the residue-series contributions. As is shown in Sec. 5, they are indeed of the right order of magnitude to account for the enhancement in the backward intensity. Physically, this arises from the focusing of the diffracted rays on the axis, which compensates for the exponential damping along the sphere surface. This confirms the basic correctness of Van de Hulst's conjecture. It also provides an impressive example of "Regge-pole dominance" of the scattering amplitude.

However, as is seen in Sec. 5, the residue-series contribution to the third term of the Debye expansion is unable to account for the detailed behavior of the backward-scattered intensity as a function of β. This behavior has recently been studied by Bryant and Cox,[8] by numerical summation of the partial-wave series. They found a very complicated fine structure, showing a quasiperiodic pattern with very prominent and irregular peaks. This behavior must be due to contributions from higher-order terms in the Debye expansion.

The effects produced by higher-order terms are investigated in Sec. 6, which deals almost entirely with the particular cases of forward and backward scattering. The geometrical-optic contribution to all orders is evaluated in these cases and it turns out to be quite small, as expected. The dominant term of the residue-series contribution for an arbitrary order in the Debye expansion is also evaluated. For $N > 1$, the result agrees with that obtained by Chen[9] from the geometrical theory of diffraction, in the case of a circular

[3] C. Chester, B. Friedman, and F. Ursell, Proc. Cambridge Phil. Soc. **53**, 599 (1957).
[4] F. Ursell, Proc. Cambridge Phil. Soc. **61**, 113 (1965).
[5] G. B. Airy, Trans. Cambridge Phil. Soc. **6**, 379 (1938).
[6] H. C. Van de Hulst, J. Opt. Soc. Am. **37**, 16 (1947).
[7] H. C. Van de Hulst, *Light Scattering by Small Particles* (John Wiley & Sons, New York, 1957).
[8] H. C. Bryant and A. J. Cox, J. Opt. Soc. Am. **56**, 1529 (1966).
[9] Y. M. Chen, J. Math. Phys. **5**, 820 (1964).

cylinder. For $N < 1$, it agrees with the physical interpretation given in Paper I, in terms of internal diffraction of surface waves excited by the critically incident rays. As was found in Paper I, the sense of propagation of these surface waves disagrees with the prediction of the geometrical theory of diffraction.

The rate of convergence of the Debye expansion for the residue-series contributions is also discussed in Sec. 6. It is found that they converge much more slowly than "geometrical-optic" contributions. However, for $N < 1$, when all terms have a common shadow boundary, the dominant terms can be summed to all orders, giving rise to a "renormalization" effect of the phase velocities and damping constants of surface waves. For $N > 1$, the summation to all orders is more difficult, due to the different shadow boundaries appearing in all terms. Nevertheless, with certain simplifying assumptions, the summation can still be performed, allowing us to estimate the resultant effect of all surface-wave contributions. It is found that the higher-order contributions account for the quasi-periodic fine structure found by Bryant and Cox, giving rise also to resonance effects. The main features observed in the glory, apart from polarization, are thereby explained.

Furthermore, the same effects are shown to be responsible also for the "ripple" in the total cross section for $N > 1$ (Ref. 7, p. 177). This also agrees with the explanation suggested by Van de Hulst. It is pointed out that the ripple is a very general phenomenon, affecting the intensity in any direction, but with variable amplitude, attaining its maximum at 180°. The corresponding fluctuations in other directions have been observed in numerical calculations by Penndorf.[10]

The conclusions pertaining to both Papers I and II are summed up in Sec. 7, where possible extensions and applications to nuclear physics are also discussed.

The treatment in Papers I and II deals only with a scalar field and, therefore, cannot be directly applied to light scattering. However, the whole treatment can be extended to electromagnetic scattering. The extension will be given in a subsequent paper.[11]

2. THE THIRD TERM OF THE DEBYE EXPANSION

A. Preliminary Considerations

The notation employed is everywhere the same as in Paper I, to which we refer for the definitions of all symbols that appear in the analysis.

[10] R. B. Penndorf, J. Opt. Soc. Am. **52**, 402 (1962).
[11] H. M. Nussenzveig, to be published.

The third term of the Debye expansion is given by [cf. Paper I, (3.23)]

$$f_2(\beta,\theta) = -\frac{i}{\beta}\sum_{m=-\infty}^{\infty}(-1)^m \times\int_0^{\infty}\rho(\lambda,\beta)U(\lambda,\beta)P_{\lambda-\frac{1}{2}}(\cos\theta) \times\exp(2im\pi\lambda)\lambda\,d\lambda, \quad (2.1)$$

where ρ and U are defined in Paper I, Eqs. (3.15) and (3.24), respectively. Changing λ to $-\lambda$ in the sum from $m = -\infty$ to 0, and noting that

$$\rho(-\lambda,\beta) = e^{2i\pi\lambda}\rho(\lambda,\beta), \quad U(-\lambda,\beta) = U(\lambda,\beta), \quad (2.2)$$

we can rewrite (2.1) as

$$f_2(\beta,\theta) = \frac{i}{\beta}\sum_{m=0}^{\infty}(-1)^m\int_{-\infty}^{\infty}\rho(\lambda,\beta)U(\lambda,\beta)P_{\lambda-\frac{1}{2}}(\cos\theta) \times\exp[2i(m+1)\pi\lambda]\lambda\,d\lambda. \quad (2.3)$$

With the help of Paper I, (2.12), this can also be rewritten as

$$f_2(\beta,\theta) = \frac{i}{2\beta}\int_{-\infty+i\epsilon}^{\infty+i\epsilon}\rho U P_{\lambda-\frac{1}{2}}(\cos\theta)e^{i\pi\lambda}\frac{\lambda\,d\lambda}{\cos(\pi\lambda)} = -\frac{i}{2\beta}\int_{-\infty-i\epsilon}^{\infty-i\epsilon}\rho U P_{\lambda-\frac{1}{2}}(\cos\theta)e^{i\pi\lambda}\frac{\lambda\,d\lambda}{\cos(\pi\lambda)}, \quad \epsilon > 0, \quad (2.4)$$

where the path of integration in the first integral has been shifted above the real axis. The last equality follows from the fact that the integrand is odd [cf. (2.2)].

It follows from N, (C3)–(C6), that

$$P_{\lambda-\frac{1}{2}}(\cos\theta) = e^{-i\pi\lambda}[iP_{\lambda-\frac{1}{2}}(-\cos\theta) + 2\cos(\pi\lambda)Q^{(2)}_{\lambda-\frac{1}{2}}(\cos\theta)]. \quad (2.5)$$

Substituting this identity in (2.4), we find

$$f_2(\beta,\theta) = f^{+}_{2,0} + f_{2,r} = f^{-}_{2,0} - f_{2,r}, \quad (2.6)$$

where

$$f^{\pm}_{2,0}(\beta,\theta) = \pm\frac{i}{\beta}\int_{-\infty\pm i\epsilon}^{\infty\mp i\epsilon}\rho U Q^{(2)}_{\lambda-\frac{1}{2}}(\cos\theta)\lambda\,d\lambda, \quad (2.7)$$

and

$$f_{2,r}(\beta,\theta) = -\frac{1}{2\beta}\int_{-\infty+i\epsilon}^{\infty+i\epsilon}\rho U P_{\lambda-\frac{1}{2}}(-\cos\theta)\frac{\lambda\,d\lambda}{\cos(\pi\lambda)} = -\frac{1}{2\beta}\int_{-\infty-i\epsilon}^{\infty-i\epsilon}\rho U P_{\lambda-\frac{1}{2}}(-\cos\theta)\frac{\lambda\,d\lambda}{\cos(\pi\lambda)} = \frac{1}{2\beta}\int_{-\infty+i\epsilon}^{\infty+i\epsilon}\rho U e^{2i\pi\lambda}\frac{\lambda\,d\lambda}{\cos(\pi\lambda)}. \quad (2.8)$$

In (2.7), the path of integration was made to cross the positive real axis (which is free of singularities) so that it becomes symmetric about the origin. The equality between the second and third integrals in (2.8) follows from the change of variable $\lambda \to -\lambda$, with the help of (2.2). The equality between the first and third integrals follows from the identity

$$\frac{e^{2i\pi\lambda}}{\cos(\pi\lambda)} = 2e^{i\pi\lambda} - \frac{1}{\cos(\pi\lambda)}, \tag{2.9}$$

where the first term gives no contribution because the corresponding path of integration can be shifted to the real axis and the integrand is odd.

Substituting in (2.7) the identity [N, (C2), (C5)]

$$Q^{(2)}_{\lambda-\frac{1}{2}}(\cos\theta) = e^{2i\pi\lambda}Q^{(1)}_{\lambda-\frac{1}{2}}(\cos\theta) - ie^{i\pi\lambda}P_{\lambda-\frac{1}{2}}(-\cos\theta), \tag{2.10}$$

we find once more that the second term leads to an odd integrand, so that

$$f^{\pm}_{2,0}(\beta,\theta) = \pm\frac{i}{\beta}\int_{-\infty\pm i\epsilon}^{\infty\mp i\epsilon}\rho U Q^{(1)}_{\lambda-\frac{1}{2}}(\cos\theta)e^{2i\pi\lambda}\lambda\,d\lambda. \tag{2.11}$$

Again, splitting up the integral at the origin and making $\lambda \to -\lambda$ in the integral from $-\infty \pm i\epsilon$ to 0, we find, with the help of N, (6.25),

$$f^{\pm}_{2,0}(\beta,\theta) = \mp\frac{i}{\beta}\int_0^{\infty\mp i\epsilon}\rho U P_{\lambda-\frac{1}{2}}(-\cos\theta) \times e^{i\pi\lambda}\tan(\pi\lambda)\lambda\,d\lambda. \tag{2.12}$$

On the other hand, expanding the integrand in the last member of (2.8), we find

$$f_{2,r}(\beta,\theta) = \frac{1}{\beta}\sum_{m=0}^{\infty}(-1)^m\int_{-\infty}^{\infty}\rho U P_{\lambda-\frac{1}{2}}(-\cos\theta) \times \exp[i(2m+3)\pi\lambda]\lambda\,d\lambda. \tag{2.13}$$

All of the above representations are exact. The choice of an appropriate one among the manifold possibilities is determined by the ranges of values of the refractive index and by the direction under consideration, as will be seen later.

The asymptotic behavior of $e^{i\pi\lambda}\rho U$ as $|\lambda| \to \infty$ follows from Paper I, Figs. 14 and 21. Since it is an even function of λ, it suffices to consider its asymptotic behavior in the upper half-plane, which is shown in Fig. 1. We see that it tends to zero everywhere, except in the shaded regions in the neighborhood of the imaginary axis, where its maximum degree of divergence (neglecting factors such as powers of λ) is given by

$$e^{i\pi\lambda}\rho U = \mathcal{O}(e^{\pi|\lambda|}). \tag{2.14}$$

On the other hand, $e^{2i\pi\lambda}P_{\lambda-\frac{1}{2}}(-\cos\theta)$ behaves like $e^{i\lambda(\pi+\theta)}$ in the upper half-plane, so that we can always close the contour in (2.13) and reduce it to a residue series:

$$f_{2,r}(\beta,\theta) = \tilde{f}_{2,\mathrm{res}}(\beta,\theta) + \tilde{f}'_{2,\mathrm{res}}(\beta,\theta) = \frac{2\pi i}{\beta}\sum_{m=0}^{\infty}(-1)^m\sum_n \text{residues}\,\{\lambda\rho U P_{\lambda-\frac{1}{2}}(-\cos\theta) \times \exp[i(2m+3)\pi\lambda]\}_{\lambda_n,-\lambda_{n'}}, \tag{2.15}$$

where $\tilde{f}_{2,\mathrm{res}}$ corresponds to the sum of the residues at the poles λ_n and $\tilde{f}'_{2,\mathrm{res}}$ to those at the poles $-\lambda'_n$.

However, since [cf. N, (C7)]:

$$e^{-i\pi\lambda}Q^{(2)}_{\lambda-\frac{1}{2}}(\cos\theta) = \mathcal{O}[e^{-i\lambda(\pi-\theta)}] \quad (|\lambda| \to \infty), \tag{2.16}$$

$$e^{i\pi\lambda}Q^{(1)}_{\lambda-\frac{1}{2}}(\cos\theta) = \mathcal{O}[e^{i\lambda(\pi-\theta)}] \quad (|\lambda| \to \infty), \tag{2.17}$$

it follows from (2.14) that, for any value of θ, there is always some neighborhood of the imaginary axis where the integrand of (2.7) or (2.11) diverges at infinity [note that (2.16) improves the convergence in the lower half-plane and (2.17) in the upper one]. Thus, *there is no domain of values of θ in which $f^{\pm}_{2,0}$ [and, consequently, $f_2(\beta,\theta)$] can be reduced to a pure residue series.*

This already shows that the structure of the shadow region for the third term of the Debye expansion is quite different from that found for the previous two. We shall see that this is related with the existence of complex saddle points in the present case. Our next task is to study the location of the saddle points for (2.7) and (2.11).

B. Ray Behavior According to Geometrical Optics

In the geometrical-optics approximation, the third term of the Debye expansion is associated with rays transmitted through the sphere after one internal reflection, like the ray 3′ in Paper I, Fig. 5. Three possible types of ray trajectories, leading to three different relations between the scattering angle θ and the angle of incidence θ_1 and angle of refraction θ_2,

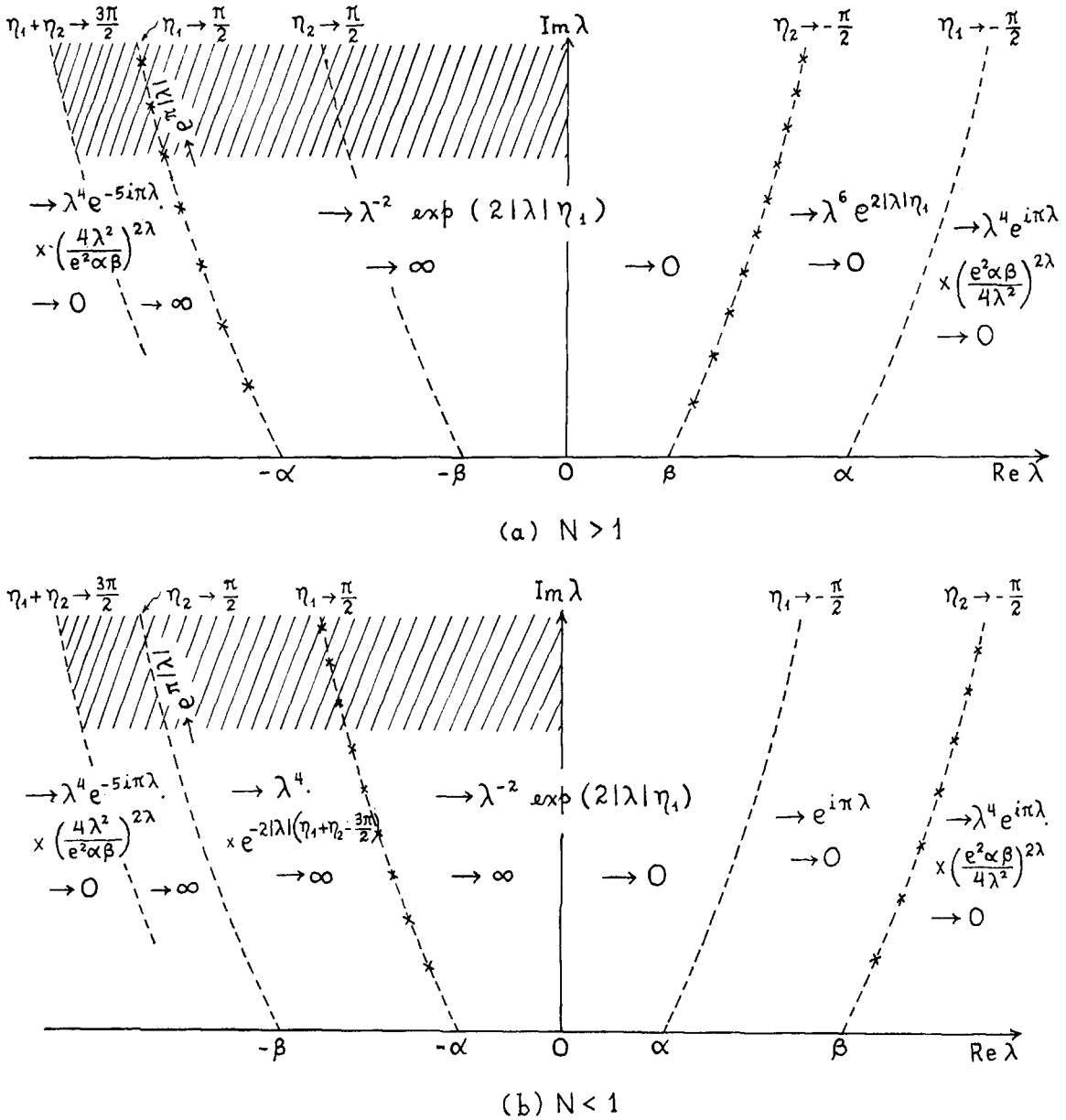

FIG. 1. Asymptotic behavior of $e^{i\pi\lambda}\rho(\lambda, \beta)U(\lambda, \beta)$ as $|\lambda| \to \infty$ in different regions of the λ plane. (a) $N > 1$; (b) $N < 1$. ×—poles. The function diverges at infinity in the shaded regions and tends to zero elsewhere. The notation is the same as in I, Fig. 14.

are shown in Fig. 2. We have, of course,

$$\sin\theta_1 = N\sin\theta_2, \quad 0 \le \frac{\theta_1}{\theta_2} \le \frac{\pi}{2}, \quad 0 \le \theta \le \pi. \tag{2.18}$$

The three possible relations are

$$\theta = 2(2\theta_2 - \theta_1) - \pi, \tag{2.19}$$

$$\theta = \pi - 2(2\theta_2 - \theta_1), \tag{2.20}$$

$$\theta = \pi + 2(2\theta_2 - \theta_1). \tag{2.21}$$

It is readily verified that any possible ray trajectory leads to one of these three relations. Relation (2.19) holds for $2(2\theta_2 - \theta_1) > \pi$, i.e., $\theta_1 > \theta_{1,c}$, where

$$\sin\theta_{1,c} = \sin\left(2\theta_{2,c} - \frac{\pi}{2}\right) = \frac{N^2}{4}\left[1 + \left(1 + \frac{8}{N^2}\right)^{\frac{1}{2}}\right], \tag{2.22}$$

which is only possible for $N < 1$ [Fig. 2(a)].

If $N < 1$ and $\theta_1 < \theta_{1,c}$, we have to employ (2.20). This relation also holds for $N > 1$, provided that

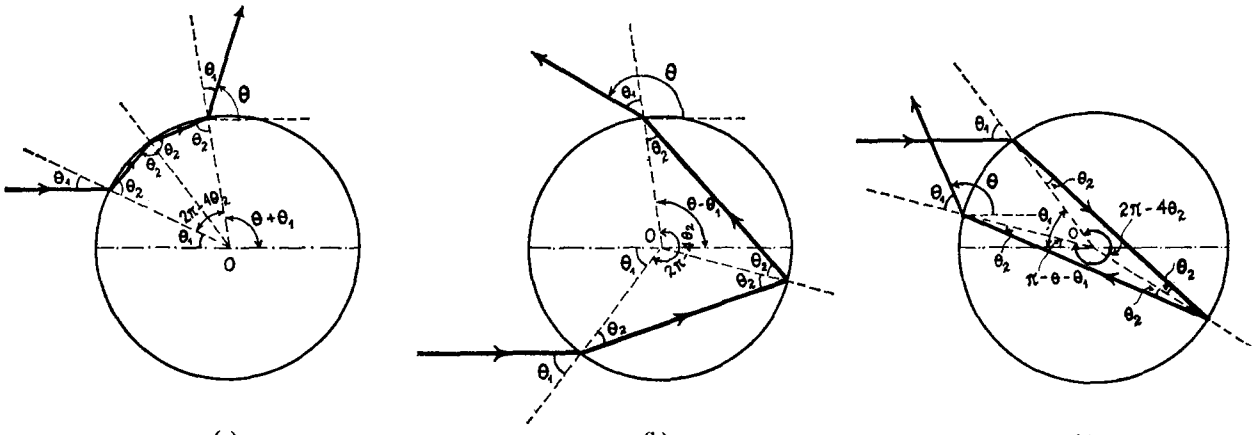

(a) (b) (c)

FIG. 2. Three possible ray trajectories according to geometrical optics and the corresponding relations among θ, θ_1, and θ_2. All possible trajectories for this class of rays lead to one of these three relations. (a) $N < 1$, $2(2\theta_2 - \theta_1) > \pi$, $\theta = 2(2\theta_2 - \theta_1) - \pi$; (b) $1 < N < 2$, $0 < 2(2\theta_2 - \theta_1) < \pi$, $\theta = \pi - 2(2\theta_2 - \theta_1)$; (c) $N > 2$, $2(2\theta_2 - \theta_1) < 0$, $\theta = \pi + 2(2\theta_2 - \theta_1)$.

$2\theta_2 - \theta_1 > 0$. The angle θ_{1A} such that

$$2\theta_{2A} - \theta_{1A} = 0 \tag{2.23}$$

is characterized by

$$\cos\theta_{1A} = \tfrac{1}{2}(N^2 - 2), \tag{2.24}$$

so that such an angle exists only for

$$\sqrt{2} \leq N \leq 2. \tag{2.25}$$

Thus, if

$$1 < N < \sqrt{2}, \tag{2.26}$$

we have $0 < 2(2\theta_2 - \theta_1) < \pi$, and (2.20) is the only valid relation. On the other hand, if N is in the range (2.25), we must employ (2.20) for $\theta_1 < \theta_{1A}$ and (2.21) for $\theta_1 > \theta_{1A}$. Finally, if $N > 2$, we have $2\theta_2 - \theta_1 < 0$, so that (2.21) is the only valid relation [Fig. 2(c)].

In all cases, $\theta_1 = 0$ yields $\theta = \pi$, corresponding to the central ray that is reflected backwards after transmission. For $N < 1$, the limiting incident ray that is transmitted corresponds to the critical angle,

$$\theta_1 = \theta_l = \sin^{-1} N, \quad \theta_2 = \pi/2 \quad (N < 1), \tag{2.27}$$

and, according to (2.19), the corresponding scattering angle is $\theta = \theta_t$, where

$$\theta_t = \pi - 2\theta_l = 2\cos^{-1} N \quad (N < 1). \tag{2.28}$$

This is the same shadow boundary angle already found in Paper I, Fig. 8(b) and Paper I, Fig. 13(b).

For $N > 1$, the limiting incident ray is

$$\theta_1 = \frac{\pi}{2}, \quad \theta_2 = \theta_l = \sin^{-1}\frac{1}{N} \quad (N > 1). \tag{2.29}$$

In the range (2.26), according to (2.20), the corresponding scattering angle is $\theta = \theta_L$, where

$$\theta_L = 4\left(\frac{\pi}{2} - \theta_l\right) = 2\theta_t = 4\cos^{-1}\frac{1}{N} \quad (1 < N < \sqrt{2}), \tag{2.30}$$

whereas, for $N > \sqrt{2}$, we have to employ (2.21) and we find for the limiting scattering angle

$$\theta_L = 4\theta_l \quad (N > \sqrt{2}). \tag{2.31}$$

Let

$$y = \sin\frac{\theta}{2} = \pm\cos(2\theta_2 - \theta_1), \tag{2.32}$$

where the + sign corresponds to the relations (2.20) and (2.21), and the − sign to (2.19). Taking into account (2.18), we find

$$\frac{dy}{d\theta_1} = \mp\frac{\sin(2\theta_2 - \theta_1)}{N\cos\theta_2}(2\cos\theta_1 - N\cos\theta_2). \tag{2.33}$$

The sign of $dy/d\theta_1$ tells us whether the scattering angle is an increasing or decreasing function of the angle of incidence. The change from − to + sign in (2.33) occurs only for $N < 1$, at $\theta_1 = \theta_{1c}$ [cf. (2.22)], which, by (2.19), corresponds to $\theta = 0$. Otherwise, $dy/d\theta_1$ changes sign only at $\theta_1 = \theta_{1A}$ [cf. (2.23)], which occurs only in the range (2.25) and corresponds to $\theta = \pi$, and for $\theta_1 = \theta_{1R}$, where

$$2\cos\theta_{1R} = N\cos\theta_{2R}, \tag{2.34}$$

which leads to

$$\sin\theta_{1R} = s = \left(\frac{4 - N^2}{3}\right)^{\frac{1}{2}},$$
$$\cos\theta_{1R} = c = \left(\frac{N^2 - 1}{3}\right)^{\frac{1}{2}}. \tag{2.35}$$

This is only possible for $1 < N < 2$. The corresponding scattering angle is $\theta = \theta_R$, where

$$y_R = \sin\frac{\theta_R}{2} = \frac{(8 + N^2)c}{3N^2}, \quad \cos\frac{\theta_R}{2} = \frac{s^3}{N^2}. \quad (2.36)$$

As will be seen later, θ_R is the *rainbow angle*.

According to (2.30) or (2.31), we have

$$y_L = \sin\frac{\theta_L}{2} = \sin(2\theta_l) = \frac{2M}{N^2}, \quad (2.37)$$

where [cf. Paper I, (2.53)]

$$M = (N^2 - 1)^{\frac{1}{2}} \quad (N > 1). \quad (2.38)$$

Thus, in the range (2.26), θ_R is always smaller than the limiting angle θ_L. However, in the range (2.25), we have

$$\theta_R < \theta_L \quad (N < N_0), \quad \theta_R > \theta_L \quad (N > N_0), \quad (2.39)$$

where

$$N_0 = (6\sqrt{3} - 8)^{\frac{1}{2}} \approx 1.547. \quad (2.40)$$

The above discussion enables us to give a complete description of the behavior of θ as a function of θ_1, for all ranges of the refractive index. The results are graphically displayed in Fig. 3.

Let us start from $\theta = \pi$ at $\theta_1 = 0$. Fig. 3(a) shows that for $N < 1$, θ first decreases from π to 0 as θ_1 increases from 0 to θ_{1c} [cf. (2.22)], and then increases again from 0 to θ_t [cf. (2.28)] as θ_1 increases from θ_{1c} to θ_l. Thus the domain $0 \leq \theta \leq \theta_t$ is covered twice: once by rays arising from (2.19) and once more by those from (2.20); there are two rays passing through

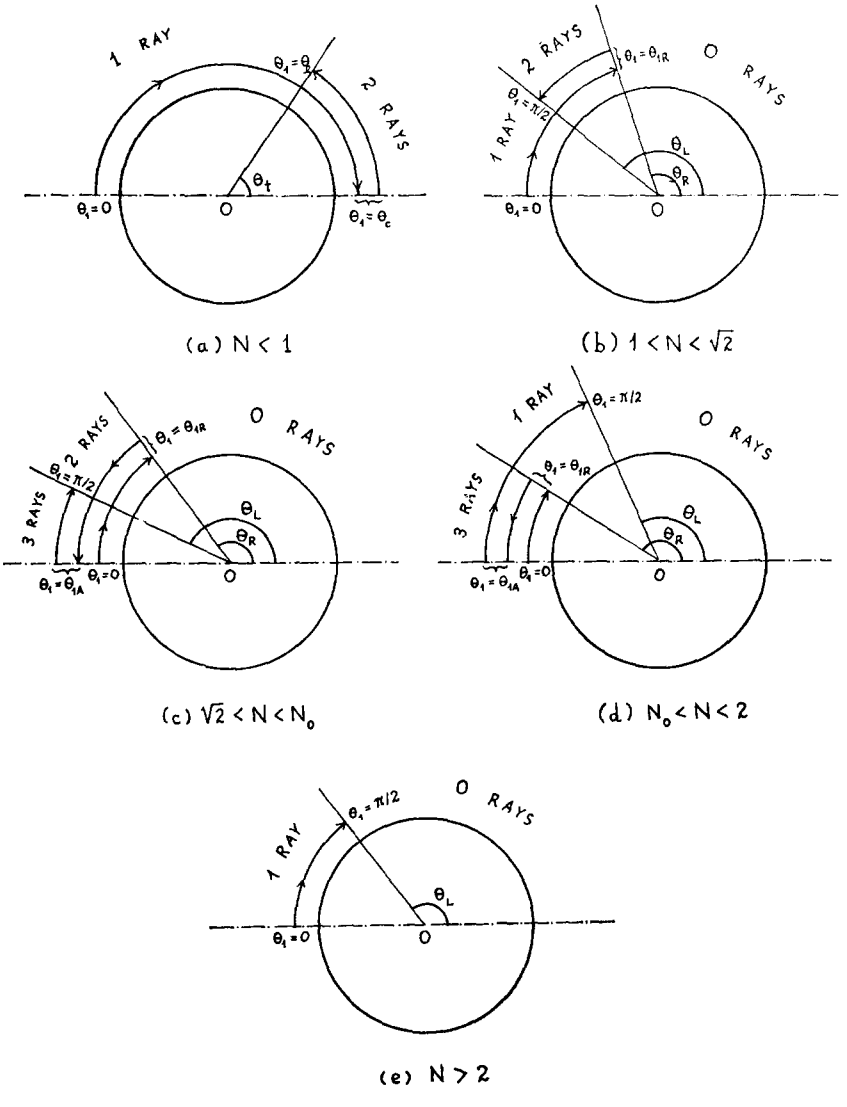

FIG. 3. Division into regions according to geometrical optics, for all ranges of the refractive index N. The behavior of θ as a function of θ_1 is indicated by the circular arrows, which point in the direction of increasing θ_1. The values of θ_1 at the turning points are indicated. The number of geometrical rays passing through a given direction is indicated in each region.

each direction in this region. There is no geometrical shadow (0-ray) region for $N < 1$: there is only a 1-ray/2-ray shadow boundary.

For $1 < N < \sqrt{2}$ [Fig. 3(b)], we have a turning point at $\theta_1 = \theta_{1R}$; the corresponding scattering angle θ_R is the angle of minimum deviation. The rainbow appears around this angle, which is a 2-ray/0-ray shadow boundary. The angle θ_L is a 1-ray/2-ray shadow boundary.

For $\sqrt{2} < N < 2$, there is, in addition to $\theta_1 = \theta_{1R}$, another turning point at $\theta_1 = \theta_{1A}$ [cf. (2.24)], beyond which (2.20) is replaced by (2.21). For $\theta_1 > \theta_{1A}$, θ decreases from π to θ_L [cf. (2.31)], where, by (2.39), $\theta_L > \theta_R$ for $N < N_0$ [Fig. 3(c)] and $\theta_L < \theta_R$ for $N > N_0$ [Fig. 3(d)]. Thus, for $N < N_0$, the rainbow occurs at a 2-ray/0-ray boundary, whereas for $N > N_0$ it occurs at a 3-ray/1-ray boundary, which should make it more difficult to observe. In the whole domain $\sqrt{2} < N < 2$, the neighborhood of the backward direction is covered by three rays.

Finally, for $N > 2$ [Fig. 3(e)], there are no turning points: we find only a 1-ray and a 0-ray region, just as for the previous terms of the Debye expansion.

C. The Saddle Points for $1 < N < \sqrt{2}$

From now on we shall deal mainly with the range $1 < N < \sqrt{2}$, for which the ray directions are determined by (2.20). The appropriate representation for $f^{\pm}_{2,0}(\beta, \theta)$ in this range is given by (2.7). In fact, as will now be seen, the saddle points on the real axis for the integrand of (2.7) are associated with the rays (2.20).

To determine the saddle points, let us consider the behavior of the integrand in the neighborhood of the real axis, between $\lambda = 0$ and $\lambda = \beta$, where the real saddle points must lie. The integrand differs from the corresponding one in Paper I, (5.29) only by a factor $-\rho(\lambda, \beta)$, so that we can employ approximations similar to those leading to Paper I, (5.36). With the change of variables [Paper I, (5.35)],

$$\lambda = \beta \sin w_1 = \alpha \sin w_2, \tag{2.41}$$

we find [cf. Paper I, (3.15)]

$$\begin{aligned}\rho(\lambda, \beta) = i&\left(\frac{\cos w_1 - N \cos w_2}{\cos w_1 + N \cos w_2}\right) \\ &\times \exp\left\{2i\beta\left[N \cos w_2 + \left(w_2 - \frac{\pi}{2}\right) \sin w_2\right]\right\} \\ &\times \left\{1 - \frac{i}{4\alpha \cos w_2}(1 + \tfrac{5}{3}\tan^2 w_2)\right. \\ &\left. - \frac{i \tan^2 w_1}{\alpha \cos w_2} + \mathcal{O}(\beta^{-2})\right\}.\end{aligned} \tag{2.42}$$

Taking into account Paper I, (5.36)–(5.38), this leads to

$$\begin{aligned}&\frac{i}{\beta}\int \rho U Q^{(2)}_{\lambda-\frac{1}{2}}(\cos\theta)\lambda \, d\lambda \\ &\quad \approx -2e^{-i\pi/4} N \left(\frac{2\beta}{\pi \sin\theta}\right)^{\frac{1}{2}} \\ &\qquad \times \int C(w_1, \beta, \theta) \exp\left[i\beta\omega(w_1, \theta)\right] dw_1,\end{aligned} \tag{2.43}$$

where

$$\begin{aligned}\omega(w_1, \theta) = 2\Big[&2N \cos w_2 - \cos w_1 \\ &+ \left(2w_2 - w_1 - \frac{\pi - \theta}{2}\right) \sin w_1\Big],\end{aligned} \tag{2.44}$$

$$\begin{aligned}&C(w_1, \beta, \theta) \\ &\quad = (\sin w_1)^{\frac{1}{2}} \cos^2 w_1 \cos w_2 \frac{(\cos w_1 - N \cos w_2)}{(\cos w_1 + N \cos w_2)^3} \\ &\qquad \times \left\{1 + \frac{i}{\beta}\left[\frac{1}{4 \cos w_1}(1 + \tfrac{5}{3}\tan^2 w_1)\right.\right. \\ &\qquad - \frac{1}{2N \cos w_2}(1 + \tfrac{5}{3}\tan^2 w_2) - \frac{2 \tan^2 w_1}{N \cos w_2} \\ &\qquad \left.\left. + \frac{\tan^2 w_2}{\cos w_1} - \frac{\cot\theta}{8 \sin w_1}\right] + \mathcal{O}(\beta^{-2})\right\}.\end{aligned} \tag{2.45}$$

In the derivation of these results, in addition to [N, Eq. (C7)], we have employed the Debye asymptotic expansions [Paper N, (A16)] for $H^{(1,2)}_{\lambda}(\beta)$. The domain of validity of these expansions in the λ plane[12] is represented in Fig. 4 by the oblong-shaped region bounded by the curves in broken line, from which the domain

$$|\lambda| - \beta = \mathcal{O}(\beta^{\frac{1}{3}}) \tag{2.46}$$

also has to be excluded. Thus, we can employ (2.43)–(2.45) to locate not only real, but also complex saddle points (if any) contained within this region.

Taking into account Paper I, Eq. (5.39), we find

$$\partial\omega/\partial w_1 = 2 \cos w_1 [2w_2 - w_1 - \tfrac{1}{2}(\pi - \theta)], \tag{2.47}$$

so that the saddle points are determined by

$$\bar{w}_1 = \theta_1, \quad \bar{w}_2 = \theta_2, \quad \bar{\lambda} = \beta \sin\theta_1 = \alpha \sin\theta_2, \tag{2.48}$$

[12] G. N. Watson, *Theory of Bessel Functions* (Cambridge University Press, London, 1962), 2nd ed., p. 265.

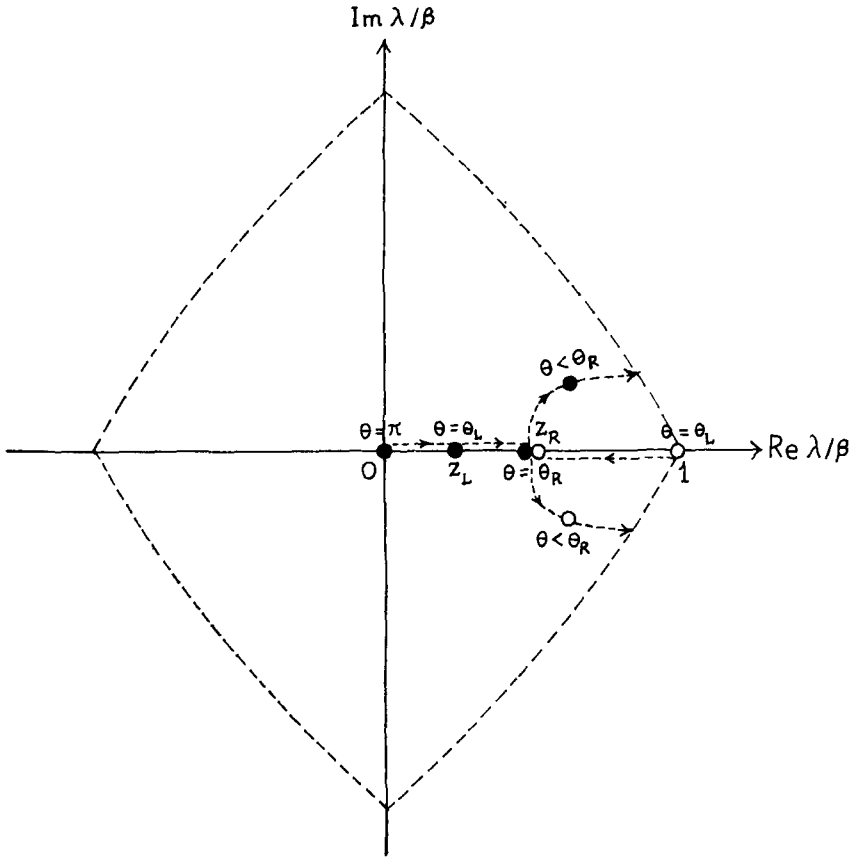

FIG. 4. Saddle-point trajectories in the λ plane as a function of θ for $1 < N < \sqrt{2}$. ●—z''; ○—z', where $z = \bar{\lambda}/\beta$ [cf. (A7)]. The limiting angle θ_L is given by (2.30) and the rainbow angle θ_R by (2.36). The two saddle points coalesce at $\theta = \theta_R$. For $\theta < \theta_R$, they move apart in complex conjugate directions. The oblong-shaped region is the domain of validity of the asymptotic expansions employed in (2.43)–(2.45).

where θ_1 and θ_2 are related to θ by (2.20). This justifies our choice of the representation (2.7). [As is readily seen with the help of [I, Eq. (C7)], had we chosen, instead, the representation (2.11), the resulting saddle points would correspond to (2.21). Thus, this would be the appropriate choice for $N > 2$.]

In order to determine the saddle points, we have to find the real and complex roots of (2.48), (2.20) that lie within the domain under consideration. This is done in Appendix A. The results are graphically displayed in Fig. 4, which shows the trajectories described by the saddle points in the λ plane as θ changes.

For $\theta_L < \theta < \pi$, the 1-ray region in Fig. 3(b), there is only one saddle point, given by $\bar{\lambda}/\beta = \sin\theta_1 = z''$, where z'' is defined in (A7). This saddle point moves from the origin to the point z_L as θ decreases from π to θ_L.

At $\theta = \theta_L$ [cf. (2.30)], another saddle point z' [cf. (A7)] appears at $\bar{\lambda}/\beta = 1$ and, as θ decreases from θ_L to θ_R, the two saddle points move towards each other. [This is not quite correct, since the Debye expansions employed in (2.43)–(2.45) fail in the domain (2.46); we shall see in Sec. 3 how to treat the region $\theta \approx \theta_L$.] Their confluence takes place at the rainbow angle θ_R. Thus, for $\theta_R < \theta < \theta_L$, there are two real saddle points, corresponding to the 2-ray region in Fig. 3(b).

Finally, for $\theta < \theta_R$, the two saddle points become complex. They leave the real axis at right angles and describe complex-conjugate trajectories. This corresponds to the 0-ray region in Fig. 3(b). However, the saddlepoint positions are given by (A7) only as long as they fall within the oblong-shaped domain indicated in Fig. 4. Outside of this domain, i.e., deep within the geometrical shadow region, the results are no longer valid. To evaluate the complex saddle points under these conditions, we would have to substitute (2.43)–(2.45) by the appropriate representation, valid outside of the oblong-shaped region. However, as will be seen in Sec. 3C, the contribution from the complex saddle points no longer dominates the amplitude in the deep shadow region, so that the corresponding results will not be required.

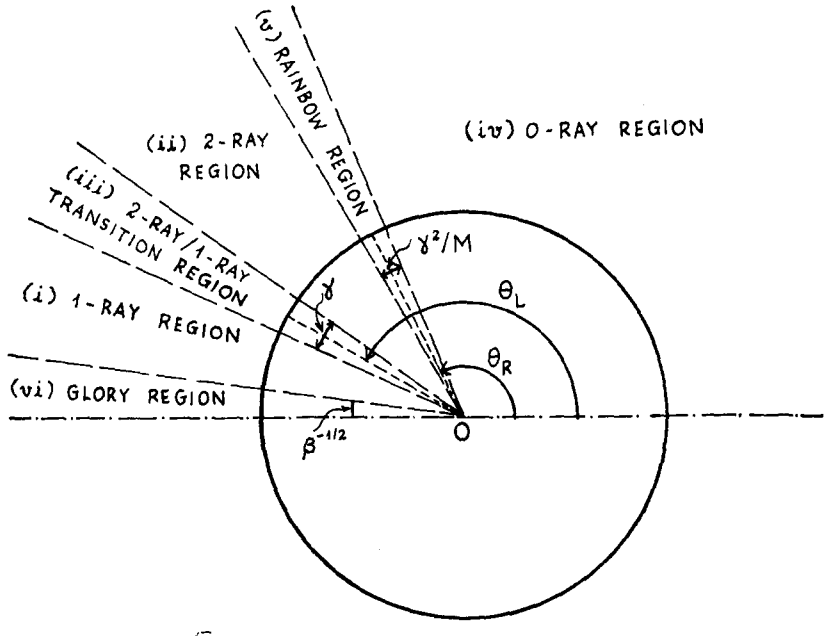

FIG. 5. Division into regions for $1 < N < \sqrt{2}$; θ_R = rainbow angle; θ_L = 2-ray/1-ray boundary angle. The angular width of the transition regions is also indicated.

3. BEHAVIOR IN THE NORMAL REGIONS

According to geometrical optics [cf. Fig. 3(b)], there are three different angular regions for $1 < N < \sqrt{2}$. They are distinguished by the number of geometrical rays passing through a given direction: 0-ray ($0 < \theta < \theta_R$), 2-ray ($\theta_R < \theta < \theta_L$) and 1-ray ($\theta_L < \theta < \pi$).

If we consider also the corresponding transition regions, including a transition region near the backward direction, we find six angular regions requiring separate treatments, as shown in Fig. 5. The width $\Delta\theta$ of each transition region will be derived later on.

Region (v), corresponding to the rainbow, and region (vi), where the glory is found, are treated in Secs. 4 and 5, respectively. The remaining regions, which will be called "normal" regions, are treated in the present Section.

A. The 1-Ray Region

This is the region

$$\theta - \theta_L \gg \gamma, \quad \pi - \theta \gg \beta^{-\frac{1}{2}}, \tag{3.1}$$

where θ_L is defined by (2.30) and $\gamma = (2/\beta)^{\frac{1}{3}}$, as in [I, Eq. (2.49)]. The restriction to $\pi - \theta \gg \beta^{-\frac{1}{2}}$ allows us to employ the asymptotic expansion [N, Eq. (C7)] for $Q^{(2)}_{\lambda-\frac{1}{2}}(\cos\theta)$ in (2.7), thus leading to the representation (2.43)–(2.45).

For $\theta > \theta_L$, we have seen that there is a single saddle point, given by

$$\bar{\lambda}/\beta = \sin\theta_1 = N \sin\theta_2 = z'', \tag{3.2}$$

where z'' is defined by (A7).

It follows from (2.47) that

$$\left(\frac{\partial^2\omega}{\partial w_1^2}\right)_{w_1=\theta_1} = \frac{2\cos\theta_1}{N\cos\theta_2}(2\cos\theta_1 - N\cos\theta_2). \tag{3.3}$$

Let

$$\cos\theta_1/\cos\theta_{1R} = \sqrt{3}\tan\phi \quad (0 < \phi < \pi/2),$$

where $\cos\theta_{1R}$ is given by (2.35). Then, (3.3) becomes

$$(4\cos\theta_1)^{-1}(\partial^2\omega)/(\partial w_1^2)_{w_1=\theta_1} = \sin\phi - \tfrac{1}{2},$$

so that

$$\left(\frac{\partial^2\omega}{\partial w_1^2}\right)_{\theta_1} > 0, \quad \text{for} \quad \theta_1 < \theta_{1R},$$

$$\left(\frac{\partial^2\omega}{\partial w_1^2}\right)_{\theta_1} < 0, \quad \text{for} \quad \theta_1 > \theta_{1R}. \tag{3.4}$$

In the present case (cf. Fig. 4), we have $\theta_1 < \theta_{1R}$, so that the steepest-descent path crosses the real axis at the saddle point at an angle of $\pi/4$. This leads us to choose $f^-_{2,0}$ (rather than $f^+_{2,0}$) in (2.7). The steepest-descent path is schematically represented by the curve in full line in Fig. 6. It must begin and end at

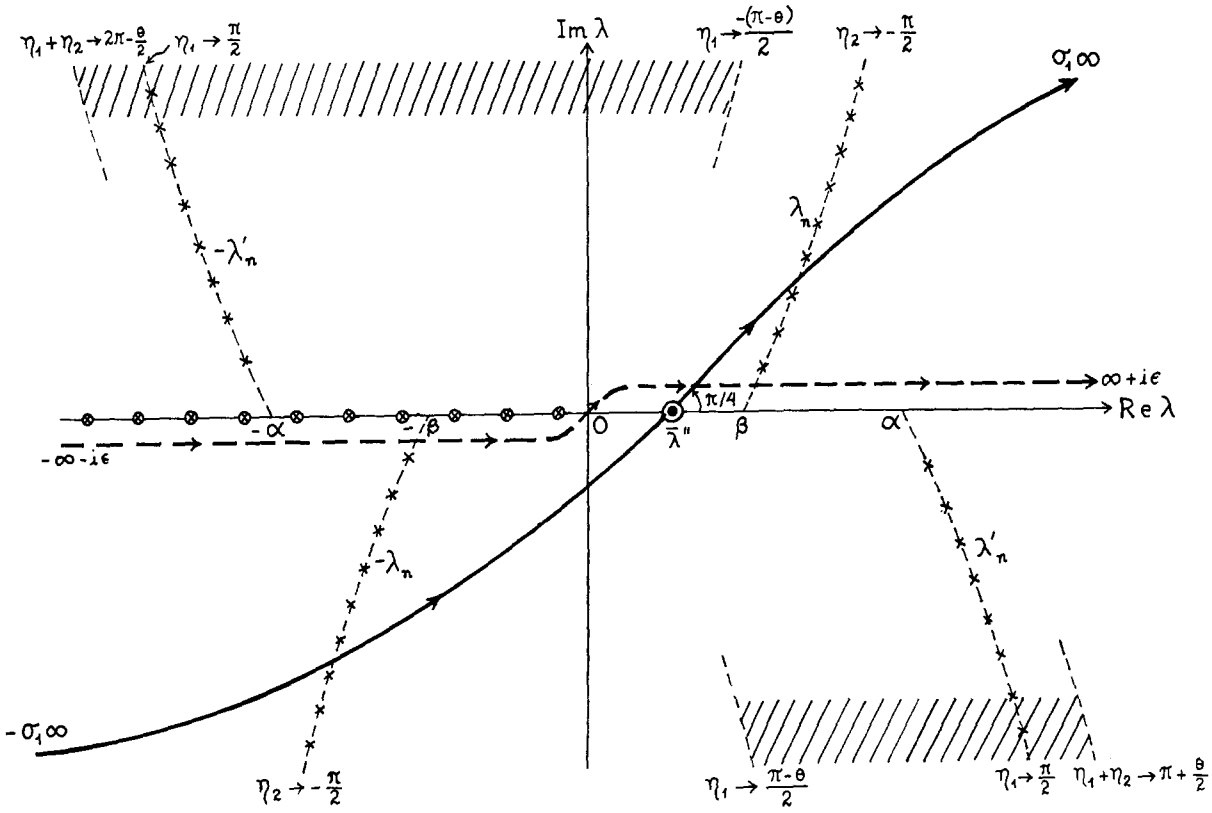

FIG. 6. Behavior of the integrand of (2.7) and the paths of integration in the λ plane ($\theta > \theta_L$). ×—poles of ρU; ⊗—poles of $Q^{(2)}_{\lambda-\frac{1}{2}}$ at the negative half-integers; ⊙—saddle point. The integrand diverges as $|\lambda| \to \infty$ within the shaded regions and tends to zero elsewhere (apart from the poles). The original path of integration, shown in broken line, must be deformed onto the steepest-descent path, shown in solid line; this gives rise to residues at the poles λ_n and $-\lambda_n$.

infinity outside of the shaded regions, where the integrand diverges [cf. Fig. 1 and (2.16)]. In order to deform the path of integration in (2.7) from $(-\infty - i\epsilon,\ \infty + i\epsilon)$ (curve in broken line in Fig. 6) to the steepest-descent path $(-\sigma_1\infty,\ \sigma_1\infty)$, we have to go across the poles λ_n and $-\lambda_n$, so that we find

$$f^{-}_{2,0}(\beta,\theta) = -\frac{i}{\beta}\int_{-\sigma_1\infty}^{\sigma_1\infty}\rho U Q^{(2)}_{\lambda-\frac{1}{2}}(\cos\theta)\lambda\, d\lambda + \frac{2\pi}{\beta}\sum_n \{\text{residue } [\lambda\rho U Q^{(2)}_{\lambda-\frac{1}{2}}(\cos\theta)]_{\lambda_n} - \text{residue } [\lambda\rho U Q^{(2)}_{\lambda-\frac{1}{2}}(\cos\theta)]_{-\lambda_n}\}. \quad (3.5)$$

It is irrelevant for our purpose whether the number of poles crossed is finite or infinite. This depends on the shape of the path far away from the saddle point, which will not be investigated here. Actually, only poles close to the real axis give a significant contribution. For simplicity, the residues at all the poles have been included in (3.5) and subsequent relations, but only trivial changes are required if the number is finite.

Since $\lambda = -\lambda_n$ is a triple pole (cf. I, Sec. 3B), we have

$$\text{residue } [\lambda\rho U Q^{(2)}_{\lambda-\frac{1}{2}}(\cos\theta)]_{-\lambda_n} = \frac{1}{2!}\frac{d^2}{d\lambda^2}[(\lambda+\lambda_n)^3\lambda\rho U Q^{(2)}_{\lambda-\frac{1}{2}}(\cos\theta)]_{-\lambda_n}.$$

Changing $\lambda \to -\lambda$ on the right-hand side, and taking into account (2.2), we find

$$\text{residue } [\lambda\rho U Q^{(2)}_{\lambda-\frac{1}{2}}(\cos\theta)]_{-\lambda_n} = \text{residue } [\lambda e^{2i\pi\lambda}\rho U Q^{(2)}_{-\lambda-\frac{1}{2}}(\cos\theta)]_{\lambda_n}. \quad (3.6)$$

It follows from N, Eq. (C5) and (C6), that

$$Q^{(2)}_{-\lambda-\frac{1}{2}}(\cos\theta) = Q^{(1)}_{\lambda-\frac{1}{2}}(\cos\theta) - \frac{i}{\cos(\pi\lambda)}P_{\lambda-\frac{1}{2}}(-\cos\theta). \quad (3.7)$$

Substituting (3.6) and (3.7) in (3.5), and taking into account I, (2.12), we get

$$f_{2,0}^{-}(\beta,\theta) = -\frac{i}{\beta}\int_{-\sigma_1\infty}^{\sigma_1\infty}\rho U Q^{(2)}_{\lambda-\frac{1}{2}}(\cos\theta)\lambda\,d\lambda + 2\bar{f}_{2,\mathrm{res}}(\beta,\theta) + \frac{2\pi}{\beta}\sum_n \text{residue}\,\{\lambda\rho U[Q^{(2)}_{\lambda-\frac{1}{2}}(\cos\theta) - e^{2i\pi\lambda}Q^{(1)}_{\lambda-\frac{1}{2}}(\cos\theta)]\}_{\lambda_n}, \tag{3.8}$$

where $\bar{f}_{2,\mathrm{res}}$ is the residue series at the poles λ_n defined in (2.15).

It follows from N, Eq. (C3)–(C4), that

$$Q^{(2)}_{\lambda-\frac{1}{2}}(\cos\theta) - e^{2i\pi\lambda}Q^{(1)}_{\lambda-\frac{1}{2}}(\cos\theta) = -ie^{i\pi\lambda}P_{\lambda-\frac{1}{2}}(-\cos\theta). \tag{3.9}$$

Substituting the result in (3.8) and taking into account (2.15), we find that (2.6) finally becomes

$$f_2(\beta,\theta) = f_{2,g}(\beta,\theta) + f_{2,\mathrm{res}}(\beta,\theta) + f'_{2,\mathrm{res}}(\beta,\theta) \qquad (\theta_L < \theta < \pi), \tag{3.10}$$

where

$$f_{2,g}(\beta,\theta) = -\frac{i}{\beta}\int_{-\sigma_1\infty}^{\sigma_1\infty}\rho U Q^{(2)}_{\lambda-\frac{1}{2}}(\cos\theta)\lambda\,d\lambda, \tag{3.11}$$

$$f_{2,\mathrm{res}}(\beta,\theta) = -\frac{2\pi i}{\beta}\sum_{m=0}^{\infty}(-1)^m \times \sum_n \text{residue}\,\{\lambda\rho U P_{\lambda-\frac{1}{2}}(-\cos\theta) \times \exp[i(2m+1)\pi\lambda]\}_{\lambda_n}, \tag{3.12}$$

and

$$f'_{2,\mathrm{res}}(\beta,\theta) = \frac{2\pi i}{\beta}\sum_{m=1}^{\infty}(-1)^m \times \sum_n \text{residue}\,\{\lambda\rho U P_{\lambda-\frac{1}{2}}(-\cos\theta) \times \exp[i(2m+1)\pi\lambda]\}_{-\lambda_n}. \tag{3.13}$$

Let us consider first the "geometrical-optic" term $f_{2,g}(\beta,\theta)$. The expansion for the integrand in the vicinity of the saddle point follows from (2.43)–(2.45), and the saddle point is determined by (2.48) and (2.20). The path of integration is the image of that shown in Fig. 6 in the w_1-plane.

The saddlepoint evaluation of (3.11) now proceeds by applying the analog of N, Eq. (6.12), which differs from I, Eq. (4.34) only by the substitutions:

$$B \to C, \quad \delta \to \omega, \quad |\delta''| \to -\omega'', \quad |\delta''|^{\frac{1}{2}} \to -i(\omega'')^{\frac{1}{2}}. \tag{3.14}$$

A rather tedious calculation finally leads to the result

$$f_{2,g}(\beta,\theta) = -\left(\frac{\sin\theta_1}{\sin\theta}\right)^{\frac{1}{2}}\frac{(2N\cos\theta_1\cos\theta_2)^{\frac{3}{2}}}{(2\cos\theta_1 - N\cos\theta_2)^{\frac{1}{2}}} \times \frac{(N\cos\theta_2 - \cos\theta_1)}{(N\cos\theta_2 + \cos\theta_1)^3} \times \exp[2i\beta(2N\cos\theta_2 - \cos\theta_1)] \times \left\{1 - \frac{i\mathfrak{G}(\theta_1,\theta)}{64\beta\cos\theta_1} + \mathcal{O}(\beta^{-2})\right\}, \tag{3.15}$$

where

$$\mathfrak{G}(\theta_1,\theta) = 8\cot\theta_1\left[\cot\theta + \frac{\cot\theta_1}{2(2\chi-1)}\right] + 6(9\chi - 11) - \frac{15}{2\chi-1} - \frac{9}{(2\chi-1)^2} + \tan^2\theta_1\left[56\chi^3 - 3\chi^2 + \tfrac{39}{2}\chi - \frac{79}{2} - \frac{33}{2(2\chi-1)} - \frac{51}{4(2\chi-1)^2} - \frac{15}{4(2\chi-1)^3}\right], \tag{3.16}$$

and, as in I, (5.47),

$$\chi = \left(\frac{dw_2}{dw_1}\right)_{\bar{w}_1} = \frac{\cos\theta_1}{N\cos\theta_2}. \tag{3.17}$$

The relation between θ_1 and θ follows from (3.2) and Appendix A, so that, in principle, everything can be explicitly written as a function of θ, but the resulting expressions would be enormously complicated.

The result (3.15) should be compared with I, Eq. (5.45). It contains an additional factor corresponding to the internal Fresnel reflection coefficient, as well as the phase factor appropriate to the ray path shown in Fig. 2(b). The denominator $(2\cos\theta_1 - N\cos\theta_2)^{\frac{1}{2}}$ would vanish only at the rainbow angle (2.34), but this falls outside of the region (3.1).

Let us consider next the residue series at the poles λ_n, given by (3.12). Substituting ρ and U by their definitions I, Eq. (3.15) and I, Eq. (3.24), and taking

into account I, Eqs. (3.4)–(3.8), we find [cf. I, Eq. (5.17)]:

$$f_{2,\mathrm{res}}(\beta,\theta) = -\frac{32i}{\pi\beta^3}\sum_{m=0}^{\infty}(-1)^m \times \sum_n \text{residue}\left\{\frac{c_m(\lambda,\beta,\theta)}{[d(\lambda,\beta)]^3}\right\}_{\lambda_n}, \quad (3.18)$$

where, as in I, Eq. (4.38),

$$d(\lambda,\beta) = [1\ \beta] - N[2\ \alpha] \quad (3.19)$$

and

$$c_m(\lambda,\beta,\theta) = \lambda \exp[i(2m+1)\pi\lambda]\frac{H_\lambda^{(1)}(\alpha)}{[H_\lambda^{(1)}(\beta)]^2[H_\lambda^{(2)}(\alpha)]^3} \times ([1\ \beta] - N[1\ \alpha])P_{\lambda-\frac{1}{2}}(-\cos\theta). \quad (3.20)$$

The residue of the expression within curly brackets in (3.18) at a triple pole is given by (cf. Ref. 9, Appendix II):

$$\text{residue}\left\{\frac{c_m(\lambda,\beta,\theta)}{[d(\lambda,\beta)]^3}\right\}_{\lambda_n} = \frac{c_m}{2\dot{d}^3}\left[\frac{\ddot{c}_m}{c_m} - 3\frac{\dot{c}_m}{c_m}\frac{\ddot{d}}{\dot{d}} + 3\left(\frac{\ddot{d}}{\dot{d}}\right)^2 - \frac{\dddot{d}}{\dot{d}}\right]_{\lambda_n}, \quad (3.21)$$

where the dots denote partial derivatives with respect to λ and all quantities in the second member are to be evaluated at the pole λ_n.

Let us evaluate (3.21) to lowest order, just as we did for I, (5.22) [in Sec. 5C, we shall have to reevaluate (3.21) with much greater accuracy]. For this purpose, we employ the asymptotic expansions N, (A16) for $H_\lambda^{(1,2)}(\alpha)$ and N, (C11) for $P_{\lambda-\frac{1}{2}}(-\cos\theta)$ (this is allowed since $\pi - \theta \gg \beta^{-1}$), and the expansions given in I, Appendix A, for $H_\lambda^{(1)}(\beta)$ and its derivatives with respect to λ and β. Keeping only the dominant term in each expansion and neglecting corrections of order γ^2, we find the following final result:

$$\begin{aligned} f_{2,\mathrm{res}}(\beta,\theta) &\approx \frac{e^{i\pi/12}}{M^2}\left(\frac{\gamma}{\pi\sin\theta}\right)^{\frac{1}{2}}\exp(4iM\beta) \\ &\times \Big\{ i\sum_n (a_n')^{-2}[(\zeta_{2,0}^+)^2 + M\zeta_{2,0}^+]\exp(i\lambda_n\zeta_{2,0}^+) \\ &+ \sum_{m=1}^{\infty}(-1)^m\sum_n (a_n')^{-2}\{i[(\zeta_{2,m}^+)^2 + M\zeta_{2,m}^+] \\ &\times \exp(i\lambda_n\zeta_{2,m}^+) - [(\zeta_{2,m}^-)^2 + M\zeta_{2,m}^-] \\ &\times \exp(i\lambda_n\zeta_{2,m}^-)\}\Big\}, \end{aligned} \quad (3.22)$$

where [cf. (2.30)]

$$\zeta_{2,m}^{\pm} = 2m\pi - 2\theta_t \pm \theta = 2m\pi - \theta_L \pm \theta \quad (m = 0, 1, 2, \cdots). \quad (3.23)$$

For the general evaluation of the dominant term in the residue-series contribution at the poles λ_n, of which (3.22) is a particular case, see Appendix C.

Just as in Paper I [Eq. (5.24)], we can rewrite this result as follows:

$$\begin{aligned} f_{2,\mathrm{res}}(\beta,\theta) &\approx i(\sin\theta)^{-\frac{1}{2}}\exp(4iM\beta) \\ &\times \Big\{\sum_n D_n^2 D_{21}D_{12}[\tilde{R}_{11}\zeta_{2,0}^+ + \tfrac{1}{2}D_{21}D_{12}(\zeta_{2,0}^+)^2] \\ &\times \exp(i\lambda_n\zeta_{2,0}^+) + \sum_{m=1}^{\infty}(-1)^m\sum_n D_n^2 D_{21}D_{12} \\ &\times [(\tilde{R}_{11}\zeta_{2,m}^+ + \tfrac{1}{2}D_{21}D_{12}(\zeta_{2,m}^+)^2)\exp(i\lambda_n\zeta_{2,m}^+) \\ &+ i(\tilde{R}_{11}\zeta_{2,m}^- + \tfrac{1}{2}D_{21}D_{12}(\zeta_{2,m}^-)^2)\exp(i\lambda_n\zeta_{2,m}^-)]\Big\}, \end{aligned} \quad (3.24)$$

where, as in I, (4.45) and I,(5.25),

$$D_n^2 = \tfrac{1}{2}e^{i\pi/12}(\gamma/\pi)^{\frac{1}{2}}(a_n')^{-2}, \quad (3.25)$$

$$D_{21}D_{12} = 2/M, \quad (3.26)$$

with M given by (2.38) and

$$\tilde{R}_{11} = 1. \quad (3.27)$$

The physical interpretation of this result in terms of diffracted rays is similar to that of I, (5.24) (cf. also I, Fig. 15). As shown in Figs. 7(a) and 7(b), the tangentially incident rays at T_1 and T_2, after undergoing two critical refractions and one total internal reflection, reemerge tangentially to define the 2-ray/1-ray shadow boundary at the points T_1''' and T_2''', respectively. At these points, they excite surface waves propagating from the shadow boundary into the shadow (i.e., into the 1-ray region). This gives rise to the diffracted rays $T_2T_2'T_2''T_2'''B$ [Fig. 7(a)] and $T_1T_1'T_1''T_1'''A$ [Fig. 7(b)]. The corresponding angles described along the surface are $\zeta_{2,0}^+$ and $\zeta_{2,1}^-$, respectively, and after additional turns around the sphere, the angles are given by (3.23).

As in I, Sec. 5B, there are again infinitely many paths leading to the same direction of emergence for this class of diffracted rays. Their common feature is

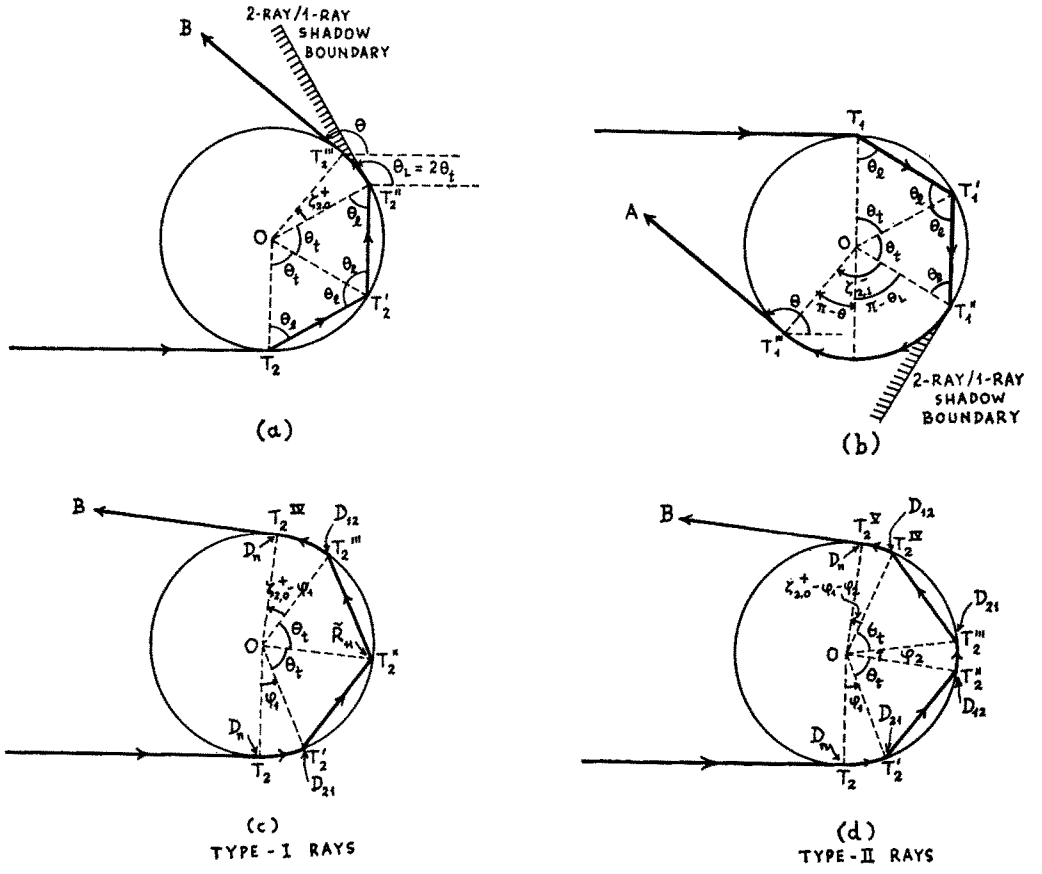

FIG. 7. Physical interpretation of (3.24). The limiting rays (a) $T_2T_2'T_2''$ and (b) $T_1T_1'T_1''$ which define the 2-ray/1-ray shadow boundary excite surface waves propagating into the shadow, generating the diffracted rays (a) $T_2T_2'T_2''T_2'''B$ and (b) $T_1T_1'T_1''T_1'''A$, in the direction θ. The corresponding angles described along the surface are $\zeta_{2,0}^+$ and $\zeta_{2,1}^-$, respectively. There are infinitely many possible paths for this class of diffracted rays: (c) type-I rays describe an angle ϕ_1 as surface waves before penetrating again into the sphere; (d) type-II rays describe two angles, ϕ_1 and ϕ_2, before emerging to describe the final angle $\zeta_{2,0}^+ - \phi_1 - \phi_2$.

that, for all of them, the diffracted rays take two "shortcuts" across the sphere. They can be subdivided into two types (cf. Ref. 9), as illustrated in Figs. 7(c) and 7(d) for $\zeta_{2,0}^+$.

Type-I rays [Fig. 7(c)] are those which, after excitation at T_2 (with diffraction coefficient D_n), describe an angle ϕ_1 ($0 \leq \phi_1 \leq \zeta_{2,0}^+$) as surface waves, are critically refracted into the sphere at T_2' (coefficient D_{21}), undergo total internal reflection at T_2'' (coefficient $\tilde{R}_{11}$), reemerge at T_2''' (coefficient D_{12}) to describe the final angle $\zeta_{2,0}^+ - \phi_1$, and finally leave the surface tangentially at T_2^{IV} (coefficient D_n). As in I, Sec. 5B, the contribution from those paths such that an angle between ϕ_1 and $\phi_1 + d\phi_1$ is described is proportional to $d\phi_1$, so that the total contribution from type-I rays is proportional to

$$D_n^2 D_{21} D_{12} \tilde{R}_{11} \int_0^{\zeta_{2,0}^+} d\phi_1 = D_n^2 D_{21} D_{12} \tilde{R}_{11} \zeta_{2,0}^+. \quad (3.28)$$

Type-II rays [Fig. 7(d)] differ from type-I only by the fact that, instead of undergoing total internal reflection at T_2'', they are critically refracted to the outside (coefficient D_{12}), describe another angle ϕ_2 ($0 \leq \phi_1 + \phi_2 \leq \zeta_{2,0}^+$) as surface waves, and are critically refracted to the inside at T_2'''; thereafter, they behave as type-I rays. The total contribution from type-II rays is therefore proportional to

$$D_n^2 (D_{21} D_{12})^2 \iint_{0 \leq \phi_1 + \phi_2 \leq \zeta_{2,0}^+} d\phi_1 \, d\phi_2$$

$$= D_n^2 (D_{21} D_{12})^2 \int_0^{\zeta_{2,0}^+} d\phi_1 \int_0^{\zeta_{2,0}^+ - \phi_1} d\phi_2$$

$$= \tfrac{1}{2} D_n^2 (D_{21} D_{12})^2 (\zeta_{2,0}^+)^2. \quad (3.29)$$

The phase factor $\exp(4iM\beta)$ in (3.24) accounts for the optical path difference associated with the two shortcuts. A similar discussion for a cylinder has been given by Chen.[9]

Finally, let us consider the residue series at the poles $-\lambda'_n$, given by (3.13). With the help of (3.6), we can rewrite (3.13) as

$$f'_{2,\mathrm{res}}(\beta,\theta) = \frac{2\pi i}{\beta}\sum_{m=1}^{\infty}(-1)^m \sum_n \text{residue} \times \{\lambda\rho U P_{\lambda-\frac{1}{2}}(-\cos\theta) \times \exp[-i(2m-1)\pi\lambda]\}_{\lambda_{n'}}. \quad (3.30)$$

Except for the change in sign and the exclusion of $m = 0$, we can still apply (3.18)–(3.21), the main difference being that the residues are now to be evaluated at λ'_n, rather than λ_n.

The approximations employed for the evaluation of (3.30) are the same as for I, (5.27), except that (3.20) contains also $H_\lambda^{(1)}(\alpha)$. According to I, (3.35) and I, (A1), we have

$$H^{(1)}_{\lambda'_n}(\alpha) \approx 2\frac{e^{-i\pi/3}}{\gamma'}\,\mathrm{Ai}\,(e^{i\pi/3}x_n), \quad (3.31)$$

where $\gamma' = (2/\alpha)^{\frac{1}{3}}$, as in I, (5.62). It follows from the Wronskian relation N, (D3), that

$$\mathrm{Ai}\,(e^{i\pi/3}x_n) = -\frac{e^{i\pi/6}}{2\pi a'_n}. \quad (3.32)$$

Taking into account these results, we finally obtain

$$f'_{2,\mathrm{res}}(\beta,\theta) \approx \frac{e^{i\pi/12}N^2}{4\pi M}\frac{\exp(2M\beta)}{(\pi\gamma'\sin\theta)^{\frac{1}{2}}} \times \Big\{\sum_n (a'_n)^{-4}(\tilde\zeta^+_{2,0})^2\exp(-i\lambda'_n\tilde\zeta^+_{2,0}) + \sum_{m=1}^{\infty}(-1)^m\sum_n (a'_n)^{-4}[(\tilde\zeta^+_{2,m})^2 \times \exp(-i\lambda'_n\tilde\zeta^+_{2,m}) - i(\tilde\zeta^-_{2,m})^2 \times \exp(-i\lambda'_n\tilde\zeta^-_{2,m})]\Big\}, \quad (3.33)$$

where

$$\tilde\zeta^{\pm}_{2,m} = 2m\pi - 2i\cosh^{-1}N \pm \theta. \quad (3.34)$$

For $N < 1$, the general evaluation of the dominant term in the residue-series contribution at the poles λ'_n is given in Appendix D.

This result should be compared with I, (5.27). As in that case, $f'_{2,\mathrm{res}}$ is exponentially small as compared with $f_{2,\mathrm{res}}$, and can therefore be neglected. As will be seen in Sec. 7F the reverse is true for $N < 1$, and the analytic continuation of (3.33) to that case has a physical interpretation similar to that of I, (5.65).

The limitation to $\theta - \theta_L \gg \gamma$ in the domain of validity of the above results [cf. (3.1)] arises from (3.22): This is the domain where the least strongly damped series, involving $\exp(i\lambda_n\zeta^+_{2,0})$, is rapidly convergent.

B. The 2-Ray Region

This is the region

$$\theta_L - \theta \gg \gamma, \quad \theta - \theta_R \gg \gamma^2/M. \quad (3.35)$$

In this region, in addition to the real saddle point z'', with $\theta_1 < \theta_{1R}$, there is another real saddle point z', with $\theta_1 > \theta_{1R}$ (cf. Fig. 4 and Appendix A).

According to (3.4), the steepest-descent path at the new saddle point z' crosses the real axis at an angle of $-\pi/4$, so that the path of integration shown in Fig. 6 must be replaced by the new path shown in solid line in Fig. 8.

In order to deform the path of integration in (2.7) from $(-\infty - i\epsilon,\ \infty + i\epsilon)$ (curve in broken line in Fig. 8) to the new path $(-\sigma_1\infty,\ \sigma_2\infty)$, we have to go across the poles $-\lambda_n$ and λ'_n so that, instead of (3.10), we find

$$f_2(\beta,\theta) = \tilde f_{2,g}(\beta,\theta) + \tilde f_{2,\mathrm{res}}(\beta,\theta) + \tilde f'_{2,\mathrm{res}}(\beta,\theta), \quad (3.36)$$

where

$$\tilde f_{2,g}(\beta,\theta) = -\frac{i}{\beta}\int_{-\sigma_1\infty}^{\sigma_2\infty}\rho U Q^{(2)}_{\lambda-\frac{1}{2}}(\cos\theta)\lambda\,d\lambda, \quad (3.37)$$

$$\tilde f_{2,\mathrm{res}}(\beta,\theta) = f_{2,\mathrm{res}}(\beta,\theta) - \frac{2\pi}{\beta} \times \sum_n \text{residue}\,[\lambda\rho U Q^{(2)}_{\lambda-\frac{1}{2}}(\cos\theta)]_{\lambda_n} \quad (3.38)$$

$$\tilde f'_{2,\mathrm{res}}(\beta,\theta) = f'_{2,\mathrm{res}}(\beta,\theta) - \frac{2\pi}{\beta} \times \sum_{n=1}^{n_0}\text{residue}\,[\lambda\rho U Q^{(2)}_{\lambda-\frac{1}{2}}(\cos\theta)]_{\lambda_{n'}}, \quad (3.39)$$

where $f_{2,\mathrm{res}}$ and $f'_{2,\mathrm{res}}$ are given by (3.12) and (3.13), respectively, and n_0 is the total number of poles λ'_n crossed by the contour. In order to determine the total number n_0 of poles λ'_n crossed, a detailed investigation of the shape of the steepest-descent path far away from the saddle points would be required. For our purposes, it is sufficient to know that the contribution from the poles λ'_n can be neglected.

The "geometrical-optic" term (3.37) now contains two contributions, one from each saddle point. The contribution from the left saddle point z'' is still given by (3.15)–(3.17); that from the right saddle point z' is similar, except that we must now employ I,

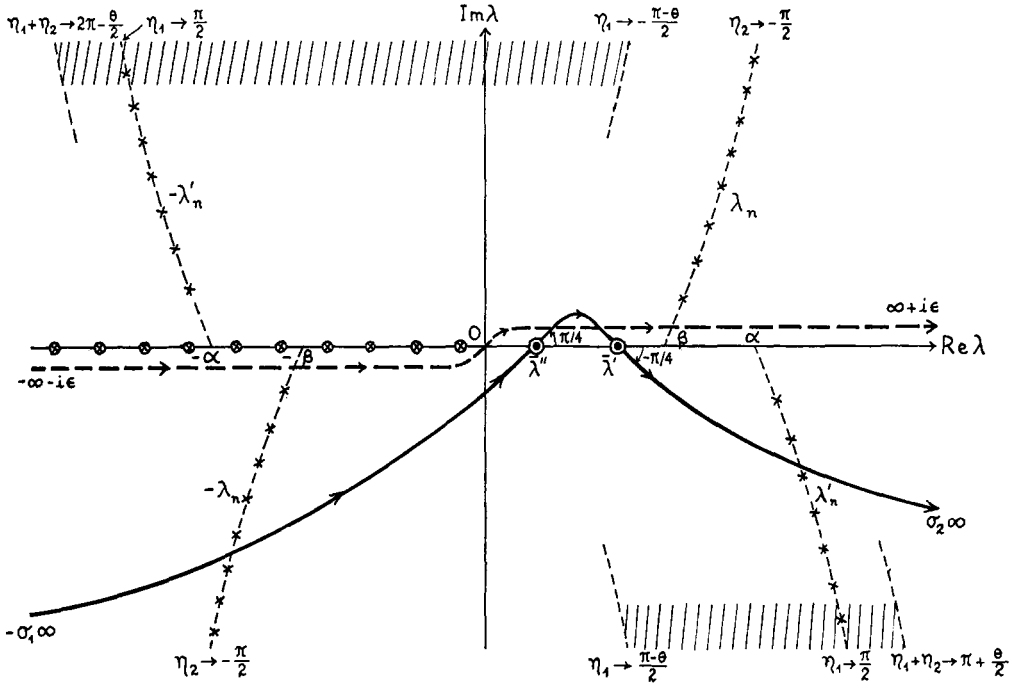

FIG. 8. Path of integration in (2.7) for $\theta_R < \theta < \theta_L$. ×—poles of ρU; ⊗—poles of $Q^{(2)}_{\lambda-\frac{1}{2}}$; ⊙—saddle points. The original path of integration, shown in broken line, must be deformed onto the path shown in solid line; this gives rise to residues at the poles $-\lambda_n$ and λ_n' (cf. Fig. 6).

(4.34), so that we find

$$\tilde{f}_{2,g}(\beta,\theta) = \tilde{f}'_{2,g}(\beta,\theta) + \tilde{f}''_{2,g}(\beta,\theta), \qquad (3.40)$$

where

$$\tilde{f}'_{2,g}(\beta,\theta) = i\left\{\left(\frac{\sin\theta_1}{\sin\theta}\right)^{\frac{1}{2}} \frac{(2N\cos\theta_1\cos\theta_2)^{\frac{3}{2}}}{(N\cos\theta_2 - 2\cos\theta_1)^{\frac{1}{2}}} \times \frac{(N\cos\theta_2 - \cos\theta_1)}{(N\cos\theta_2 + \cos\theta_1)^3} \times \exp\left[2i\beta(2N\cos\theta_2 - \cos\theta_1)\right] \times \left[1 - \frac{i\mathfrak{G}(\theta,\theta_1)}{64\beta\cos\theta_1}\right]\right\}_{\sin\theta_1=z'}, \qquad (3.41)$$

$$\tilde{f}''_{2,g}(\beta,\theta) = -\left\{\left(\frac{\sin\theta_1}{\sin\theta}\right)^{\frac{1}{2}} \frac{(2N\cos\theta_1\cos\theta_2)^{\frac{3}{2}}}{(2\cos\theta_1 - N\cos\theta_2)^{\frac{1}{2}}} \times \frac{(N\cos\theta_2 - \cos\theta_1)}{(N\cos\theta_2 + \cos\theta_1)^3} \times \exp\left[2i\beta(2N\cos\theta_2 - \cos\theta_1)\right] \times \left[1 - \frac{i\mathfrak{G}(\theta,\theta_1)}{64\beta\cos\theta_1}\right]\right\}_{\sin\theta_1=z''}, \qquad (3.42)$$

where $\mathfrak{G}(\theta,\theta_1)$ is still given by (3.16), and z', z'' are given by (A7).

In particular, near the rainbow angle, with

$$\theta = \theta_R + \epsilon, \qquad (3.43)$$

$$\gamma^2/M \ll \epsilon \ll \beta^{-\frac{1}{2}}, \qquad (3.44)$$

the saddle points are given by (A23), and we can also employ (A25)–(A26). Taking the slowly-varying factors outside the exponentials in (3.41)–(3.42) at the rainbow angle $\theta = \theta_R$, $\theta_1 = \theta_{1R}$, we then find

$$\tilde{f}_{2,g}(\beta,\theta_R+\epsilon) = -\frac{16}{27}e^{-i\pi/4}\frac{N^2}{(8+N^2)^{\frac{1}{2}}}\frac{c^{\frac{1}{2}}}{s^{\frac{3}{2}}} \times \exp\left[6ic\beta + is\beta\epsilon + \mathcal{O}(\beta\epsilon^2)\right] \times \sin\left[\frac{s\beta}{2}\left(\frac{4c}{3s}\epsilon\right)^{\frac{3}{2}} + \frac{\pi}{4}\right]\left(\frac{4c}{3s}\epsilon\right)^{-\frac{1}{4}} \times \left[1 + \mathcal{O}\left(\frac{1}{\beta\epsilon^{\frac{3}{2}}}\right)\right] \qquad (\gamma^2/M \ll \epsilon \ll \beta^{-\frac{1}{2}}), \qquad (3.45)$$

where c and s are defined by (2.35). This oscillatory behavior of the amplitude arises from interference between the two geometrical contributions (3.41) and (3.42), which have nearly equal amplitudes close to the rainbow angle.

To the same order of approximation employed in the derivation of (3.22), the residue series (3.38) differs from that result only by the omission of the terms in $\zeta^+_{2,0}$:

$$\tilde{f}_{2,\mathrm{res}}(\beta,\theta) \approx \frac{e^{i\pi/12}}{M^2}\left(\frac{\gamma}{\pi\sin\theta}\right)^{\frac{1}{2}} \times \exp(4iM\beta)\sum_{m=1}^{\infty}(-1)^m\sum_n (a'_n)^{-2} \times \{i[(\zeta^+_{2,m})^2 + M\zeta^+_{2,m}]\exp(i\lambda_n\zeta^+_{2,m}) - [(\zeta^-_{2,m})^2 + M\zeta^-_{2,m}]\exp(i\lambda_n\zeta^-_{2,m})\}. \quad (3.46)$$

This is just what we should get, since the surface wave excited at T''_2 [Fig. 7(a)] now has to describe an angle $2\pi - (\theta_L - \theta) = \zeta^+_{2,1} < 2\pi$ before emerging in the direction θ.

Similarly, the last term in (3.39) is equivalent to an additional contribution in $\tilde{\zeta}^-_{2,0}$ to (3.33), so that we get

$$f'_{2,\mathrm{res}}(\beta,\theta) \approx f'_{2,\mathrm{res}}(\beta,\theta) - i\frac{e^{i\pi/12}N^2}{4\pi M}\frac{\exp(2M\beta)}{(\pi\gamma'\sin\theta)^{\frac{1}{2}}}(\tilde{\zeta}^-_{2,0})^2 \times \sum_{n=1}^{n_0}(a'_n)^{-4}\exp(-i\lambda'_n\tilde{\zeta}^-_{2,0}), \quad (3.47)$$

where $f'_{2,\mathrm{res}}(\beta,\theta)$ is given by (3.33) and $\tilde{\zeta}^-_{2,0}$ by (3.34) with $m = 0$.

Let us now discuss the domain of validity of the above results. One restriction arises from the condition that the right saddle point $\bar{\lambda}'$, given by (A3) and (A7), must not lie too close to $\lambda = \beta$,

$$\beta - \bar{\lambda}' \gg \beta^{\frac{1}{3}}, \quad (3.48)$$

in order that the Debye asymptotic expansions be valid. One can verify that, in the neighborhood of $\theta = \theta_L$,

$$1 - \frac{\bar{\lambda}'}{\beta} = \mathcal{O}[(\theta_L - \theta)^2], \quad (3.49)$$

so that (3.48) leads to $\theta_L - \theta \gg \gamma$, the first condition in (3.35).

Further restrictions arise from the condition that the correction terms in $\mathcal{G}(\theta_1,\theta)$ in (3.41)–(3.42) be small. This condition is violated near the rainbow angle. According to (3.16), (3.41), and (3.42), the magnitude of the dominant correction terms near $\theta = \theta_R$ is

$$\frac{15\sin^2\theta_1}{256\beta\,|2\chi-1|^3\cos^3\theta_1} \sim \{\beta[M(\theta-\theta_R)]^2\}^{-1}, \quad (3.50)$$

where we have employed (A22)–(A26). The requirement that (3.50) be much smaller than unity leads to the second condition in (3.35).

Another condition for the validity of the above results is that the integral (3.37) be reducible to the sum of two independent saddle point contributions. This approximation certainly fails in the neighborhood of the rainbow angle, when the two saddle points tend toward each other. A precise estimate of the error is difficult and will be postponed to Sec. 4. However, a necessary condition for the validity of this approximation is that the range of each saddle point be much smaller than the separation between the two saddle points. It can be verified that this leads precisely to the same condition already found, namely, $M(\theta - \theta_R) \gg \gamma^2$. For an explanation of the concept "range of a saddle point," see Ref. 13.

Finally, the domain of validity of (3.45) is much more restrictive. In addition to the above condition on $\theta - \theta_R$, it is necessary that the neglected terms in the exponent in (3.45) be small. This leads to the condition (3.44), so that (3.45) can be employed only in a very narrow angular domain near the rainbow angle.

C. The 0-Ray Region

This is the region

$$\theta_R - \theta \gg \gamma^2/M. \quad (3.51)$$

In this region the saddle points become complex. Their trajectories are partially shown in Fig. 4. Their behavior near the rainbow angle is given by (A23)–(A26).

Since the saddle points are complex conjugate, one of them would give rise to an increasing exponential, while the other one corresponds to the exponential decrease expected in the shadow. Thus, the path of integration in (3.37) must be taken only over the latter saddle point. With the help of Appendix A, one can verify that it is the lower saddle point that gives rise to the exponentially decreasing contribution. In Appendix A, this point is associated with the root z' (cf. Fig. 4), so that the "geometrical-optic" contribution in this region is given by (3.41) alone. This may be interpreted as a "complex ray".[14] The residue-series contributions are the same as in the 2-ray region.

[13] N. G. de Bruijn, *Asymptotic Methods in Analysis* (North-Holland Publishing Co., Amsterdam, 1958), p. 91.

[14] J. B. Keller, in *Calculus of Variations and its Applications*, Proc. Symp. Appl. Math., L. M. Graves, Ed. (McGraw-Hill Book Co., New York, 1958), Vol. 8, p. 27.

In particular, if θ is given by (3.43) with $\epsilon < 0$ and

$$\gamma^2/M \ll |\epsilon| \ll \beta^{-\frac{1}{2}}, \tag{3.52}$$

we can employ (A23)–(A26) and we find, similarly to (3.45),

$$\tilde{f}_{2,g}(\beta, \theta_R + \epsilon) \approx -\frac{8}{27} e^{-i\pi/4} \frac{N^2}{(8+N^2)^{\frac{1}{2}}} \frac{c^{\frac{1}{2}}}{s^{\frac{3}{2}}} \times \exp[6ic\beta - is\beta|\epsilon| + \mathcal{O}(\beta\epsilon^2)] \times \exp\left[-\frac{s\beta}{2}\left(\frac{4c}{3s}|\epsilon|\right)^{\frac{3}{2}}\right] \left(\frac{4c}{3s}|\epsilon|\right)^{-\frac{1}{4}} \times \left\{1 + \mathcal{O}\left(\frac{1}{\beta|\epsilon|^{\frac{3}{2}}}\right)\right\} \quad (\epsilon < 0,\ \gamma^2/M \ll |\epsilon| \ll \beta^{-\frac{1}{2}}). \tag{3.53}$$

Near the rainbow angle, the amplitude is dominated by this "complex-ray" contribution, which describes the exponential damping away from the 2-ray/0-ray shadow boundary. However, since the damping exponent is proportional to β, whereas it is proportional to $\beta^{\frac{1}{2}}$ for the residue-series contributions, the latter will eventually dominate the amplitude in the deep shadow region. Thus, the amplitude is more rapidly damped near the rainbow angle than far away from it.

D. The 1-Ray/2-Ray Transition Region

This is the region

$$|\theta - \theta_L| \lesssim \gamma. \tag{3.54}$$

In this region, we can use all the results derived for the 2-ray region, except for the contribution (3.41) from the right saddle point z', because it would now violate condition (3.48). The evaluation of this contribution is entirely similar to that in I, Sec. 5D. In fact, (3.37) differs from I, Eq. (5.29), only by a factor

$$\rho = R_{11} \frac{H_\lambda^{(1)}(\alpha)}{H_\lambda^{(2)}(\alpha)} \approx -i \exp\left\{2i\left[(\alpha^2 - \lambda^2)^{\frac{1}{2}} - \lambda \cos^{-1}\frac{\lambda}{\alpha}\right]\right\}, \tag{3.55}$$

so that we find, corresponding to I, (5.54),

$$\tilde{f}'_{2,g}(\beta, \theta) \approx -\frac{e^{-i\pi/12}[1 + \mathcal{O}(\gamma)]}{\pi M(2\pi\beta \sin\theta)^{\frac{1}{2}}} \times \int \exp\left\{4i\left[(\alpha^2 - \lambda^2)^{\frac{1}{2}} - \lambda \cos^{-1}\frac{\lambda}{\alpha}\right] + i\lambda\theta\right\} \frac{d\zeta}{A^2(\zeta)}, \tag{3.56}$$

where the notation, as well as the path of integration, are the same as in I, (5.54).

Similarly to I, (5.55), we find from this

$$\tilde{f}'_{2,g}(\beta, \theta) = -\frac{2e^{-i\pi/4}}{M} \frac{\exp[4iM\beta + i\beta(\theta - \theta_L)]}{(2\pi\beta \sin\theta)^{\frac{1}{2}}} \times [1 + \mathcal{O}(\gamma)] f\left(\frac{\theta - \theta_L}{\gamma}\right) \quad (|\theta - \theta_L| \lesssim \gamma), \tag{3.57}$$

where $f(s)$ is Fock's function, defined in I, (5.57). This expression now substitutes (3.41), whereas the remaining results obtained for the 2-ray region remain valid.

Thus, the 1-ray/2-ray transition corresponds to a normal (Fock-type) transition region. In particular, similarly to I, (5.58), we find

$$\tilde{f}'_{2,g}(\beta, \theta) \approx \frac{e^{i\pi/3}}{M}\left(\frac{\gamma}{\pi \sin\theta}\right)^{\frac{1}{2}} \exp(4iM\beta) \times \sum_n (a'_n)^{-2}[1 + \mathcal{O}(\gamma)](\theta - \theta_L) \times \exp\left[i\left(\beta + e^{i\pi/3}\frac{x_n}{\gamma}\right)(\theta - \theta_L) + i\frac{\pi}{4}\right] \quad (\theta - \theta_L \gg \gamma). \tag{3.58}$$

Within the order of approximation to which this result is valid, i.e., $\theta - \theta_L \gg \gamma$ but still $\theta - \theta_L = \mathcal{O}(\gamma)$, (3.58) is equivalent to the residue series in $\zeta^+_{2,0}$ by which (3.22) differs from (3.46) [in fact, the term $(\zeta^+_{2,0})^2$ is then $\mathcal{O}(\gamma)$ as compared with $M\zeta^+_{2,0}$].

Thus, as usual, the Fock amplitude interpolates smoothly between the 1-ray and 2-ray regions, but the corresponding representation (3.57) cannot be employed too far beyond the transition region.

4. THEORY OF THE RAINBOW

The present section deals mainly with the 2-ray/0-ray transition region (Fig. 5), i.e., the domain

$$|\theta - \theta_R| \lesssim \gamma^2/M, \tag{4.1}$$

where θ_R is the rainbow angle, given by (2.36). This is the region where the rainbow occurs.

A. The Rainbow

The mathematical problem with which we are confronted in the rainbow region is the asymptotic evaluation of the integral (3.37) in a domain where its two saddle points are very close to each other (cf. Fig. 4). As mentioned in Sec. 1, the extension of the saddle point method to this situation has only recently been given by Chester, Friedman, and Ursell.[3,4] The main features of their method are summarized in Appendix B. The present treatment is a direct application of this method.

According to (2.43)–(2.45), we may rewrite (3.37) in the form

$$f_{2,g}^{r}(\beta, \theta) = 2e^{-i\pi/4}N\left(\frac{2\beta}{\pi \sin\theta}\right)^{\frac{1}{2}} F(\kappa, \theta), \tag{4.2}$$

where

$$F(\kappa, \theta) = \int_{-\bar{\sigma}_1\infty}^{\bar{\sigma}_2\infty} g(w_1) \exp\left[\kappa f(w_1, \theta)\right] dw_1, \tag{4.3}$$

with

$$\kappa = 2\beta, \tag{4.4}$$

$$f(w_1, \theta) = i\Big[2N\cos w_2 - \cos w_1 + \left(2w_2 - w_1 - \frac{\pi - \theta}{2}\right)\sin w_1\Big], \tag{4.5}$$

$$g(w_1) = (\sin w_1)^{\frac{1}{2}} \cos^2 w_1 \cos w_2 \times \frac{(\cos w_1 - N\cos w_2)}{(\cos w_1 + N\cos w_2)^3}\left[1 + \mathcal{O}(\beta^{-1})\right], \tag{4.6}$$

where $-\bar{\sigma}_1\infty$ and $\bar{\sigma}_2\infty$ are the images of $-\sigma_1\infty$ and $\sigma_2\infty$ in the w_1-plane, respectively [cf. (3.37)]. For the sake of simplicity, the corrections of order β^{-1} will not be evaluated; their evaluation by the method given in Appendix B is straightforward, but rather cumbersome.

The two saddle points are given by

$$\bar{w}_1 = \theta_1', \theta_1'', \quad \text{with} \quad z' = \sin\theta_1', z'' = \sin\theta_1'', \tag{4.7}$$

where z' and z'' are given by (A7). In the domain (4.1), we have

$$\theta = \theta_R + \epsilon, \quad |\epsilon| \ll 1, \tag{4.8}$$

so that the expansions (A19)–(A26) can be employed. For definiteness, let us assume, to begin with, that $\epsilon > 0$, so that the two saddle points are real.

The integral (4.3) is of the form discussed in Appendix B. Let us make the change of variables (B2),

$$f(w_1, \theta) = \tfrac{1}{3}\mu^3 - \zeta(\epsilon)\mu + A(\epsilon). \tag{4.9}$$

According to (B4), (4.5), and (A1), the parameters $\zeta(\epsilon)$ and $A(\epsilon)$ are given by

$$A(\epsilon) = i[N(\cos\theta_2' + \cos\theta_2'') - \tfrac{1}{2}(\cos\theta_1' + \cos\theta_1'')], \tag{4.10}$$

$$\tfrac{2}{3}[\zeta(\epsilon)]^{\frac{3}{2}} = i[N(\cos\theta_2' - \cos\theta_2'') - \tfrac{1}{2}(\cos\theta_1' - \cos\theta_1'')], \tag{4.11}$$

where θ_2', θ_2'' are the values of θ_2 corresponding to (4.7), and we have made the association [cf. (B3)]:

$$\theta_1' \to -\zeta^{\frac{1}{2}}(\epsilon), \quad \theta_1'' \to \zeta^{\frac{1}{2}}(\epsilon). \tag{4.12}$$

In particular, for $|\epsilon| \ll 1$, we can employ the approximations (A19)–(A27), with the following results:

$$A(\epsilon) = i\left[3c + \tfrac{1}{2}s\epsilon + \frac{c(11c^2 - 15)}{72s^2}\epsilon^2 + \mathcal{O}(\epsilon^3)\right], \tag{4.13}$$

$$\frac{2}{3}[\zeta(\epsilon)]^{\frac{3}{2}} = \frac{2}{3}i\frac{(c\epsilon)^{\frac{3}{2}}}{(3s)^{\frac{1}{2}}} \times \left[1 + \frac{(875c^6 - 1257c^4 + 657c^2 + 45)}{5760(cs)^3}\epsilon + \mathcal{O}(\epsilon^2)\right], \tag{4.14}$$

where s and c are defined by (2.35).

The main contribution to the integral (4.3) arises from the neighborhood of the saddle points, where, for small enough ϵ, (4.5) may be expanded in powers of

$$\omega = w_1 - \theta_{1R}, \tag{4.15}$$

with the following result:

$$f(w_1, \theta) = i\Big[3c + \frac{s}{2}\epsilon + \frac{c}{2}\epsilon\omega - \frac{s}{4}\epsilon\omega^2 - \left(\frac{s}{8} + \frac{c\epsilon}{12}\right)\omega^3 + \mathcal{O}(\omega^4)\Big]. \tag{4.16}$$

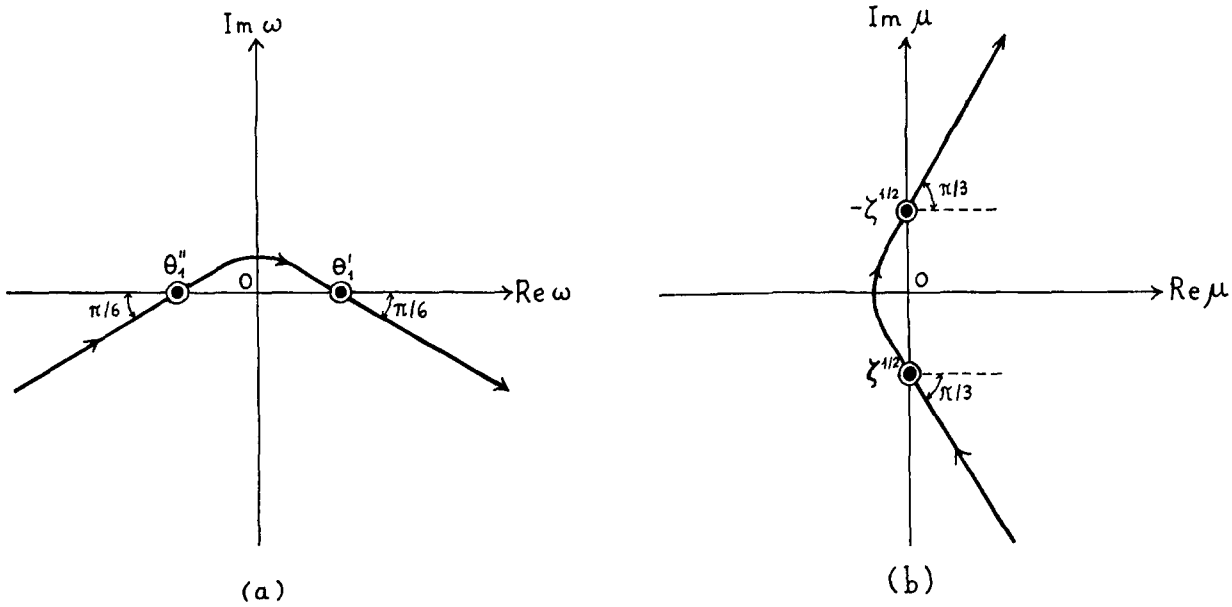

FIG. 9. The mapping of the ω plane onto the μ plane in the neighborhood of the origin.

For small enough ϵ, it also follows from (4.13)–(4.16) that, in the relevant portion of the path of integration, the transformation (4.9) is approximately given by

$$\mu^3/3 \approx -is\omega^3/8. \tag{4.17}$$

In solving (4.14) and (4.17) to determine $\zeta(\epsilon)$ and $\omega(\mu)$, care must be taken to choose the appropriate phase factors corresponding to the regular branch of the transformation. This branch is characterized by the condition that (4.12) holds on it (cf. Appendix B). The correct choice is

$$\omega \approx -2i\mu/(3s)^{\frac{1}{3}}, \tag{4.18}$$

$$\zeta(\epsilon) = e^{-i\pi}\frac{c\epsilon}{(3s)^{\frac{1}{3}}} \times \left[1 + \frac{(875c^6 - 1257c^4 + 657c^2 + 45)}{8640(sc)^3}\epsilon + \mathcal{O}(\epsilon^2)\right]. \tag{4.19}$$

In fact, if we set $\mu = -\zeta^{\frac{1}{2}}$ ($\mu = \zeta^{\frac{1}{2}}$) in (4.18), substituting ζ by (4.19), we find, respectively, $\omega = \delta'$ ($\omega = \delta''$), where δ' and δ'' are given by (A21), in agreement with (4.12).

According to (4.18), the mapping of the ω plane onto the μ plane in the relevant portion of the path of integration is as shown in Fig. 9. The path through the saddle points in Fig. 9(a) has been chosen in such a way that the transformed path in the μ-plane runs from $e^{-i\pi/3}\infty$ to $e^{i\pi/3}\infty$, as shown in Fig. 9(b).

Following (B5), we now expand

$$G(w_1, \epsilon) = g(w_1)\frac{dw_1}{d\mu} = \sum_m p_m(\epsilon)(\mu^2 - \zeta)^m + \sum_m q_m(\epsilon)\mu(\mu^2 - \zeta)^m, \tag{4.20}$$

where the coefficients $p_m(\epsilon)$, $q_m(\epsilon)$ are obtained by repeated differentiation of (4.20), setting $w_1 = \theta_1'$, $\mu = -\zeta^{\frac{1}{2}}$ and $w_1 = \theta_1''$, $\mu = \zeta^{\frac{1}{2}}$. Thus,

$$p_0(\epsilon) = \tfrac{1}{2}[G(\theta_1'', \epsilon) + G(\theta_1', \epsilon)], \tag{4.21}$$

$$q_0(\epsilon) = \tfrac{1}{2}\zeta^{-\frac{1}{2}}[G(\theta_1'', \epsilon) - G(\theta_1', \epsilon)], \tag{4.22}$$

$$p_1(\epsilon) = \tfrac{1}{4}\zeta^{-\frac{1}{2}}\left[\frac{dG}{d\mu}(\theta_1'', \epsilon) - \frac{dG}{d\mu}(\theta_1', \epsilon)\right], \tag{4.23}$$

$$q_1(\epsilon) = \tfrac{1}{4}\zeta^{-1}\left[\frac{dG}{d\mu}(\theta_1'', \epsilon) + \frac{dG}{d\mu}(\theta_1', \epsilon) - 2q_0(\epsilon)\right], \tag{4.24}$$

and so on. We shall compute explicitly only the coefficients p_0 and q_0.

Differentiating (4.5) twice with respect to μ and setting $\mu = -\zeta^{\frac{1}{2}}$, $w_1 = \theta_1'$, we get, taking into account (A1),

$$-2\zeta^{\frac{1}{2}} = i\frac{\cos\theta_1'}{N\cos\theta_2'}(2\cos\theta_1' - N\cos\theta_2')\left(\frac{dw_1}{d\mu}\right)^2_{\theta_1} \tag{4.25}$$

and, similarly for θ_1'', with $-\zeta^{\frac{1}{2}} \to \zeta^{\frac{1}{2}}$, $\theta_1' \to \theta_1''$. It follows that

$$\left(\frac{dw_1}{d\mu}\right)_{\theta_1'} = e^{-i\pi/4}\left[\frac{2N\cos\theta_2'}{\cos\theta_1'(N\cos\theta_2' - 2\cos\theta_1')}\right]^{\frac{1}{2}}\zeta^{\frac{1}{4}}, \tag{4.26}$$

$$\left(\frac{dw_1}{d\mu}\right)_{\theta_1''} = e^{-i\pi/4}\left[\frac{2N\cos\theta_2''}{\cos\theta_1''(2\cos\theta_1'' - N\cos\theta_2'')}\right]^{\frac{1}{2}}\zeta^{\frac{1}{4}}, \tag{4.27}$$

where the phase factors have been determined by the requirement that, for $|\epsilon| \ll 1$ [cf. (4.18)],

$$\left(\frac{dw_1}{d\mu}\right)_{\theta_1'} \approx \left(\frac{dw_1}{d\mu}\right)_{\theta_1''} \approx -\frac{2i}{(3s)^{\frac{1}{3}}}. \tag{4.28}$$

Employing the approximations (A23)–(A26) and (4.19) in (4.26)–(4.27), we find that (4.28) is indeed verified.

Substituting (4.26), (4.27), and (4.6) in (4.21)–(4.22), we find

$$\begin{Bmatrix} p_0 \\ q_0 \end{Bmatrix} = \frac{e^{-i\pi/4}}{4N}\zeta^{\pm\frac{1}{4}}\left[\left(\frac{\sin\theta_1''}{2\cos\theta_1'' - N\cos\theta_2''}\right)^{\frac{1}{2}}\right.$$
$$\times (2N\cos\theta_1''\cos\theta_2'')^{\frac{3}{2}}\frac{(\cos\theta_1'' - N\cos\theta_2'')}{(\cos\theta_1'' + N\cos\theta_2'')^3}$$
$$\pm\left(\frac{\sin\theta_1'}{N\cos\theta_2' - 2\cos\theta_1'}\right)^{\frac{1}{2}}(2N\cos\theta_1'\cos\theta_2')^{\frac{3}{2}}$$
$$\left.\times\frac{(\cos\theta_1' - N\cos\theta_2')}{(\cos\theta_1' + N\cos\theta_2')^3}\right][1 + \mathcal{O}(\beta^{-1})], \tag{4.29}$$

where upper and lower signs correspond to p_0 and q_0, respectively, ζ is given by (4.11) and θ_1', θ_1'' by (4.7).

In particular, for $|\epsilon| \ll 1$, we may employ (A23)–(A26) and (4.19), so that (4.29) becomes

$$p_0(\epsilon) = \frac{4i(3s)^{\frac{1}{6}}c}{27\sqrt{3}\,N}[1 + \mathcal{O}(\epsilon)], \tag{4.30}$$

$$q_0(\epsilon) = -\frac{(28 - 31s^2)}{27\sqrt{3}\,N(3s)^{\frac{7}{6}}}[1 + \mathcal{O}(\epsilon^{\frac{1}{2}})]. \tag{4.31}$$

If we now substitute (4.9) and (4.20) into (4.3), we find, by (B6),

$$F(\kappa, \theta) = 2\pi i\exp[\kappa A(\epsilon)]\left[\sum_m p_m(\epsilon)F_m(\zeta, \kappa, C_1)\right.$$
$$\left. + \sum_m q_m(\epsilon)G_m(\zeta, \kappa, C_1)\right], \tag{4.32}$$

where F_m and G_m are defined by (B7)–(B8) and the contour C_1 by (B9) (cf. Fig. 9).

Taking into account (B10) and (B12), we finally obtain

$$F(\kappa, \theta) = 2\pi i\kappa^{-\frac{1}{3}}\exp[\kappa A(\epsilon)]$$
$$\times\{[p_0(\epsilon) + \mathcal{O}(\kappa^{-1})]\,\mathrm{Ai}\,(\kappa^{\frac{2}{3}}\zeta)$$
$$- \kappa^{-\frac{1}{3}}[q_0(\epsilon) + \mathcal{O}(\kappa^{-1})]\,\mathrm{Ai}'\,(\kappa^{\frac{2}{3}}\zeta)\}, \tag{4.33}$$

where Ai (z) is the Airy function. Thus, taking into account (4.4), (4.2) finally becomes

$$\tilde{f}_{2,g}(\beta, \theta) = 4e^{i\pi/4}N\left(\frac{\pi}{\sin\theta}\right)^{\frac{1}{2}}(2\beta)^{\frac{1}{6}}\exp[2\beta A(\epsilon)]$$
$$\times\left\{p_0(\epsilon)\,\mathrm{Ai}\,[(2\beta)^{\frac{2}{3}}\zeta(\epsilon)]\right.$$
$$\left. - \frac{q_0(\epsilon)}{(2\beta)^{\frac{1}{3}}}\,\mathrm{Ai}'\,[(2\beta)^{\frac{2}{3}}\zeta(\epsilon)]\right\}[1 + \mathcal{O}(\beta^{-1})], \tag{4.34}$$

where $A(\epsilon)$, $\zeta(\epsilon)$ are given by (4.10)–(4.11), $p_0(\epsilon)$ and $q_0(\epsilon)$ by (4.29), and θ_1', θ_1'' by (4.7).

Higher-order terms in the Chester–Friedman–Ursell uniform asymptotic expansion of the scattering amplitude may be obtained, if required, by means of the procedure indicated in Appendix B. Here we shall restrict our consideration to the first two terms, given by (4.34).

In particular, for $|\epsilon| \ll 1$, we may employ (4.13), (4.19), (4.30), and (4.31), so that (4.34) becomes

$$\tilde{f}_{2,g}(\beta, \theta) = -\frac{16e^{-i\pi/4}}{27\sqrt{3}}\left(\frac{\pi}{\sin\theta}\right)^{\frac{1}{2}}c(6s\beta)^{\frac{1}{6}}$$
$$\times\exp[6ic\beta + is\beta\epsilon + i\mathcal{A}\beta\epsilon^2 + \mathcal{O}(\beta\epsilon^3)]$$
$$\times\left\{[1 + \mathcal{O}(\epsilon) + \mathcal{O}(\beta^{-1})]\right.$$
$$\times\,\mathrm{Ai}\left[-\frac{c(2\beta)^{\frac{2}{3}}\epsilon}{(3s)^{\frac{1}{3}}}(1 + \mathcal{B}\epsilon + \mathcal{O}(\epsilon^2))\right]$$
$$-\frac{i\mathcal{C}}{(2\beta)^{\frac{1}{3}}}[1 + \mathcal{O}(\epsilon^{\frac{1}{2}}) + \mathcal{O}(\beta^{-1})]$$
$$\left.\times\,\mathrm{Ai}'\left[-\frac{c(2\beta)^{\frac{2}{3}}\epsilon}{(3s)^{\frac{1}{3}}}(1 + \mathcal{B}\epsilon + \mathcal{O}(\epsilon^2))\right]\right\}, \tag{4.35}$$

where

$$\mathcal{A} = \frac{c(11c^2 - 15)}{36s^2}, \tag{4.36}$$

$$\mathcal{B} = \frac{875c^6 - 1257c^4 + 657c^2 + 45}{8640(sc)^3}, \tag{4.37}$$

$$\mathcal{C} = \frac{28 - 31s^2}{4c(3s)^{\frac{4}{3}}}. \tag{4.38}$$

The result (4.35) is a good approximation throughout the domain where the indicated error terms are small, i.e., for

$$|\epsilon| \ll \gamma. \tag{4.39}$$

This is true, in particular, within the rainbow region (4.1).

We can still employ (4.35) over part of the domain (3.44), in the 2-ray region, where the Airy functions may be replaced by their asymptotic expansions (B15)–(B16). With the help of (2.36), it is found that the result is equivalent to (3.45). The corresponding oscillations, arising from interference between the two geometrical ray contributions, give rise to the "supernumerary bows" sometimes seen on the inner side of the main rainbow.

For still larger scattering angles in the 2-ray region, we can no longer employ (4.35), but (4.34) remains valid. Again with the help of (B15)–(B16), taking into account (4.29), we find

$$\begin{aligned} \tilde{f}_{2,g}(\beta, \theta) = {} & \left(\frac{1}{\sin\theta}\right)^{\frac{1}{2}} \left(\frac{\sin\theta_1''}{2\cos\theta_1'' - N\cos\theta_2''}\right)^{\frac{1}{2}} \\ & \times (2N\cos\theta_1''\cos\theta_2'')^{\frac{1}{2}} \frac{(\cos\theta_1'' - N\cos\theta_2'')}{(\cos\theta_1'' + N\cos\theta_2'')^3} \\ & \times \exp\left[2\beta A(\epsilon) - \tfrac{4}{3}\beta\zeta^{\frac{3}{2}}(\epsilon)\right] \\ & - i\left(\frac{\sin\theta_1'}{N\cos\theta_2' - 2\cos\theta_1'}\right)^{\frac{1}{2}} \\ & \times (2N\cos\theta_1'\cos\theta_2')^{\frac{1}{2}} \frac{(\cos\theta_1' - N\cos\theta_2')}{(\cos\theta_1' + N\cos\theta_2')^3} \\ & \times \exp\left[2\beta A(\epsilon) + \tfrac{4}{3}\beta\zeta^{\frac{3}{2}}(\epsilon)\right]\Big)[1 + \mathcal{O}(\beta^{-1})]. \end{aligned} \tag{4.40}$$

In view of (4.10)–(4.11), this coincides exactly with the result (3.40)–(3.42) of the saddle-point method. Thus, the Chester–Friedman–Ursell method leads indeed to a uniform asymptotic expansion, matching smoothly the result obtained by the saddle-point method in the region where the latter is valid.

In the 0-ray region, within the domain (3.52), we may again employ (4.35), but now, since $\epsilon < 0$, we must employ the asymptotic expansions (B13)–(B14) for the Airy functions. The result is identical to (3.53), corresponding to the exponential damping on the shadow side of the rainbow (dark band between primary and secondary bows).

For still larger scattering angles in the 0-ray region, the Chester–Friedman–Ursell method would apparently have to be extended in order to match smoothly with the saddle-point method, since the coefficients (4.29) depend symmetrically on both saddle points, whereas, according to Sec. 3C, only the lower saddle point contributes to the steepest-descent result (cf. note A in Ref. 4, p. 126).

B. Comparison with Earlier Theories

An excellent review of the development of the theory of the rainbow has been given by Van de Hulst (Ref. 7, p. 240). A more detailed historical account may be found in Ref. 15.

Airy's theory[5] still remains the best approximation so far available, other than numerical summation of the partial-wave series. It is based on the application of Huygens' principle to the cubic wave front near the ray of minimum deviation. Van der Pol and Bremmer[16] applied Watson's transformation to the electromagnetic problem, but the expression thus obtained was finally reduced to Airy's approximation. The same is true for Rubinow's treatment[17] of the scalar problem. Bucerius[18] attempted to improve Airy's approximation by including terms up to the fifth order in a Taylor series expansion of the phase around the rainbow point [similar to (4.16)]. However, this does not lead to a uniform asymptotic expansion.

Airy's approximation may be obtained from (4.35) by retaining only the lowest-order term in all expansions, including those that appear in the argument of the exponential and Airy functions. This corresponds to setting

$$\mathcal{A} = \mathcal{B} = \mathcal{C} = 0. \tag{4.41}$$

Substituting also $\sin\theta$ by $\sin\theta_R$ and c and s by their values [cf. (2.35)–(2.36)], we find

$$\begin{aligned} \tilde{f}_{2,g}^{(\mathrm{Airy})}(\beta, \theta) = {} & -\frac{16}{27}\frac{3^{\frac{7}{2}}}{2^{\frac{1}{3}}} e^{-i\pi/4} \frac{N^2(N^2-1)^{\frac{1}{4}}}{(8+N^2)^{\frac{1}{2}}(4-N^2)^{\frac{2}{3}}} \beta^{\frac{1}{6}} \\ & \times \exp\left\{\frac{i\beta}{\sqrt{3}}\left[6(N^2-1)^{\frac{1}{2}} + (4-N^2)^{\frac{1}{2}}(\theta - \theta_R)\right]\right\} \\ & \times \mathrm{Ai}\left[-\frac{(N^2-1)^{\frac{1}{2}}}{(4-N^2)^{\frac{1}{3}}}\left(\frac{2\beta}{3}\right)^{\frac{2}{3}}(\theta - \theta_R)\right], \end{aligned} \tag{4.42}$$

which is Airy's approximation. The factor in front of

[15] C. B. Boyer, *The Rainbow* (Thomas Yoseloff, New York, 1959).
[16] B. van der Pol and H. Bremmer, Phil. Mag. **24**, 141, 825 (1937).
[17] S. I. Rubinow, Ann. Phys. (N.Y.) **14**, 305 (1961).
[18] H. Bucerius, Optik **1**, 188 (1946).

the Airy function agrees with that given in Ref. 17, Eq. (68), except for the sign. The argument of the Airy function is incorrectly given in Ref. 17, but the correct value appears in Ref. 7.

According to Van de Hulst (Ref. 7, pp. 246–249), Airy's approximation is a useful quantitative theory only for $\beta > 5000$ and $|\epsilon| < 0.5^\circ \sim 0.01r$; Huygens's principle may still be applied for $\beta > 2000$, but "a quantitative theory of the rainbow for the entire gap $30 < \beta < 2000$ is lacking."

As we have seen, the result of the present theory, contained in the uniform asymptotic expansion (4.34), is valid even for large deviations from the rainbow angle, matching smoothly with the results obtained within the domain of validity of the saddle-point method. While it remains to be seen whether it can be applied to values of β as low as 30, values a few times bigger should be accessible. Thus, a considerable portion of the gap appears to be bridged.

In order to estimate the accuracy of Airy's approximation, let us consider the domain (4.39), where (4.35) is valid. The main contributions to the total scattering amplitude in this domain arise from the direct-reflection term I, (4.35), and from the rainbow term (4.35), which is dominant, due to the enhancement factor $\beta^{\frac{1}{3}}$. A numerical computation of the coefficients, taking $N = 1.33$, yields

$$\begin{aligned} f(\beta, \theta_R + \epsilon) \approx & -0.0786 \\ & \times \exp(-1.86i\beta) - 0.438e^{-i\pi/4}(2\beta)^{\frac{1}{3}} \\ & \times \exp[i\beta(3.038 + 0.862\epsilon - 0.230\epsilon^2)] \\ & \times \{\mathrm{Ai}[-0.369(2\beta)^{\frac{2}{3}}\epsilon(1 + 0.202\epsilon)] \\ & - 0.688i(2\beta)^{-\frac{1}{3}} \\ & \times \mathrm{Ai}'[-0.369(2\beta)^{\frac{2}{3}}\epsilon(1 + 0.202\epsilon)]\} \\ & (N = 1.33). \quad (4.43) \end{aligned}$$

If only the rainbow term is taken into account, the minima and maxima of the intensity still occur at the zeros of the Airy function and its derivative, respectively. Their angular positions are shifted with respect to Airy's theory by amounts proportional to $\mathcal{B}\epsilon$ [cf. (4.35)]. The corrections to the intensity also involve the term $\mathcal{C}$ in (4.35), which is again of order ϵ. Both corrections can attain several percent within the domain (4.39).

For β of the order of a few hundred, the correction term involving the derivative of the Airy function becomes of the same order of magnitude as the direct reflection term, so that interference with the first term in (4.43) must be taken into account. The correction term $\mathcal{A}$ to the phase of the rainbow term (4.35) will then also play a role.

In conclusion, within the domain (4.39), the corrections to Airy's theory can attain several percent; their value increases with the deviation from the rainbow angle.

5. THEORY OF THE GLORY

A. Introduction

The last region that remains to be treated is the neighborhood of the backward direction,

$$\theta = \pi - \epsilon, \quad 0 \leq \epsilon \ll \beta^{-\frac{1}{3}}. \qquad (5.1)$$

This is the region where the glory is observed.

The glory is a strong enhancement in near-backward scattering by very small water droplets, with values of β ranging up to a few hundred. As a meteorological effect,[19a] it appears when an observer stands on a high point (mountain summit), looking at his own shadow prjoected on nearby thin clouds or mist (i.e., 180° away from the sun). Under favorable conditions, he sees the shadow of his head surrounded by a bright halo, sometimes accompanied by several colored rings. A color picture of the glory has recently been published.[19b] The glory is also frequently observed from airplanes (around the shadow of the plane). When several observers stand together, each one sees the glory only around the shadow of his own head, and not those of his companions, indicating that the effect is concentrated within a very small solid angle around 180°, corresponding to a narrow peak in the back-scattered intensity. [This remarkable effect was noticed already in the first recorded observations, made in 1735 by a Spanish captain, Antonio de Ulloa, from a mountain top in the Andes, in the course of a scientific expedition to Peru.[19]] The average value of β for which the observations have been made is of the order of 160, corresponding to water droplets with 0.028 mm average diameter (Ref. 7, p. 258).

A discussion of various attempts that have been made to explain the glory has been given by Van de Hulst (Refs. 6 and 7, p. 249). Although the first recorded observation was made more than two centuries ago, no satisfactory quantitative treatment has ever been given. The main facts that have to be explained may be classified as follows (cf. Ref. 7, p. 255):

(a) The anomalously large intensity near the backward direction for values of β ranging up to a few

[19] (a) J. M. Pernter and F. M. Exner, *Meteorologische Optik* (W. Braumüller, Vienna, 1910); (b) J. C. Brandt, Publ. Astron. Soc. Pacific **80**, 25 (1968).

hundred, as well as the fact that the phenomenon is no longer observed for larger water droplets (e.g., for $\beta \sim 10^3$).

(b) The angular distribution. With (5.1), if we denote by ϵ_j the angular radius of the jth dark ring (as it would be observed in yellow light), we have, roughly (Ref. 7, p. 257),

$$0.35 \leqslant \epsilon_1/\epsilon_2 \leqslant 0.45; \quad 1.6 \leqslant \epsilon_3/\epsilon_2 \leqslant 1.7. \quad (5.2)$$

The first dark ring is apparently rather hazy. We have

$$\epsilon_1 = \mathcal{O}(\beta^{-1}), \quad (5.3)$$

which is a measure of the narrowness of the backward peak.

The ratios (5.2) differ from those found in ordinary diffraction coronae, which correspond to the forward diffraction peak. The outer rings in the glory are also much more pronounced, i.e., the intensity decreases more slowly as we move away from the center. This disposes of an early theory according to which the glory would be a diffraction corona for light reflected from the clouds; it is undoubtedly contained in the back-scattered intensity from individual water droplets.

(c) The polarization: although few systematic data exist, there are indications that the glory is strongly polarized.

(d) Variability: the character of the rings (radius, brightness, etc.) frequently changes with time, even during a single observation.

Ultimately, the crucial test of a theory lies in how accurately it can reproduce the "exact" results, obtained by numerical summation of the partial-wave expansion. For the scalar problem, there do not seem to be many numerical results available. In the electromagnetic case, however, there exist several numerical calculations of the intensity at or near 180°. Most relevant to the present problem are those of Walter[20] and Bryant and Cox.[8]

The latter are particularly valuable, because the intensity at 180° was computed as a function of β, at intervals of 0.005, near $\beta = 200$ and $\beta = 500$. The results show a lot of fine structure that does not appear in other calculations. Specifically,

(e) Superimposed on a more slowly-varying background, the back-scattered intensity shows a rapidly-varying, quasiperiodic pattern. The period $\Delta\beta$ found for these fluctuations is given by

$$0.81 \leqslant \Delta\beta \leqslant 0.82. \quad (5.4)$$

[20] H. Walter, Optik **16**, 401 (1959)

(f) Within a single period, a few irregular peaks of varying heights and widths are found; the width ranges from $\sim$0.01 to $\sim$0.1 and the intensity can change by a factor of $\sim$100 (Ref. 8, Fig. 2), corresponding to enormous spikes.

Bryant and Cox also plotted on the same curve the intensity at 90° and the total cross section (Ref. 8, Fig. 2). They found that

(g) The total cross section also shows fluctuations with very similar character and the same period as the back-scattered intensity, but with greatly reduced magnitude, corresponding to changes of the order of one percent. At 90°, intermediate-size fluctuations are seen, but the period is *twice* that given by (5.4).

Except for the polarization, it is to be expected that most of the above features also appear in the scalar case. Thus, we shall investigate to what extent they are present here, although it must be stressed that an entirely adequate confrontation can only be made with the results obtained in the case of electromagnetic scattering.[11]

We shall see that, apart from the polarization effects, all the other features are indeed present and can be explained by the theory. However, for an explanation of the detailed structure of the intensity [(e) to (g)], higher-order terms in the Debye series have to be taken into account. Their effect is discussed in Sec. 6.

B. The Geometrical-Optic Contribution

The decomposition (3.10) made in the 2-ray region,

$$f_2(\beta, \theta) = f_{2,g}(\beta, \theta) + f_{2,\mathrm{res}}(\beta, \theta) + f'_{2,\mathrm{res}}(\beta, \theta), \quad (5.5)$$

is still valid in the domain (5.1), provided that we rewrite (3.11) in the form

$$f_{2,g}(\beta, \theta) = \frac{i}{\beta} \int_0^{\sigma_1 \infty} \rho U P_{\lambda-\frac{1}{2}}(-\cos\theta) e^{i\pi\lambda} \tan(\pi\lambda) \lambda \, d\lambda. \quad (5.6)$$

This result is obtained by taking the path of integration in (3.11) to be symmetric about the origin, then splitting it at the origin, making $\lambda \to -\lambda$ in the lower half and employing the identity

$$Q^{(2)}_{\lambda-\frac{1}{2}}(\cos\theta) - e^{2i\pi\lambda} Q^{(2)}_{-\lambda-\frac{1}{2}}(\cos\theta) = -e^{i\pi\lambda} \tan(\pi\lambda) P_{\lambda-\frac{1}{2}}(-\cos\theta), \quad (5.7)$$

which follows from N, Eq. (C6). The expressions (3.12), (3.13) for the residue-series contributions to (5.5) can be employed up to $\theta = \pi$, and so can (5.6).

Let us consider first the "geometrical-optic" term $f_{2,g}(\beta, \theta)$. Strictly speaking, this name is not entirely

appropriate, because geometrical optics would predict infinite intensity in the backward direction (which corresponds to a focal line). However, in view of the fact that in previous cases the saddle-point contributions were found to correspond to the geometrical-optic approximation, the same name will be applied here. As $\theta \to \pi$, the saddle point $\bar{\lambda}$ in (3.11) tends to the origin [cf. (3.2)]. This corresponds to the central ray, $\theta_1 = \theta_2 = 0$, which is transmitted through the sphere and then reflected backwards. Thus, we expect that the main contribution to (5.6) will arise from the neighborhood of $\lambda = 0$, or, more precisely, from the domain

$$|\lambda| \ll \beta^{\frac{1}{2}}, \tag{5.8}$$

which corresponds to the range of the saddle point.[13] [There is a misprint in the corresponding formula N, Eq. (9.48), which should read exactly like (5.8)].

We can therefore evaluate (5.6) by a method similar to that described in N, Sec. IX.C. We expand the integrand in powers of λ/β, keeping all correction terms up to $\mathcal{O}(\beta^{-1})$, and making use of the asymptotic expansion N, Eq. (C9) for $P_{\lambda-\frac{1}{2}}(-\cos\theta)$.

With the change of variable

$$\lambda = e^{i\pi/4}\left(\frac{N\beta}{2-N}\right)^{\frac{1}{2}} x = \zeta x, \tag{5.9}$$

the result is

$$\begin{aligned} f_{2,g}(\beta, \pi - \epsilon) &= \frac{4iN^2(N-1)}{(2-N)(N+1)^3} \exp\left[2i(2N-1)\beta\right] \\ &\times \left\{\left[1 - \frac{i(2-N)}{4N\beta}\right] G_{0,1} - \frac{i(N^2-4N+1)}{2N(2-N)\beta} G_{0,3} \right. \\ &+ \frac{i(N^3-2)}{12N(2-N)^2\beta} G_{0,5} + \sin^2\frac{\epsilon}{2} \\ &\times \left.\left(\frac{\zeta}{3}\sin\frac{\epsilon}{2} G_{3,2} - G_{2,1} + \frac{G_{1,0}}{4\zeta\sin\frac{\epsilon}{2}}\right) + \mathcal{O}(\beta^{-2})\right\}, \end{aligned} \tag{5.10}$$

where

$$\begin{aligned} G_{m,n}(\zeta, \epsilon) &= \int_0^\infty \exp(-x^2) \\ &\times J_m\left(2\zeta x \sin\frac{\epsilon}{2}\right) \tan(\pi\zeta x) x^n \, dx. \end{aligned} \tag{5.11}$$

Evaluating these integrals by the technique developed in N, Appendix F, we find the following final result:

$$\begin{aligned} f_{2,g}(\beta, \pi - \epsilon) &= -\frac{2N^2(N-1)}{(2-N)(N+1)^3} \\ &\times \exp\left[2i(2N-1)\beta\right] \exp\left[-\frac{iN\beta\epsilon^2}{4(2-N)}\right] \\ &\times \left\{1 + \frac{i(2N^3-10N^2+17N-8)}{2N(2-N)^2\beta} \right. \\ &- \left.\frac{(N^2+1)\epsilon^2}{8(2-N)^2} - \frac{iN(N^3-2)\beta\epsilon^4}{192(2-N)^4} + \mathcal{O}(\beta^{-2})\right\} \end{aligned}$$

$$(0 \leq \epsilon \ll \beta^{-\frac{1}{2}}). \tag{5.12}$$

It can be verified that (5.12) coincides with the expansion of (3.15)–(3.16) in powers of ϵ^2, within the domain under consideration. Thus, (3.15)–(3.16) are uniformly valid up to $\theta = \pi$.

No geometrical-optic rays other than the central one contribute to the second term of the Debye expansion in this region. As shown in Fig. 3(c), such rays can appear near the backward direction only for $N > \sqrt{2}$. (They are sometimes called "glory rays," but the corresponding effect should not be confused with the one under consideration.) Thus, the total scattering amplitude near the backward direction, in the geometrical-optic approximation, is given by

$$\begin{aligned} f_g(\beta, \pi - \epsilon) &= f_{0,g}(\beta, \pi - \epsilon) + f_{2,g}(\beta, \pi - \epsilon) \\ &+ f_{p>2,g}(\beta, \pi - \epsilon), \end{aligned} \tag{5.13}$$

where $f_{0,g}(\beta, \pi - \epsilon)$ is given by I, (4.52), $f_{2,g}(\beta, \pi - \epsilon)$ by (5.12), and $f_{p>2,g}(\beta, \pi - \epsilon)$ represents the total geometrical-optic contribution from higher-order terms in the Debye expansion. It corresponds essentially to the central-ray contributions after multiple internal reflections within the sphere, and may therefore be anticipated to be much smaller than the remaining two terms in (5.13). This is confirmed in Sec. 6B by explicit computation.

In particular, for $N = 1.33$, $\beta = 130$, which is close to the average value for which the glory is observed, the total contribution from the first two terms of (5.13) at $\theta = \pi$ is found to be

$$f_{0,g}(130, \pi) + f_{2,g}(130, \pi) \approx 0.101 + 0.176i \quad (N = 1.33). \tag{5.14}$$

The "exact" scattering amplitude corresponding to these values can be computed from its partial-wave expansion I, (2.1), with the help of partial-wave

tables[21] (the term $l = 0$ has to be separately added). The result is

$$f(130, \pi) \approx -0.0104 + 0.798i \quad (N = 1.33). \quad (5.15)$$

Comparing (5.14) with (5.15), we see that it not only has the wrong phase, but also accounts only for about 7% of the total intensity! As has already been mentioned (cf. Sec. 6B), higher-order geometrical-optic contributions are negligible. The angular distribution and β-dependence of (5.13) are also entirely different from those found in the glory.

We conclude that geometrical optics accounts only for a small fraction of the total intensity near the backward direction (in the relevant range of values of β) and is completely unable to explain the glory. The attempt by Ray[22] to explain the glory by means of diffraction of light rays reflected near the backward direction is thus seen to be incorrect. The same applies to a discussion by Bricard.[23]

C. Qualitative Discussion

Since the glory is not due to geometrical-optic contributions, it must arise from residue-series contributions. Thus, it must correspond to a case of strong "Regge-pole dominance" of the scattering amplitude. Heretofore, we have found such cases only in shadow regions (where the amplitude would vanish in the geometrical-optic approximation). This is the first example of such dominance in a lit region.

Physically, this implies that the glory is due to surface waves. This was first suggested by Van de Hulst (Refs. 6; 7, p. 373), who conjectured that diffracted rays taking two shortcuts across the sphere, i.e., of the type shown in Fig. 7, are responsible for the glory.

For $N = 1.33$, the total angle $\pi - \theta_L$ that must be described by the surface waves before emerging in the backward direction [cf. Fig. 7(a), (b)], is approximately 15°. The question then is whether the exponential damping of the surface waves along this arc would not prevent them from making an appreciable contribution. This quantitative problem was not treated by Van de Hulst.

There are two qualitative pieces of evidence that tend to support the general correctness of Van de Hulst's conjecture. One of them is Bryant and Cox's numerical study[8] of partial sums of the Mie series as a function of the number of partial waves retained. They found that, at $\theta = 180°$, by far the most important contribution to the sum arises from the edge domain I, (1.14), which, as we know, corresponds to nearly-grazing incident rays.

The other piece of evidence is experimental. It has been shown by Fahlen and Bryant[24] that the circumference of a water droplet, viewed at 180° with respect to the illuminating beam, appears like a thin luminous line. The explanation of this effect is that the surface of the droplet is a caustic of diffracted rays. Just as in the well-known phenomenon of the luminosity of a diffracting edge as seen from the shadow,[25] the eye (or the photographic plate) performs an inadmissible extrapolation. From the behavior at finite distances, it is inferred that the circumference of the droplet is an actual light source, whereas the true intensity there is, of course, finite. Thus, Fahlen and Bryant's observation provides direct experimental evidence for the existence of intense surface-wave contributions along the backward direction.

Both the above pieces of evidence strongly support the inference that surface waves are responsible for the dominant contribution to the glory. This is not necessarily equivalent to Van de Hulst's conjecture, which proposed a specific model for the surface-wave contributions, namely, diffracted rays of the type shown in Fig. 7. We shall see that, while these rays indeed give a significant contribution, surface-wave contributions from higher-order terms in the Debye expansion also play an important role.

The present treatment enables us to make a quantitative evaluation of the Van de Hulst-type surface-wave contribution. It corresponds to $f_{2,\mathrm{res}}(\beta, \pi - \epsilon)$ and is given by (3.18)–(3.21). Before performing a numerical evaluation, however, let us give a qualitative discussion of the behavior of the amplitude up to the third term in the Debye expansion. To this order, we have

$$f(\beta, \pi - \epsilon) \approx f_{0,g}(\beta, \pi - \epsilon) + f_{2,g}(\beta, \pi - \epsilon) + f_{2,\mathrm{res}}(\beta, \pi - \epsilon), \quad (5.16)$$

where the first two terms are the same as in (5.13) (the remaining contributions up to this order may be neglected).

For sufficiently large β and $\epsilon \gg \beta^{-1}$, the third term is approximately given by (3.22). In the domain under consideration, $\epsilon \lesssim \beta^{-\frac{1}{2}}$, the asymptotic expansion N,

[21] R. O. Gumprecht and C. M. Sliepcevich, *Tables of Light Scattering Functions for Spherical Particles* (University of Michigan Press, Ann Arbor, 1951).

[22] B. Ray, Proc. Ind. Assoc. Cultiv. Sci. **8**, 23 (1923); Nature **111**, 83 (1923).

[23] J. Bricard, in *Handbuch der Physik* (Springer-Verlag, Berlin, 1957), Bd. XLVIII, p. 351.

[24] T. S. Fahlen and H. C. Bryant, J. Opt. Soc. Am. **56**, 1635 (1966).

[25] A. Sommerfeld, *Optics* (Academic Press Inc., New York, 1954), p. 262.

(C11) for $P_{\lambda-\frac{1}{2}}(-\cos\theta)$, employed in the derivation of (3.22), is no longer valid and must be replaced by N, (C9). With this replacement and neglecting correction terms $\mathcal{O}(\beta^{-1})$ in I, (4.52) and (5.12), we find that (5.16) becomes

$$f(\beta, \pi-\epsilon) \approx -\frac{1}{2}\left(\frac{N-1}{N+1}\right) \times \exp(-2i\beta)\left[1+\frac{4N^2}{(2-N)(N+1)^2}\exp(4iN\beta)\right] + 2\frac{e^{i\pi/3}}{\gamma M^2}\exp(4iM\beta)(\pi-\theta_L)(\pi-\theta_L+M)J_0(\beta\epsilon) \times \sum_n (a_n')^{-2}\exp[i\lambda_n(\pi-\theta_L)] \quad (0 \leq \epsilon \ll \beta^{-1}). \tag{5.17}$$

In the residue series, we have neglected all terms beyond $m = 0$ [cf. (3.22)], which correspond to surface waves making more than one turn around the sphere, since such contributions are extremely small.

It must be emphasized that the expression for $f_{2,\mathrm{res}}(\beta, \pi-\epsilon)$ in (5.17), where only the lowest-order term in each asymptotic expansion has been kept, is certainly not a good approximation for $\beta \sim 10^2$. Many more terms would have to be included in the evaluation of the residues, as will be seen in Sec. 5D. However, our present purpose is to make a rough estimate of the order of magnitude of this term and of its qualitative behavior as a function of β and ϵ. For this purpose, the simple expression given in (5.17) is entirely adequate.

Taking $N = 1.33$ and employing the asymptotic expansions for the poles given in I, Appendix A, (5.17) becomes

$$\begin{aligned} f(\beta, \pi-\epsilon) &\approx -0.0708\exp(-2i\beta)[1+1.95\exp(5.32i\beta)] \\ &\quad + 1.69\exp\left(3.77i\beta + 0.243i\beta^{\frac{1}{3}} + i\frac{\pi}{3}\right) \\ &\quad \times J_0(\beta\epsilon)\beta^{\frac{1}{3}}\exp(-0.421\beta^{\frac{1}{3}}) \\ &\quad \times \{1+0.762\exp[(-0.315+0.182i)\beta^{\frac{1}{3}}] \\ &\quad + 0.657\exp[(-0.574+0.331i)\beta^{\frac{1}{3}}] + \cdots\}, \end{aligned} \tag{5.18}$$

where, within the curly brackets, we have taken into account only the contributions from the first three poles. Now let us compare the behavior of (5.18) as a function of β and ϵ with some of the features (a)–(g) of the glory, described in Sec. 5A.

(a) The ratio of the residue-series contribution to the geometrical-optic contribution to the amplitude is of the order of

$$|f_{2,\mathrm{res}}(\beta, \pi-\epsilon)/f_g(\beta, \pi-\epsilon)| \sim 15\beta^{\frac{1}{3}}\exp(-0.4\beta^{\frac{1}{3}}). \tag{5.19}$$

This is of order 10 for $\beta \sim 10^2$ and of order unity for $\beta \sim 10^3$.

Thus, in the domain where the glory is observed, the residue series is indeed the dominant term in the amplitude, and its order of magnitude is just right to account for the discrepancy between (5.14) and (5.15).

The physical factor that enhances the surface-wave contribution is their focusing along the axis, analogous to the Poisson spot: a whole cone of diffracted rays come together, rather than just two. This is responsible for the change from a factor $\beta^{-\frac{1}{6}}$ in (3.22) to a factor $\beta^{\frac{1}{3}}$ in (5.17); the amplification factor due to focusing is of order $\beta^{\frac{1}{2}}$ [cf. also N, (5.11)].

On the other hand, the damping coefficient in the attenuation factor of the surface waves also increases like $\beta^{\frac{1}{3}}$, so that, for large enough β (a few times 10^3), the geometrical-optic contribution becomes dominant. Together with the increasing smallness of the solid angle defined by (5.3), this explains why the glory is not observed for larger water droplets.

(b) Within the domain of values of β where the glory is observed, the angular distribution is determined by the dominant term in (5.18), namely,

$$i(\beta, \pi-\epsilon) \propto J_0^2(\beta\epsilon), \tag{5.20}$$

where i denotes the intensity.

The above angular distribution also follows directly from the fact that the dominant contribution to the glory arises from partial waves in the edge domain [cf. I, (1.14)]:

$$l_- \sim \beta - c\beta^{\frac{1}{3}} \ll l \ll l_+ \sim \beta + c\beta^{\frac{1}{3}}, \tag{5.21}$$

corresponding to nearly-grazing incident rays. In fact, for such values of l, N, (C9), yields

$$P_l[\cos(\pi-\epsilon)] \approx J_0(\beta\epsilon). \tag{5.22}$$

Similar considerations have been made by Van de Hulst (Refs. 6; 7, p. 253), who also observed that (5.20) would explain the slow intensity decrease at large angles, in contrast with ordinary diffraction coronae, for which

$$i(\theta) \propto J_1^2(\beta\theta)/(\beta\theta)^2. \tag{5.23}$$

In the former case, i decreases like $(\beta\epsilon)^{-1}$; in the latter, like $(\beta\theta)^{-3}$.

The ratios of dark-ring radii according to (5.20) are given by the ratios of zeros of $J_0(x)$:

$$\epsilon_1/\epsilon_2 \approx 0.44, \quad \epsilon_3/\epsilon_2 \approx 1.6. \tag{5.24}$$

These results are compatible with (5.2), and (5.3) is also verified, although the comparison is not too significant, because we are considering a scalar theory. For the same reason we cannot discuss feature (c).

(d) The observed variability of the glory pattern must be related to the variability of the average radius and the dispersion in the radii of water droplets in thin clouds or mist, and their evolution as a function of time. It is an indication that the back-scattered intensity is extremely sensitive to small variations in the parameter β. Thus, it is a consequence of feature (f), and it should be explained together with this feature.

In order to compare (5.18) with features (e)–(g), we have to consider its detailed behavior as a function of β, in the range $10^2 \leqslant \beta \leqslant 10^3$, and within a small interval of variation of β,

$$\beta = \beta_0 + \delta\beta, \quad |\delta\beta| \leqslant 1, \quad |\delta\beta|/\beta_0 \ll 1. \tag{5.25}$$

It follows that

$$\beta^{\frac{1}{3}} \approx \beta_0^{\frac{1}{3}} + \frac{1}{3}\frac{\delta\beta}{\beta_0^{\frac{2}{3}}} \tag{5.26}$$

may actually be replaced by $\beta_0^{\frac{1}{3}}$ in (5.18).

Thus, (5.18) may be rewritten as

$$f(\beta_0 + \delta\beta, \pi - \epsilon) \approx A[1 + B\exp(-0.45i\delta\beta) + C\exp(-5.77i\delta\beta)], \quad |B| \leqslant \tfrac{1}{2}, \quad |C| \leqslant \tfrac{1}{4} \quad (10^2 \leqslant \beta_0 \leqslant 10^3, |\delta\beta| \leqslant 1), \tag{5.27}$$

where A, B, and C are complex parameters depending on β_0, which remain approximately constant within the above interval $\delta\beta$. The first term within the square brackets arises from the dominant term $f_{2,\mathrm{res}}$ in (5.16), the second one from $f_{2,g}$ and the third one from $f_{0,g}$.

It is clear that (5.27) cannot explain features (e)–(g). Instead of a quasiperiodic pattern, with period given by (5.4), and rapid intensity variations, by factors of up to 100, (5.27) describes two much less prominent modulations, resulting from the interference between geometrical-optic and surface-wave contributions. The largest modulation corresponds to a much greater period ($\sim$14) and a much smaller intensity variation (by less than a factor of 4).

While (5.17) is only a rough approximation for $\beta \sim 10^2$, the more exact evaluation of the residue series that will now be undertaken cannot account for the discrepancy between (5.27) and features (e)–(g). Thus, these features must arise from the interference with surface-wave contributions to higher-order terms in the Debye expansion. It will be shown in Sec. 6D that this is indeed the correct explanation.

D. The Residue-Series Contribution

For a more accurate evaluation of the residue-series contribution $f_{2,\mathrm{res}}$, we start from the exact expressions (3.18)–(3.20). We have to compute the terms appearing in (3.21).

The partial derivatives $\dot{d}$, $\ddot{d}$, and $\dddot{d}$ in (3.21) can be computed with the help of I, (A25)–(A27), (for the terms involving $[1\ \beta]$) and I, (A23) (for the terms involving $[2\ \alpha]$). The Hankel functions and their derivatives can be computed by means of I, (A11)–(A20).

By taking the logarithmic derivative of (3.20) with respect to λ, we find

$$\frac{\dot{c}_m}{c_m} = \frac{1}{\lambda} + i(2m+1)\pi + \frac{\dot{H}_\lambda^{(1)}(\alpha)}{H_\lambda^{(1)}(\alpha)} - 3\frac{\dot{H}_\lambda^{(2)}(\alpha)}{H_\lambda^{(2)}(\alpha)} - 2\frac{\dot{H}_\lambda^{(1)}(\beta)}{H_\lambda^{(1)}(\beta)} + \frac{[1\dot{\ }\beta] - N[1\dot{\ }\alpha]}{[1\ \beta] - N[1\ \alpha]} + \frac{\dot{P}_{\lambda-\frac{1}{2}}(-\cos\theta)}{P_{\lambda-\frac{1}{2}}(-\cos\theta)}, \tag{5.28}$$

and, differentiating once more with respect to λ,

$$\frac{\ddot{c}_m}{c_m} = \left(\frac{\dot{c}_m}{c_m}\right)^2 - \frac{1}{\lambda^2} + \psi\{H_\lambda^{(1)}(\alpha)\} - 3\psi\{H_\lambda^{(2)}(\alpha)\} - 2\psi\{H_\lambda^{(1)}(\beta)\} + \psi\{[1\ \beta] - N[1\ \alpha]\} + \psi\{P_{\lambda-\frac{1}{2}}(-\cos\theta)\}, \tag{5.29}$$

where we have introduced the notation

$$\psi\{f(\lambda)\} = \frac{\dot{\dot{f}}}{f} - \left(\frac{\dot{f}}{f}\right)^2. \tag{5.30}$$

In order to evaluate (3.20) and (5.28)–(5.29), we again employ the expansions given in I, Appendix A for $H_\lambda^{(1)}(\beta)$, $[1\ \beta]$ and their derivatives, the expansion N, (A16) for $H_\lambda^{(1,2)}(\alpha)$ and their derivatives (thus, $[1\ \alpha]$ is given by I, (A23) with $i \to -i$) and the expansion N, (C11) for $P_{\lambda-\frac{1}{2}}(-\cos\theta)$.

The numerical evaluation of $f_{2,\mathrm{res}}(\beta, \theta)$ has been carried out at the point $\beta = 130$, $\theta = \pi$, for $N = 1.33$. The first neglected term in all asymptotic expansions employed was $\mathcal{O}(\beta^{-2})$, and contributions from the first five poles λ_n were taken into account. The result is given by

$$f_{2,\mathrm{res}}(130, \pi) \approx -0.165 + 0.483i \quad (N = 1.33). \tag{5.31}$$

Comparing this with (5.14), we see that $f_{2,\mathrm{res}}$ is indeed dominant over the geometrical-optic contribution. The order of magnitude of (5.31) (but not the numerical value!) also agrees with the estimates made with the help of (5.18).

Adding (5.31) to (5.14), we find

$$f_{0,g}(130, \pi) + f_{2,g}(130, \pi) + f_{2,\mathrm{res}}(130, \pi) \approx -0.064 + 0.659i \quad (N = 1.33). \tag{5.32}$$

Comparing this with the exact result (5.15), we see that $f_{2,\mathrm{res}}$ corrects the phase in the right direction and leads to a value for $|f|$ of about 85% of the exact value (70% for the intensity). The remainder of the discrepancy must be accounted for by contributions from higher-order terms in the Debye expansion. The discussion given in Sec. 6 leads us to expect that, for other values of β, higher-order terms in the Debye expansion may account for a larger fraction of the intensity, and the relatively good agreement between (5.32) and (5.15) may be somewhat fortuitous. This should be checked by extending the computation to other values of β.

In conclusion, we see that Van de Hulst-type surface waves indeed give rise to an important contribution to the glory, but we must still investigate the effect of higher-order terms.

6. HIGHER-ORDER TERMS

A. Introduction

So far we have discussed only the first three terms in the Debye expansion I, (3.21). With regard to the remaining terms, the following questions may be asked: (i) Can they be evaluated by similar procedures? (ii) Do they give a significant contribution? (iii) Do they give rise to any new physical effects?

The answer to (i) is clearly affirmative. The higher the order of a term in the Debye expansion, the larger will be the number of associated saddle points and the number of regions to be treated. However, the techniques for the evaluation of higher-order terms are essentially the same as those developed for the first three terms, with only slight extensions required.

For $N = 1.33$, as has already been mentioned (I, Sec. 3C), more than 98.5% of the total intensity is contained in the first three terms. For higher values of N, geometrical-optic contributions decrease less rapidly with the order, because the internal reflection coefficient increases. However, the amplitude of the direct-reflection term also increases and the transmitted contribution becomes relatively less important. Thus, the first three terms probably suffice for most applications.

In the neighborhood of some special directions, higher-order terms can give appreciable contributions. Thus, for $N = 1.33$, the secondary rainbow (around $\theta = 128.7°$), though much fainter than the primary one, still has noticeable intensity. It can be treated by exactly the same method as the primary rainbow (Sec. 4A). We have also found indications that higher-order residue-series contributions may be important in the glory (Sec. 5C). We shall see that they give rise to the rapid fluctuations in intensity mentioned in Sec. 5A, and that this effect occurs in all directions, although the amplitude of the fluctuations is largest near the backward direction.

We shall confine our attention almost entirely to the backward and forward directions. The results are not limited to the range $1 < N < \sqrt{2}$. However, the cases $N > 1$ and $N < 1$ still require separate treatments.

B. Higher-Order Geometrical-Optic Contributions to $f(\beta, 0)$ and $f(\beta, \pi)$

The $(p + 1)$th term of the Debye expansion is given by I, (3.23) and I, (3.26). With the help of the reflection properties (2.2), as well as the identity I, (2.12), these representations may be rewritten in different ways, depending on whether p is even or odd:

$$\begin{aligned} f_{2j}(\beta, \theta) &= (-1)^{j+1} \frac{i}{\beta} \sum_{m=0}^{\infty} (-1)^m \\ &\quad \times \int_{-\infty}^{\infty} U \rho^{2j-1} P_{\lambda-\frac{1}{2}}(\cos\theta) e^{2i(m+j)\pi\lambda} \lambda \, d\lambda \\ &= (-1)^{j+1} \frac{i}{2\beta} \int_{-\infty+i\epsilon}^{\infty+i\epsilon} U(e^{i\pi\lambda}\rho)^{2j-1} P_{\lambda-\frac{1}{2}}(\cos\theta) \frac{\lambda \, d\lambda}{\cos(\pi\lambda)} \\ &= (-1)^{j} \frac{i}{2\beta} \int_{-\infty-i\epsilon}^{\infty-i\epsilon} U(e^{i\pi\lambda}\rho)^{2j-1} P_{\lambda-\frac{1}{2}}(\cos\theta) \frac{\lambda \, d\lambda}{\cos(\pi\lambda)} ; \end{aligned} \tag{6.1}$$

$$\begin{aligned} f_{2j+1}(\beta, \theta) &= \frac{(-1)^{j+1}}{\beta} \sum_{m=0}^{\infty} (-1)^m \\ &\quad \times \int_{-\infty}^{\infty} U(e^{i\pi\lambda}\rho)^{2j} P_{\lambda-\frac{1}{2}}(-\cos\theta) e^{i(2m+1)\pi\lambda} \lambda \, d\lambda \\ &= \frac{(-1)^{j+1}}{2\beta} \int_{-\infty+i\epsilon}^{\infty+i\epsilon} U(e^{i\pi\lambda}\rho)^{2j} P_{\lambda-\frac{1}{2}}(-\cos\theta) \frac{\lambda \, d\lambda}{\cos(\pi\lambda)} \\ &= \frac{(-1)^{j}}{2\beta} \int_{-\infty-i\epsilon}^{\infty-i\epsilon} U(e^{i\pi\lambda}\rho)^{2j} P_{\lambda-\frac{1}{2}}(-\cos\theta) \frac{\lambda \, d\lambda}{\cos(\pi\lambda)} . \end{aligned} \tag{6.2}$$

By procedures similar to those employed in (2.4)–(2.12), these results can also be written in the form

$$f_{2j}(\beta, \theta) = f_{2j,0}(\beta, \theta) + f_{2j,r}(\beta, \theta), \tag{6.3}$$

$$f_{2j+1}(\beta, \theta) = f_{2j+1,0}(\beta, \theta) + f_{2j+1,r}(\beta, \theta), \tag{6.4}$$

where

$$f_{2j,r}(\beta, \theta) = \frac{(-1)^j}{2\beta} \int_{-\infty - i\epsilon}^{\infty - i\epsilon} U(e^{i\pi\lambda}\rho)^{2j-1} \times e^{-i\pi\lambda} P_{\lambda-\frac{1}{2}}(-\cos\theta) \frac{\lambda\, d\lambda}{\cos(\pi\lambda)}, \tag{6.5}$$

$$f_{2j+1,r}(\beta, \theta) = \frac{(-1)^{j+1} i}{2\beta} \int_{-\infty - i\epsilon}^{\infty - i\epsilon} U(e^{i\pi\lambda}\rho)^{2j} \times e^{i\pi\lambda} P_{\lambda-\frac{1}{2}}(\cos\theta) \frac{\lambda\, d\lambda}{\cos(\pi\lambda)}, \tag{6.6}$$

$$\begin{aligned} f_{2j,0}(\beta, \theta) &= (-1)^j \frac{i}{\beta} \int_{-\infty - i\epsilon}^{\infty + i\epsilon} U(e^{i\pi\lambda}\rho)^{2j-1} \times e^{-i\pi\lambda} Q^{(2)}_{\lambda-\frac{1}{2}}(\cos\theta)\, \lambda\, d\lambda \\ &= (-1)^{j+1} \frac{i}{\beta} \int_0^{\infty + i\epsilon} U(e^{i\pi\lambda}\rho)^{2j-1} \times P_{\lambda-\frac{1}{2}}(-\cos\theta) \tan(\pi\lambda)\, \lambda\, d\lambda, \end{aligned} \tag{6.7}$$

$$\begin{aligned} f_{2j+1,0}(\beta, \theta) &= (-1)^j \frac{i}{\beta} \int_{-\infty - i\epsilon}^{\infty + i\epsilon} U(e^{i\pi\lambda}\rho)^{2j} Q^{(2)}_{\lambda-\frac{1}{2}}(\cos\theta)\, \lambda\, d\lambda \\ &= (-1)^{j+1} \frac{i}{\beta} \int_0^{\infty + i\epsilon} U(e^{i\pi\lambda}\rho)^{2j} \times P_{\lambda-\frac{1}{2}}(\cos\theta) \tan(\pi\lambda)\, \lambda\, d\lambda. \end{aligned} \tag{6.8}$$

Note that (2.6)–(2.12) are particular cases of these results.

If we take $f_{2j,0}$ at $\theta = \pi$ and $f_{2j+1,0}$ at $\theta = 0$, the corresponding integrals (6.7), (6.8) have a saddle point at $\lambda = 0$. For $N < 2j$ and $N < 2j + 1$, respectively, the corresponding steepest-descent path makes an angle of $\pi/4$ with the positive λ-axis. The integrand differs from that of (2.12) only by powers of $e^{i\pi\lambda}\rho$, so that, according to Fig. 1 and I, Fig. 21, the path of integration can be deformed into the steepest-descent path.

Neglecting corrections of order β^{-1}, we can employ the approximations

$$\tan(\pi\lambda) \approx i, \tag{6.9}$$

$$U(\lambda, \beta) \approx \frac{4N}{(N+1)^2} \exp\left[2i(N-1)\beta - \frac{i\lambda^2}{N\beta}(N-1)\right], \tag{6.10}$$

$$e^{i\pi\lambda}\rho(\lambda, \beta) \approx -i \frac{(N-1)}{(N+1)} \exp\left(2iN\beta + \frac{i\lambda^2}{N\beta}\right), \tag{6.11}$$

valid near the saddle point.

The evaluation of the saddle-point contribution finally yields

$$f^{(c)}_{2j,0}(\beta, \pi) = -\frac{N^2}{N^2-1} \exp(-2i\beta) \times \frac{z^j}{\left(j - \frac{N}{2}\right)} [1 + \mathcal{O}(\beta^{-1})], \tag{6.12}$$

$$f^{(c)}_{2j+1,0}(\beta, 0) = \frac{N^2}{(N+1)^2} \exp[2i(N-1)\beta] \times \frac{z^j}{\left[j - \left(\frac{N-1}{2}\right)\right]} [1 + \mathcal{O}(\beta^{-1})], \tag{6.13}$$

where

$$z = \left(\frac{N-1}{N+1}\right)^2 \exp(4iN\beta). \tag{6.14}$$

Note that (5.12) and I, (5.48) are particular cases of these results.

The superscript (c) in (6.12) and (6.13) is to indicate that they represent contributions corresponding to the centrally incident ray in geometrical optics. The parameter z is identical to that which appears in the theory of the Fabry–Perot interferometer (Ref. 25, p. 47), representing the amplitude and phase change for double traversal of the sphere diameter. In general there may be other geometrical-optic contributions to the amplitude at $\theta = 0$ or π, arising from incident rays with nonzero impact parameters.

The total geometrical-optic contribution from central rays to the scattering amplitude at $\theta = \pi$ and $\theta = 0$ from higher-order terms in the Debye expansion is given by

$$\begin{aligned} f^{(c)}_{p>2,g}(\beta, \pi) &= \sum_{j=2}^{\infty} f^{(c)}_{2j,0}(\beta, \pi) \\ &= -\frac{N^2}{N^2-1} \exp(-2i\beta) \times \left[\varphi\left(z, \frac{N}{2}\right) - \frac{2z}{2-N}\right][1 + \mathcal{O}(\beta^{-1})], \end{aligned} \tag{6.15}$$

$$\begin{aligned} f^{(c)}_{p>2,g}(\beta, 0) &= \sum_{j=1}^{\infty} f^{(c)}_{2j+1,0}(\beta, 0) \\ &= \frac{N^2}{(N+1)^2} \exp[2i(N-1)\beta] \times \varphi\left(z, \frac{N-1}{2}\right)[1 + \mathcal{O}(\beta^{-1})], \end{aligned} \tag{6.16}$$

where

$$\varphi(z, \lambda) = \sum_{j=1}^{\infty} \frac{z^j}{(j - \lambda)} \quad (|z| < 1, \lambda \neq 1, 2, 3, \cdots). \tag{6.17}$$

This function is related to Lerch's transcendent[26]

$$\Phi(z, s, \alpha) = \sum_{n=0}^{\infty} \frac{z^n}{(n + \alpha)^s} \quad (|z| < 1, \alpha \neq 0, -1, -2, \cdots) \tag{6.18}$$

by

$$\varphi(z, \lambda) = \Phi(z, 1, -\lambda) + \lambda^{-1}. \tag{6.19}$$

For $N = 1.33$, we have $|z| \approx 0.02$, so that (6.15) is a very small correction. For instance,

$$f^{(c)}_{p>2,g}(130, \pi) \approx -0.0007 + 0.0001i, \tag{6.20}$$

is to be compared with (5.14). As mentioned in Sec. 5B, the correction is negligible.

C. Higher-Order Residue-Series Contributions to $f(\beta, \pi)$ for $N > 1$

The residue-series contribution at the poles λ_n to $f_p(\beta, \pi)$ is of the form

$$f_{p,\mathrm{res}}(\beta, \pi) = -\frac{2\pi i^r}{\beta} \sum_{m=0}^{\infty} (-1)^m \times \sum_n \text{residue } [\lambda U \rho^{p-1} e^{i(2m+s)\pi\lambda}]_{\lambda_n}, \tag{6.21}$$

where r and s are integers related to p, that have to be determined by detailed study of the deformation of the path of integration in (6.2), (6.5) near $\theta = \pi$. According to (3.12) and I, (5.7), we have

$$r = s = 1 \quad \text{for} \quad p = 1, \quad p = 2. \tag{6.22}$$

We shall evaluate only the dominant high-frequency contribution to (6.21). Thus, we restrict ourselves to the term $m = 0$ and we keep only the lowest-order term in each asymptotic expansion. The result, like (5.17), is certainly not a good approximation for $\beta \sim 10^2$, although it does yield the right order of magnitude. However, it is adequate for a qualitative discussion of the effects due to higher-order terms. For an accurate numerical computation, techniques similar to those employed in Sec. 5D would be required.

[26] W. Magnus, F. Oberhettinger, and R. P. Soni, *Formulas and Theorems for the Special Functions of Mathematical Physics* (Springer-Verlag, Berlin, 1966), 3rd ed., p. 32.

Substituting $U(\lambda, \beta)$ and $\rho(\lambda, \beta)$ by their explicit expressions, we find [cf. (3.18)–(3.20)]

$$f_{p,\mathrm{res}}(\beta, \pi) \approx (-1)^{p+1} i^r \frac{32}{\pi\beta^3} \sum_n r_{n,p}, \tag{6.23}$$

where

$$r_{n,p} = \text{residue} \left\{ \frac{c_p(\lambda, \beta)}{[d(\lambda, \beta)]^{p+1}} \right\}_{\lambda_n}, \tag{6.24}$$

$$c_p(\lambda, \beta) = \frac{\lambda e^{is\pi\lambda} [H^{(1)}_\lambda(\alpha)]^{p-1}}{[H^{(1)}_\lambda(\beta)]^2 [H^{(2)}_\lambda(\alpha)]^{p+1}} ([1\ \beta] - N[1\ \alpha])^{p-1}, \tag{6.25}$$

and $d(\lambda, \beta)$ is given by (3.19).

The evaluation of the dominant term in $r_{n,p}$ is carried out in Appendix C. Substituting the result, given by (C26), in (6.23), we get

$$f_{p,\mathrm{res}}(\beta, \pi) \approx i^{r+1} \frac{e^{i\pi/3}}{\gamma} \exp\left[ip\left(2M\beta - \frac{\pi}{2}\right)\right] L_p^{(-1)}\left(\frac{-2\zeta_p}{M}\right) \times \sum_n (a'_n)^{-2} \exp(i\lambda_n\zeta_p)[1 + \mathcal{O}(\gamma^2)], \tag{6.26}$$

where $L_p^{(-1)}$ is a generalized Laguerre polynomial, defined by (C24), and M and ζ_p are defined by (2.38) and (C19), respectively. The value of the integers in (6.21) and (C19) is determined by the requirement that ζ_p corresponds to an angle between 0 and 2π,

$$\zeta_p \equiv \pi - p\theta_t \,(\mathrm{mod}\, 2\pi), \quad 0 \leq \zeta_p < 2\pi. \tag{6.27}$$

In particular, for $p = 1$ and $p = 2$, it follows from (6.22) that (6.26) is in agreement with I, (5.20), and with the extension of (3.46) to $\theta = \pi$. Similarly to I, (5.24), and to (3.24), the above result can also be rewritten as follows [cf. (C24)]:

$$f_{p,\mathrm{res}}(\beta, \pi) \approx i^{r+1} e^{i\pi/4} (2\pi\beta)^{\frac{1}{2}} \exp\left[ip\left(2M\beta - \frac{\pi}{2}\right)\right] \times \sum_n D_n^2 D_{21} D_{12} \Big[(\tilde{R}_{11})^{p-1} \zeta_p + (p-1)(\tilde{R}_{11})^{p-2} D_{12} D_{21} \frac{\zeta_p^2}{2!} + \frac{(p-1)(p-2)}{2!} (\tilde{R}_{11})^{p-3} (D_{12}D_{21})^2 \frac{\zeta_p^3}{3!} + \cdots + (D_{12}D_{21})^p \frac{\zeta_p^p}{p!} \Big] \times \exp(i\lambda_n\zeta_p)[1 + \mathcal{O}(\gamma^2)], \tag{6.28}$$

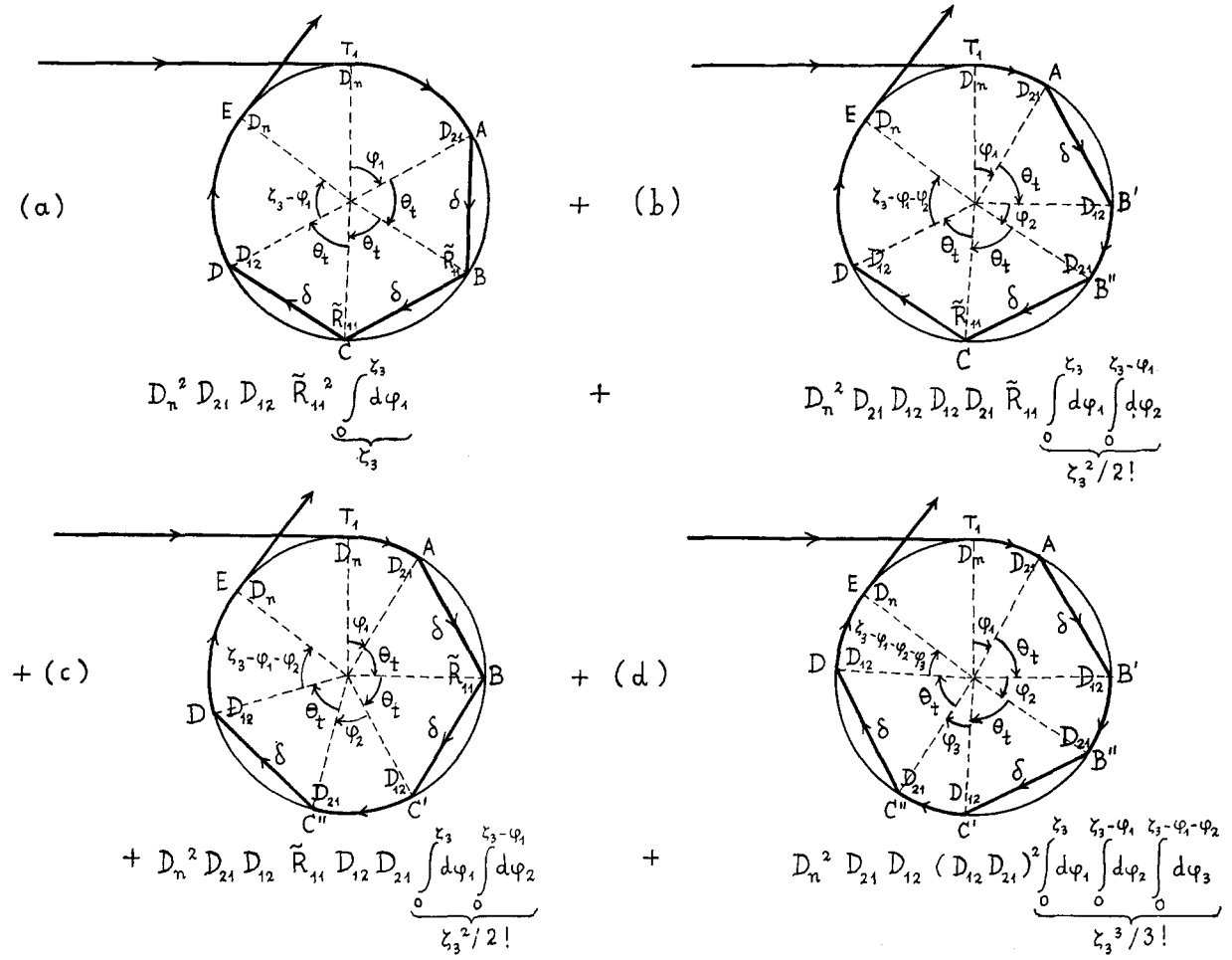

FIG. 10. Physical interpretation of (6.28) for $p = 3$. The four types of diagram that contribute in this case are shown, together with the contribution from each type. The diffraction, transmission, or reflection coefficients at each vertex are indicated. The total angle described along the surface is ζ_3. There is a phase factor exp $(3i\delta)$, where $\delta = 2M\beta$ is the optical phase difference associated with each "shortcut."

where D_n^2 is given by (3.25), $D_{21}D_{12}$ by (3.26) and $\tilde{R}_{11} = 1$, as in (3.27). An equivalent result for a cylinder was obtained by Chen [Ref. 9, Eq. (1.33)], by applying the geometrical theory of diffraction.

The physical interpretation of (6.28) is a generalization of that given in Fig. 7 for $p = 2$. The terms which arise for $p = 3$ are shown in Fig. 10. For simplicity, this figure is drawn for a scattering angle $\theta \neq \pi$. Referring to this figure as an illustration, we can describe the physical interpretation of each term in (6.28).

As has been emphasized in I, Sec. 3A, the Debye expansion corresponds to a description in terms of surface interactions, and its pth term represents the effect of $(p + 1)$ interactions at the surface. For a surface wave, one of them is its excitation at the point T_1 (with diffraction coefficient D_n) and final reconversion into a tangentially emerging ray at E (again with coefficient D_n). Another one is the initial critical refraction into the sphere at A (coefficient D_{21}) and final reemergence at D (factor D_{12}). These two interactions account for the common factor $D_n^2 D_{21} D_{12}$ in (6.28).

Once inside the sphere, there remain $(p - 1)$ interactions at the surface. Each of them can belong to either one of two types [cf. Figs. 7(c), 7(d)]: (I), internal reflection, with coefficient $\tilde{R}_{11}$; (II), critical refraction to the outside (coefficient D_{12}), followed by traveling along an arc as a surface wave, and by a new critical refraction into the sphere (coefficient D_{21}). These two types of elementary interactions are illustrated in Fig. 11. Each of them can be regarded as a "vertex," provided that the path V′V″ traveled along the surface for a type-II vertex is separately taken into account. The "coupling constant" associated with a type-I vertex is $\tilde{R}_{11}$, and for a type-II vertex it is $D_{12}D_{21}$. With this interpretation, the terms of (6.28) correspond to diagrams with $(p - 1)$ "internal"

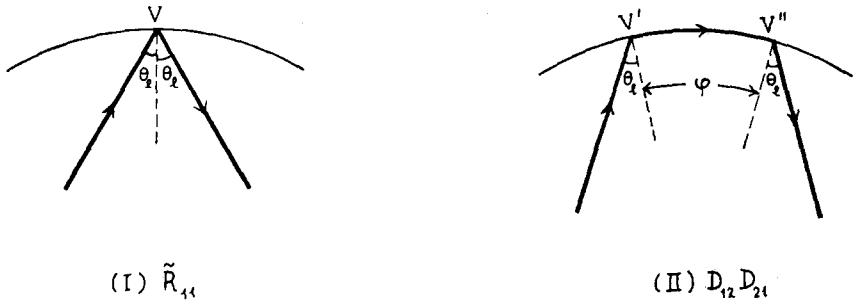

FIG. 11. The two possible types of elementary interactions of a diffracted ray at the surface ("vertices") and the corresponding "coupling constants."

vertices, besides the two "external" ones already described above. An equivalent way to classify them is that they are all associated with p shortcuts across the sphere.

The simplest diagram with $(p-1)$ internal vertices is one with $(p-1)$ type-I vertices [Fig. 10(a)]. Diagrams of this kind can have any value for the angle φ_1 between 0 and ζ_p, so that they contribute

$$(\tilde{R}_{11})^{p-1}\int_0^{\zeta_p} d\varphi_1 = (\tilde{R}_{11})^{p-1}\zeta_p,$$

which is the first term within square brackets in (6.28).

If we now substitute one type-I vertex in each diagram of the above class by a type-II vertex, there are $(p-1)$ different ways to do this [Figs. 10(b), (c)], so that we get a contribution [cf. (3.29)]

$$(p-1)(\tilde{R}_{11})^{p-2}D_{12}D_{21}\int_0^{\zeta_p} d\varphi_1\int_0^{\zeta_p-\varphi_1} d\varphi_2 = (p-1)(\tilde{R}_{11})^{p-2}D_{12}D_{21}\frac{\zeta_p^2}{2!},$$

which is the second term in (6.28).

Similarly, if we substitute two type-I vertices by type-II vertices, this can be done in $(p-1)(p-2)$ ways, but an interchange between the two type-II vertices leaves the result unchanged, so that this class of diagrams [Fig. 10(d)] contributes

$$\frac{(p-1)(p-2)}{2!}(\tilde{R}_{11})^{p-3}(D_{12}D_{21})^2 \times\int_0^{\zeta_p} d\varphi_1\int_0^{\zeta_p-\varphi_1} d\varphi_2\int_0^{\zeta_p-\varphi_1-\varphi_2} d\varphi_3,$$

which is the third term in (6.28)—and so on.

The "propagator" between two vertices is either $\exp(2iM\beta)$, the phase factor associated with a shortcut, or $\exp(i\lambda_n\phi_j)$, the damping factor for a surface wave along the angle ϕ_j. Since there are p shortcuts and the total angle described along the surface is ζ_p, this leads to the factor $\exp(2ipM\beta)\exp(i\lambda_n\zeta_p)$ in (6.28). The factors $\exp(-i\pi/2)$ represent the phase delay associated with passage through the focal points for diffracted rays at the poles.

It also follows from the above argument that, for an angle θ such that $\pi-\theta \gg \beta^{-\frac{1}{2}}$, the dominant terms of the residue-series contribution at high frequencies must be of the form

$$f_{p,\mathrm{res}}(\beta,\theta) = f^{+}_{p,\mathrm{res}}(\beta,\theta) + f^{-}_{p,\mathrm{res}}(\beta,\theta), \quad (6.29)$$

where

$$f^{\pm}_{p,\mathrm{res}}(\beta,\theta) = \frac{i^{n_\pm}}{(\sin\theta)^{\frac{1}{2}}}\exp(2ipM\beta) \times\sum_{m=0}^{\infty}(-1)^m\sum_n D_n^2 D_{21}D_{12}\Big[(\tilde{R}_{11})^{p-1}\zeta^{\pm}_{m,p} + (p-1)(\tilde{R}_{11})^{p-1}D_{12}D_{21}\frac{(\zeta^{\pm}_{m,p})^2}{2!} + \cdots + (D_{12}D_{21})^{p-1}\frac{(\zeta^{\pm}_{m,p})^p}{p!}\Big]\exp(i\lambda_n\zeta^{\pm}_{m,p}) \quad (\pi-\theta \gg \beta^{-\frac{1}{2}}), \quad (6.30)$$

where $n_\pm$ is an integer and

$$\zeta^{\pm}_{m,p} = \zeta^{\pm}_p + 2m\pi, \quad (6.31)$$

the angles $\zeta^{\pm}_p$ being the minimum angles described by surface waves excited at T_1 or T_2 (Fig. 7) before emerging in the direction θ. In (6.30), waves making any number of turns around the sphere have been added, but usually only $m=0$ needs to be taken into account. The difference between the factors appearing in (6.28) and (6.30) corresponds to the replacement [cf. N, (C8)]

$$P_{\lambda-\frac{1}{2}}(1) = 1 \to P_{\lambda-\frac{1}{2}}(-\cos\theta) \approx (2\pi\beta\sin\theta)^{-\frac{1}{2}} \times\left\{\exp\left[i\lambda(\pi-\theta)-i\frac{\pi}{4}\right] + \exp\left[-i\lambda(\pi-\theta)+i\frac{\pi}{4}\right]\right\}. \quad (6.32)$$

The extra factor $\beta^{\frac{1}{2}}$ in (6.28) is a measure of the focusing effect along the axis. Note that (3.24) is a particular case of (6.29).

D. Higher-Order Effects in the Glory

In order to discuss the effect of the higher-order contributions (6.26), the first question that must be answered is: How many such contributions need to be taken into account? The slow convergence of the Debye expansion for residue-series contributions, arising from the high internal reflection coefficient (3.27), is apparent from (6.28).

Let us investigate the asymptotic behavior of (6.26) for large p. The asymptotic behavior of $L_p^{(-1)}(-x)$ for large p and fixed x is given by[27]

$$L_p^{(-1)}(-x) = \sqrt{\frac{x}{p}}\, e^{-x/2}\Big\{I_1[2(px)^{\frac{1}{2}}] + \frac{x}{4p} I_3[2(px)^{\frac{1}{2}}] + \cdots\Big\}, \quad (6.33)$$

where $I_n(z)$ is the modified Bessel function of order n. In particular, if $\sqrt{px} \gg 1$, (6.33) becomes

$$L_p^{(-1)}(-x) = \frac{x^{\frac{1}{4}} e^{-x/2}}{2(\pi)^{\frac{1}{2}} p^{\frac{3}{4}}} \exp\,[2(px)^{\frac{1}{2}}]\left[1 + \mathcal{O}\left(\frac{1}{(px)^{\frac{1}{2}}}\right)\right] \quad [(px)^{\frac{1}{2}} \gg 1]. \quad (6.34)$$

Under these conditions, (6.26) becomes

$$f_{p,\mathrm{res}}(\beta, \pi) \approx \frac{i^{r+1} e^{i\pi/3}}{2(\pi)^{\frac{1}{2}}\gamma}\left(\frac{2\zeta_p}{M}\right)^{\frac{1}{4}} p^{-\frac{3}{4}} \times \exp\left[2^{\frac{3}{2}}\left(\frac{p\zeta_p}{M}\right)^{\frac{1}{2}} + ip\left(2M\beta - \frac{\pi}{2}\right)\right] \times \sum_n (a_n')^{-2} \exp\left[i\left(\lambda_n + \frac{i}{M}\right)\zeta_p\right] \times [1 + \mathcal{O}(\gamma^2)] \quad [(p\zeta_p/M)^{\frac{1}{2}} \gg 1]. \quad (6.35)$$

It would appear from this result that $|f_{p,\mathrm{res}}|$ is unbounded as $p \to \infty$. However, it must be remembered that (6.26) is the dominant term in an asymptotic expansion for *fixed* p and sufficiently large β, whereas we are now interested in the asymptotic behavior for *fixed* β and increasingly large p. Since the number of correction terms [indicated in (6.26) as $\mathcal{O}(\gamma^2)$] also increases with p, (6.26) eventually no longer represents the dominant term for sufficiently large p: It is modified by the accumulated effect of a large number of correction terms (e.g., γ^{-2} terms, each of order γ^2).

We shall now give a heuristic argument to show that the resultant effect due to correction terms must be to bring about an exponential damping factor for large p. To see this, let us go back to the discussion of the rate of convergence of the Debye expansion in I, Sec. 3A. In terms of the partial-wave series, the Debye expansion I, (3.21) can be rewritten as follows:

$$f(\beta, \pi) - f_0(\beta, \pi) = -\frac{i}{\beta}\sum_{l=0}^{\infty}(-1)^l(l + \tfrac{1}{2})U_l\sum_{p=1}^{\infty}(\rho_l)^{p-1}, \quad (6.36)$$

where

$$U_l(\beta) = U(l + \tfrac{1}{2}, \beta), \quad \rho_l(\beta) = \rho(l + \tfrac{1}{2}, \beta). \quad (6.37)$$

According to the discussion given in Sec. 5C, the residue-series contributions are associated with partial waves in the edge domain [cf. I, (1.14)], so that, at least in order of magnitude, we can identify

$$f_{p,\mathrm{res}}(\beta, \pi) \sim -\frac{i}{\beta}\sum_{l=l_-}^{l_+}(-1)^l(l + \tfrac{1}{2})U_l(\rho_l)^{p-1}, \quad (6.38)$$

where l_- and l_+ are given by (5.21). Thus, the rate of convergence of the Debye expansion for the residue-series contributions is determined by the magnitude of the spherical reflection coefficient $|\rho_l|$ in the edge domain (5.21).

It follows from I, (3.15) and I, (3.8)–(3.11), that

$$|\rho_l|^2 = 1 - \frac{16}{\pi^2\beta^2} \times |H_{l+\frac{1}{2}}^{(1)}(\beta)H_{l+\frac{1}{2}}^{(2)}(\alpha)([1\,\beta] - N[2\,\alpha])|^{-2}. \quad (6.39)$$

Substituting the Hankel functions and their logarithmic derivatives by the corresponding asymptotic expansions in the edge domain (I, Appendix A), we finally get [cf. I, (4.58)]

$$|\rho_l|^2 \approx 1 - \frac{\gamma}{M}|\mathrm{Ai}\,(-z_l)|^{-2} = 1 - 2\epsilon_l \quad (l_- \lesssim l \lesssim l_+), \quad (6.40)$$

where

$$z_l = e^{-i\pi/3}\gamma(l + \tfrac{1}{2} - \beta), \quad (6.41)$$

so that $|z_l| = \mathcal{O}(1)$ in the edge domain.

On the other hand, it follows from I, (3.24), I, (3.5)–(3.8), and I, Appendix A, that

$$|U_l(\beta)| = |T_{21}T_{12}| \approx \frac{\gamma}{\pi M}|\mathrm{Ai}\,(-z_l)|^{-2} \quad (l_- \lesssim l \lesssim l_+). \quad (6.42)$$

[27] *The Bateman Manuscript Project: Higher Transcendental Functions, Vol. II*, A. Erdélyi, W. Magnus, F. Oberhettinger, and F. G. Tricomi, Eds. (McGraw-Hill Book Co., Inc., New York, 1953), p. 199.

Substituting these results in the remainder after P terms of (6.38), we find

$$\left|\sum_{p=P+1}^{\infty} f_{p,\mathrm{res}}(\beta,\pi)\right| \leqslant \frac{\gamma}{\pi M}\sum_{l=l_-}^{l_+}|\mathrm{Ai}\,(-z_l)|^{-2}\frac{|\rho_l|^P}{|1-\rho_l|}$$

$$\approx \frac{2}{\pi}\sum_{l=l_-}^{l_+}|\rho_l|^P \approx 2c\beta^{\frac{1}{3}}\bar{\rho}^P, \quad (6.43)$$

where

$$\bar{\rho} = 1-\epsilon, \quad \epsilon \sim \gamma, \quad (6.44)$$

is an average value of ρ_l in the edge domain, and c is defined by (5.21).

Finally, (6.43) becomes, for large enough P,

$$\left|\sum_{p=P+1}^{\infty} f_{p,\mathrm{res}}(\beta,\pi)\right| \leqslant 2c\beta^{\frac{1}{3}}(1-\epsilon)^P \sim 2c\beta^{\frac{1}{3}}e^{-\epsilon P}$$

$$\sim 2c\beta^{\frac{1}{3}}e^{-\gamma P}. \quad (6.45)$$

Comparing this with (5.18), we see that the remainder after P terms of the Debye expansion for the residue-series contributions is negligible, as compared with the second term $f_{2,\mathrm{res}}(\beta,\pi)$, if

$$P \sim \beta^{\frac{2}{3}}. \quad (6.46)$$

This gives the maximum number of terms that would have to be kept in the Debye expansion.

Actually, (6.46) is probably an overestimate. We can interpret (6.43) as implying that, due to the correction factors indicated in (6.26), the internal reflection coefficient for diffracted rays is brought down from its "geometrical-optic" value $\tilde{R}_{11} = 1$ to

$$\tilde{R}_{11} \sim \bar{\rho} = 1-\epsilon. \quad (6.47)$$

From (6.28), this is seen to imply that, in (6.26), we should make the replacement

$$L_p^{(-1)}\left(-\frac{2\zeta_p}{M}\right) \to \bar{\rho}^P L_p^{(-1)}\left(-\frac{2\zeta_p}{M\bar{\rho}}\right). \quad (6.48)$$

According to (6.45), the damping factor $\bar{\rho}^p$ becomes effective for $p \gtrsim \gamma^{-1}$, leading to the estimate

$$\beta^{\frac{1}{3}} \leqslant P \leqslant \beta^{\frac{2}{3}}. \quad (6.49)$$

Since the number of terms in (6.38) is $\sim\beta^{\frac{1}{3}}$, it might seem more expedient, in practice, to evaluate the residue-series contribution directly, by numerical summation of the edge-domain terms in the partial-wave expansion. This is related to a proposal made by Ljunggrén.[28] However, the objections to this procedure would be: (i) the identification (6.38) should be regarded merely as an order-of-magnitude estimate; (ii) it is difficult to determine the precise values of l_- and l_+ in (6.38), and the value of the sum undergoes considerable fluctuations as extra terms are added (cf. Ref. 8, Fig. 3); (iii) the physical interpretation in terms of surface waves enables us to understand the qualitative behavior of the results, as will now be seen.

In order to determine the resultant effect of higher-order surface-wave contributions, we have to sum the contributions (6.26) for all values of p, up to a maximum value P verifying (6.49). One of the main difficulties in this summation is the dependence of ζ_p on p, corresponding to the different position of the shadow boundary for each term of the Debye expansion.

We want to discuss the qualitative behavior of the resultant surface-wave contribution. For this purpose, an accurate evaluation is not required. We shall carry out the summation by making several simplifying assumptions:

(A) Only the contribution from the first pole λ_1 is taken into account.

This is certainly adequate for an order-of-magnitude evaluation. According to (6.26), the total residue-series contribution to the backward scattering amplitude is then given by

$$f_{\mathrm{res}}(\beta,\pi) \approx -\frac{e^{i\pi/3}}{a_1'^2\gamma}\Psi(N,\beta), \quad (6.50)$$

where

$$\Psi(N,\beta) = \sum_p \exp\left[ip\left(2M\beta-\frac{\pi}{2}\right)+i\lambda_1\zeta_p\right]$$

$$\times L_p^{(-1)}\left(-\frac{2\zeta_p}{M}\right). \quad (6.51)$$

The next problem is: Over what values of p does the sum range? In principle, we have to sum over all p, up to P. However, we can clearly restrict ourselves to the diffracted rays that emerge closest to the backward direction, because other contributions contain an extra damping factor of at least $\exp(i\lambda_n\theta_t)$, corresponding to an additional shortcut (cf. Fig. 10). Thus, in (6.27), we impose the extra condition

$$0 \leq \zeta_p < \theta_t. \quad (6.52)$$

[28] T. Ljunggrén, Arkiv Fysik 1, 1 (1949).

TABLE I. Values of ζ_p for the lowest values of p.

$N = 1.33, \quad \theta_t = 1.43978$

p	2	6	10	15	19	24	28
ζ_p	0.26204	0.78612	1.31021	0.39452	0.91860	0.00029	0.52699

$N = 1.40, \quad \theta_t = 1.55039$

p	2	6	10	14	18	22	26
ζ_p	0.040819	0.12246	0.20410	0.28574	0.36738	0.44901	0.53065

The values of ζ_p satisfying the conditions (6.27), (6.52) for the lowest values of p are listed in Table I for $N = 1.33$ and for $N = 1.40$. The latter value is close to the critical refractive index $N = \sqrt{2}$, for which the diffracted rays are "at resonance." In fact, for $N = \sqrt{2}$, as shown in Fig. 12, a diffracted ray comes back to the starting point after each four additional shortcuts taken through the sphere. Moreover, in this limiting case, there are diffracted rays emerging exactly in the backward direction, i.e., with $\zeta_p = 0$, for

$$p = 4n + 2 \quad (n = 0, 1, 2, \cdots). \tag{6.53}$$

For $N = 1.40$, the angle ζ_2 corresponds to only 2.3°, as compared with 15° for $N = 1.33$. For $N = \sqrt{2}$, there are additional complications, as we see from Figs. 3(b), 3(c), for $p = 2$, because this is the borderline between having one ray or three rays near the backward direction; thus, a special treatment would be required.

There is another resonance, corresponding to a period of five shortcuts (inscribed regular pentagon instead of square), for

$$N = [\cos(\pi/5)]^{-1} \approx 1.236. \tag{6.54}$$

The value $N = 1.33$ is about halfway between this value and $N = \sqrt{2}$ (but still closer to $\sqrt{2}$), so that the corresponding values of p given by Table I:

$$p = 2, 6, 10, 15, 19, 24, 28, \cdots \quad (N = 1.33) \tag{6.55}$$

show a mixture of periodicities 4 and 5, with predominance of the period 4.

On the other hand, for $N = 1.40$, the values of p are of the form (6.53) up to $p = 74$. According to (6.49), larger values of p would not give any appreciable contribution within the range of values of β for which the glory is observed. Thus, we can make a further simplifying assumption:

(B) The summation in (6.51) is restricted to the values of p given by (6.53).

This is certainly a much better approximation for $N = 1.40$ than for $N = 1.33$, and it becomes better the closer N is to $\sqrt{2}$. The effect of deviations from assumption (B), like those found in (6.55), will be discussed later.

For $N = 1.40$, it follows from (6.30) and Table I that

$$\zeta_{4n+2} = (2n + 1)\zeta_2, \tag{6.56}$$

up to the same value of p for which (B) holds. Thus, it is consistent with (B) to assume also that

(C) The angles ζ_{4n+2} are given by (6.56) for all n.

For large enough n, (6.56) will violate condition (6.52). In particular, the damping factor $\exp(i\lambda_1\zeta_p)$ in (6.51), which would be bounded by $|\exp(i\lambda_1\theta_t)|$, will decrease exponentially as $n \to \infty$, according to (6.56). However, for large values of n, where the exponential decrease becomes significant, there would be such a decrease anyway, arising from the multiple internal reflection factor $\bar{\rho}^p$ [cf. (6.45)]. Thus, for N sufficiently close to $\sqrt{2}$, (C) is a reasonable assumption.

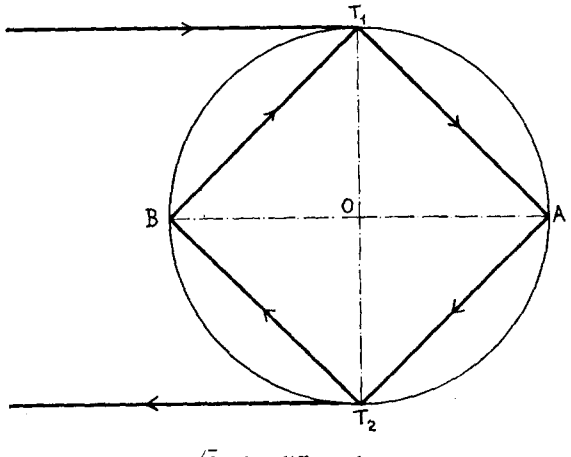

FIG. 12. For $N = \sqrt{2}$, the diffracted rays are at resonance: they come back to the starting point after four shortcuts, forming a square.

The last simplifying assumption we shall make is

(D) The angle ζ_p may be replaced by an average value $\bar{\zeta}$ in the argument of the Laguerre polynomial in (6.51):

$$L_p^{(-1)}(-2\zeta_p/M) \to L_p^{(-1)}(-x), \tag{6.57}$$

where

$$x = 2\bar{\zeta}/M \quad (0 \leq \bar{\zeta} < \theta_t). \tag{6.58}$$

Since the Laguerre polynomial is a slowly varying function of ζ_p as compared with $\exp(i\lambda_1\zeta_p)$ [cf. (6.34)], assumption (D) is also reasonable for an order-of-magnitude evaluation.

The effect of the simplifying assumptions (A) to (D) is to replace (6.51) by

$$\Psi(N, \beta) \approx \Psi(x, \delta) = \sum_{n=0}^{\infty} e^{i(4n+2)\delta} L_{4n+2}^{(-1)}(-x), \tag{6.59}$$

where δ is a complex number given by

$$\delta = 2M\beta - \frac{\pi}{2} + \tfrac{1}{2}\lambda_1\zeta_2 + i\epsilon \quad (\operatorname{Im}\delta > 0). \tag{6.60}$$

The term $i\epsilon$ ($\epsilon > 0$) has been added to represent the effective damping due to other contributions. It corresponds mainly to the effect of the internal reflection coefficient $\tilde{\rho}$ [cf. (6.48)]. This source of damping would still be present even for $\zeta_2 = 0$ ($N = \sqrt{2}$), and it is, in fact, responsible for the convergence of the Debye expansion for the residue-series contributions, as we have seen above.

The main virtue of the approximation (6.59) is that $\Psi(x, \delta)$ can be evaluated exactly, with the help of the generating function for generalized Laguerre polynomials (Ref. 27, p. 242):

$$\sum_{p=0}^{\infty} L_p^{(\alpha)}(x) z^p = (1 - z)^{-\alpha-1} \exp\left(\frac{xz}{z-1}\right) \quad (|z| < 1). \tag{6.61}$$

Setting $\alpha = -1$ and $z = e^{i\delta}$ ($\operatorname{Im}\delta > 0$), we get [cf. (C24)–(C25)]

$$\Phi(x, \delta) = \sum_{p=0}^{\infty} e^{ip\delta} L_p^{(-1)}(-x) = \exp\left(\frac{xe^{i\delta}}{1 - e^{i\delta}}\right)$$
$$= \exp\left(-\frac{x}{2}\right) \exp\left(\frac{ix}{2}\cot\frac{\delta}{2}\right) \quad (\operatorname{Im}\delta > 0). \tag{6.62}$$

To get $\Psi(x, \delta)$, it suffices to take

$$\Psi(x, \delta) = \frac{1}{4}\left[\Phi(x, \delta) - \Phi\left(x, \delta + \frac{\pi}{2}\right) + \Phi(x, \delta + \pi) - \Phi\left(x, \delta + \frac{3\pi}{2}\right)\right], \tag{6.63}$$

so that

$$\Psi(x, \delta) = \tfrac{1}{4}\exp\left(-\frac{x}{2}\right) \times \left\{\exp\left(\frac{ix}{2}\cot\frac{\delta}{2}\right) + \exp\left(-\frac{ix}{2}\tan\frac{\delta}{2}\right) - \exp\left[\frac{ix}{2}\cot\left(\frac{\delta}{2} + \frac{\pi}{4}\right)\right] - \exp\left[-\frac{ix}{2}\tan\left(\frac{\delta}{2} + \frac{\pi}{4}\right)\right]\right\}. \tag{6.64}$$

In particular, if $\operatorname{Im}\delta$ is large, i.e.,

$$\exp(-\operatorname{Im}\delta) \ll 1, \tag{6.65}$$

we can employ the approximation

$$\tan\frac{\delta}{2} \approx i + 2\exp(-\operatorname{Im}\delta)\sin(\operatorname{Re}\delta), \tag{6.66}$$

so that (6.64) becomes

$$\Psi(x, \delta) \approx \tfrac{1}{2}\{\cos[xe^{-\operatorname{Im}\delta}\sin(\operatorname{Re}\delta)] - \cos[xe^{-\operatorname{Im}\delta}\cos(\operatorname{Re}\delta)]\}$$
$$\approx \frac{x^2}{4}\exp(-2\operatorname{Im}\delta)\cos(2\operatorname{Re}\delta)$$
$$= \frac{x^2}{4}\operatorname{Re}(e^{2i\delta}) \quad (e^{-\operatorname{Im}\delta} \ll 1,\ x \lesssim 1). \tag{6.67}$$

Let us study the behavior of $\Psi(x, \delta)$ as a function of δ. We have [cf. (6.59)]:

$$\Psi\left(x, \delta + \frac{\pi}{2}\right) = -\Psi(x, \delta), \tag{6.68}$$

so that it suffices to consider the interval

$$0 \leq \operatorname{Re}\delta < \pi/2. \tag{6.69}$$

The behavior of Ψ within this interval depends very sensitively on the magnitude of the damping, i.e., on $\operatorname{Im}\delta$.

For strong damping, $e^{-\operatorname{Im}\delta} \ll 1$, we have, by (6.67), $|\Psi| \ll 1$, and Ψ oscillates like $\cos(2\operatorname{Re}\delta)$. In the opposite extreme of weak damping, $\operatorname{Im}\delta \ll 1$, it follows from (6.64) that $|\Psi|$ has oscillations with rapidly-varying period within the interval (6.69), but it is still bounded by

$$|\Psi(x, \delta)| \lesssim 1. \tag{6.70}$$

We shall now discuss the implications of these results for the theory of the glory. It follows from (6.50) and (6.59) that

$$|f_{\text{res}}(\beta, \pi)| \approx 2.034(\beta/2)^{\frac{1}{3}}|\Psi(x, \delta)|. \tag{6.71}$$

On the other hand, according to Sec. 5, the intensity

in the glory is dominated by the residue-series contribution:

$$i(\beta, \pi) \approx |f_{\text{res}}(\beta, \pi)|^2. \tag{6.72}$$

Let us consider the behavior of $i(\beta, \pi)$ as a function of β. It follows from (6.68) and (6.71)–(6.72) that the intensity is a periodic function of Re δ, with period $\pi/2$. According to (6.60), the corresponding period $\Delta\beta$ in β, near $\beta = \beta_0$, is given by

$$\Delta\beta = \frac{\pi}{4M + \zeta_2\left(\dfrac{d \operatorname{Re} \lambda_1}{d\beta}\right)_{\beta_0}}. \tag{6.73}$$

Within the domain of validity of the approximation I, (3.29), for λ_1, this becomes

$$\Delta\beta \approx \frac{\pi}{4M + \zeta_2\left[1 + \dfrac{x_1}{12}\left(\dfrac{2}{\beta_0}\right)^{\frac{2}{3}}\right]} \quad (\beta_0^{\frac{1}{3}} \gg 1). \tag{6.74}$$

Notice that, actually, (6.71) is not strictly periodic in β, both because $\Delta\beta$ depends (not very strongly) on β and because Im δ also changes with β. Furthermore, the strict periodicity in Re δ follows from assumptions (B) and (C), which are not very good approximations for $N = 1.33$. However, we should still find a quasi-periodic pattern, with period given approximately by (6.73), superimposed on a more slowly varying background.

For $\beta_0 = 200$, $N = 1.333$, (6.74) gives

$$\Delta\beta \approx 0.83, \tag{6.75}$$

in excellent agreement with the corresponding value (5.4) found by Bryant and Cox.[8] This provides the explanation of feature (e) in the glory (Sec. 5A). We see that the quasiperiodicity arises from the proximity to the resonance situation shown in Fig. 12, with a return to nearly the original position after each four additional shortcuts.

Let us now turn to feature (f), the behavior of $i(\beta, \pi)$ within a single period. For $\beta_0 \approx 200$, $N = 1.33$, it follows from (6.60), I, (3.29) and Table I, that $e^{-\operatorname{Im}\delta} \sim 10^{-2} \ll 1$, so that (6.67) holds. According to (6.67), the total residue-series contribution has the same order of magnitude as the second term in the Debye expansion. As we have seen in Sec. 5C, this term accounts correctly for the order of magnitude of the intensity in the glory.

On the other hand, the relatively slow oscillations of $|\Psi|$ given by (6.67) do not agree with the behavior described in feature (f) (Sec. 5A). However, the assumptions made in the derivation of this result are violated for $N = 1.33$. In particular, assumptions (B) and (C), which led to strong damping of high-p contributions, are already violated for $p = 15$ and $p = 24$ (cf. Table I). The latter, in particular, corresponds to a very small ζ_p. According to (6.49), these terms are still significant for $\beta_0 \sim 200$. In view of (6.33)–(6.35), their contributions can be quite large, and they probably account for the large spikes in the backward intensity; e.g., the interference between $p = 2$ and $p = 15$ may give rise to narrow peaks. The irregular behavior of the intensity within a period is thus related to the mixture of periodicities 4 and 5 in (6.55).

As N approaches closer to the resonance at $\sqrt{2}$, the assumptions leading to (6.71) become increasingly better justified. The damping also decreases with ζ_2 [cf. (6.60)], so that (6.64) should be applied. Thus we should find a number of oscillations with rapidly varying period within a single interval $\Delta\beta$. The character of these oscillations is strongly dependent on the damping, i.e., on the deviation of the refractive index from resonance. This extremely sensitive dependence of the intensity on β and N explains feature (d) (Sec. 5A), the variability of the glory.

The ratio of the surface-wave contribution to $f(\beta, \pi)$ to the geometrical-optic contribution is roughly given by [cf. (5.19)]:

$$|f_{\text{res}}(\beta, \pi)/f_g(\beta, \pi)| \sim \beta^{\frac{1}{3}} \exp(-\bar{\zeta} \operatorname{Re} \lambda_1), \tag{6.76}$$

but it can become much larger at resonance. However, by (6.70) and (6.71), the magnitude of the resonance peaks is bounded by

$$|f_{\text{res}}(\beta, \pi)| \leqslant \beta^{\frac{1}{3}}, \tag{6.77}$$

and this is also the upper bound for the ratio (6.76).

The origin of this upper bound can be understood by going back to the partial-wave series. By I, (2.1) and (6.38), we have

$$f_{\text{res}}(\beta, \pi) \approx \frac{1}{i\beta} \sum_{l=l_-}^{l_+} (-1)^l (l + \tfrac{1}{2})[S_l(k) - 1]. \tag{6.78}$$

The unitarity condition for the S matrix gives

$$|S_l(k) - 1| \leq 2, \tag{6.79}$$

where the extreme value 2 is attained when the lth partial wave is resonant. Substituting (6.79) in (6.78), and taking into account (5.21), we are led to an upper bound of the form (6.77).

Thus, the upper bound (6.77) corresponds to *saturation of the unitarity limit*. It would arise from having most partial waves within the edge domain

(5.21) close to resonance. This provides a link between the geometrical picture of diffracted-ray resonances illustrated in Fig. 12 and the more familiar concept of resonances in individual partial waves. The former are due to poles of the Debye expansion; the latter correspond to Regge poles close to the real axis [cf. I, Fig. 3 and the discussion about the physical interpretation of I, (2.34)–(2.35)]. The relationship between the two sets of poles and the two pictures is similar to that between the Debye expansion and the partial-wave description: surface-wave resonances can be regarded as a collective effect of many nearly-resonant partial waves, and conversely.

In conclusion, we see that higher-order surface-wave contributions are responsible for the main features of the glory that were left unexplained in Sec. 5 (quasiperiodicity, behavior within a period, and variability). All these effects are related to the existence of resonances like that shown in Fig. 12.

E. The Total Cross Section and the Ripple

Let us now go over to the forward scattering amplitude. According to I, (4.67), I, (5.48), and (6.16), it can be written in the following form:

$$f(\beta, 0) = f_d(\beta, 0) + f_F(\beta, 0) + f_g(\beta, 0) + \tilde{f}_{\text{res}}(\beta, 0), \tag{6.80}$$

where

$$f_d(\beta, 0) = i\beta/2 \tag{6.81}$$

is the contribution from the forward diffraction peak,

$$f_F(\beta, 0) = i\left[\frac{M_0}{\gamma} - \frac{i}{M} + \frac{8}{15} M_1\gamma - \frac{iM_0}{6}\frac{(4N^2-3)}{M^3}\gamma^2 + \mathcal{O}(\gamma^3)\right] \tag{6.82}$$

is the contribution from the Fock correction terms,

$$f_g(\beta, 0) = -\frac{2N^2}{(N-1)(N+1)^2}\exp[2i(N-1)\beta] \times \left\{1 + \frac{i}{\beta}\left[1 - \frac{1}{N} + \frac{1}{2(N-1)}\right] + \mathcal{O}(\beta^{-2})\right\} + \frac{N^2}{(N+1)^2}\exp[2i(N-1)\beta]\varphi\left(z, \frac{N-1}{2}\right) \tag{6.83}$$

is the geometrical-optic contribution (neglecting noncentral rays) and, finally, $\tilde{f}_{\text{res}}(\beta, 0)$ is the residue-series contribution.

In particular, taking $N = 1.33$, $\beta = 130$, we find

$$f_d(130, 0) + f_F(130, 0) + f_g(130, 0) \approx 65i + (-3.223 + 2.449i) + (1.081 + 1.644i) = -2.142 + 69.093i \quad (N = 1.33), \tag{6.84}$$

whereas the corresponding "exact" result, computed in the same way as (5.15), is

$$f(130, 0) = -2.529 + 68.988i \quad (N = 1.33). \tag{6.85}$$

Thus, the residue-series contribution must be given by

$$\tilde{f}_{\text{res}}(130, 0) \approx -0.387 - 0.105i \quad (N = 1.33). \tag{6.86}$$

Though smaller than the Fock and geometrical-optic contributions in (6.84), this still has comparable order of magnitude.

The total cross section is related to $f(\beta, 0)$ by the optical theorem:

$$\sigma_{\text{tot}} = \frac{4\pi a^2}{\beta}\,\text{Im}\, f(\beta, 0). \tag{6.87}$$

Taking into account (6.80)–(6.83), we find

$$\frac{\sigma_{\text{tot}}}{2\pi a^2} = 1 + \left\{\text{Re}\, M_0\gamma^2 + \tfrac{8}{15}\text{Re}\, M_1\gamma^4 + \frac{\text{Im}\, M_0}{6}\frac{(4N^2-3)}{M^3}\gamma^5\right\} + \frac{2N^2}{(N+1)^2\beta}\left\{-\frac{2}{N-1}\sin[2(N-1)\beta] + \text{Im}\left[e^{2i(N-1)\beta}\varphi\left(z, \frac{N-1}{2}\right)\right]\right\} + \frac{\sigma_{\text{res}}}{2\pi a^2} + \mathcal{O}(\beta^{-2}), \tag{6.88}$$

where the first term arises from the diffraction peak, the second and third ones (expressions within curly brackets) from the Fock and (central-ray) geometrical-optic contributions, and σ_{res} denotes the residue-series contribution.

The diffraction and Fock terms in (6.88) give rise to a slowly varying background which is monotonically decreasing, approaching the asymptotic value unity as $\beta \to \infty$. This leads to the well-known result that the asymptotic cross section is twice the geometrical cross section ($\sigma_{\text{tot}} \to 2\pi a^2$).

The geometrical-optic contribution gives rise to relatively slow oscillations with period

$$\Delta_1\beta = \frac{\pi}{N-1} \tag{6.89}$$

and amplitude decreasing like β^{-1}, superimposed on the background. These oscillations arise from interference between waves diffracted around the sphere and those geometrically transmitted through it. An analogous effect has been observed in neutron

scattering at energies of several million electron volts ("giant resonances"), and a similar explanation has been proposed.[29]

Very accurate numerical calculations of the total cross section, based on the partial-wave series and done at very small intervals, have shown, superimposed on these broad oscillations, a quasiperiodic structure, corresponding to rather irregular fluctuations with short period and variable amplitude. These secondary fluctuations are generally known as the "ripple" (Ref. 7, p. 177, Fig. 32[30]). Most calculations have been performed for $\beta \leqslant 20$, but the ripple also appears in Bryant and Cox's curves for σ_{tot} near $\beta = 200$ (Ref. 8, Fig. 2). Moreover, as has already been mentioned in Sec. 5A [feature (g)], these curves show a striking parallelism with the scattered intensity at 180°, with similar peaks, located at nearly the same values of β, but with greatly reduced amplitude. This parallelism strongly suggests that the ripple must correspond to the contribution from σ_{res} in (6.88).

Let us compute the contribution. According to I, (5.30), (3.38), and (6.21), the residue-series contribution to $f_p(\beta, 0)$ must be of the form

$$\tilde{f}_{p,\text{res}}(\beta, 0) = -\frac{2\pi}{\beta} i^{r-1} \sum_{m=0}^{\infty} (-1)^m \sum_n \text{residue } \{\lambda U \rho^{p-1} \times \exp[i(2m + s + 1)\pi\lambda]\}_{\lambda_n}, \quad (6.90)$$

where r and s are integers related to p, and (6.22) remains valid.

By comparison with (6.21), we see that the only difference in (6.90) is an additional factor $-ie^{i\pi\lambda}$. Thus, according to (6.26),

$$\tilde{f}_{p,\text{res}}(\beta, 0) \approx i^r \frac{e^{i\pi/3}}{\gamma} \times \exp\left[ip\left(2M\beta - \frac{\pi}{2}\right)\right] L_p^{(-1)}(-2\tilde{\zeta}_p/M) \times \sum_n (a_n')^{-2} \exp(i\lambda_n \tilde{\zeta}_p)[1 + \mathcal{O}(\gamma^2)], \quad (6.91)$$

where [cf. (6.30)]

$$\tilde{\zeta}_p \equiv 2\pi - p\theta_t \pmod{2\pi}, \quad 0 \leq \tilde{\zeta}_p < 2\pi. \quad (6.92)$$

In particular, for $p = 1$ and $p = 2$, (6.91) agrees with I, (5.32), and with the extension of (3.46) to $\theta = 0$ [cf. (6.32)].

The dominant contributions arise from values of p such that [cf. (6.52)]

$$0 \leq \tilde{\zeta}_p < \theta_t. \quad (6.93)$$

For $N = 1.33$, this implies that the lowest value of p to contribute is $p = 4$. Employing (6.91) to estimate the order of magnitude of this contribution for $\beta = 130$, we find that it is of order unity, in agreement with (6.86).

For $N = 1.40$, up to large values of p, the dominant contributions arise from [cf. (6.53)]

$$p = 4n \quad (n = 1, 2, 3, \cdots), \quad (6.94)$$

whereas, for $N = 1.33$, we find deviations from (6.94) already for rather low values of p, as in Table I.

By employing assumptions similar to those made for the derivation of (6.50), we find

$$\tilde{f}_{\text{res}}(\beta, 0) = \sum_p \tilde{f}_{p,\text{res}}(\beta, 0) \approx -\frac{(-i)^r e^{i\pi/3}}{\gamma a_1'^2} \tilde{\Psi}(N, \beta), \quad (6.95)$$

where

$$\tilde{\Psi}(N, \beta) \approx \tilde{\Psi}(\tilde{x}, \delta) = \sum_{n=1}^{\infty} \exp(4in\delta) L_{4n}^{(-1)}(-\tilde{x}), \quad (6.96)$$

with

$$\tilde{x} = 2\tilde{\zeta}/M \quad (0 \leq \tilde{\zeta} < \theta_t), \quad (6.97)$$

where $\tilde{\zeta}$ is an average value of $\tilde{\zeta}_p$, and δ is given by the *same* expression (6.60). In fact, (6.56) is replaced by

$$\tilde{\zeta}_{4n} = n\tilde{\zeta}_4 = 2n\zeta_2, \quad (6.98)$$

with ζ_2 still given by (6.30).

It is readily seen, with the help of (C25), that (6.63)–(6.64) are replaced by

$$\begin{aligned}\tilde{\Psi}(\tilde{x}, \delta) &= \frac{1}{4}\left[\Phi(\tilde{x}, \delta) + \Phi\left(\tilde{x}, \delta + \frac{\pi}{2}\right) + \Phi(\tilde{x}, \delta + \pi) + \Phi\left(\tilde{x}, \delta + \frac{3\pi}{2}\right)\right] - 1 \\ &= \frac{1}{4}\exp\left(-\frac{\tilde{x}}{2}\right)\left\{\exp\left(\frac{i\tilde{x}}{2}\cot\frac{\delta}{2}\right) + \exp\left(-\frac{i\tilde{x}}{2}\tan\frac{\delta}{2}\right) + \exp\left[\frac{i\tilde{x}}{2}\cot\left(\frac{\delta}{2} + \frac{\pi}{4}\right)\right] + \exp\left[-\frac{i\tilde{x}}{2}\tan\left(\frac{\delta}{2} + \frac{\pi}{4}\right)\right]\right\} - 1. \quad (6.99)\end{aligned}$$

Instead of (6.68), we now have

$$\tilde{\Psi}\left(\tilde{x}, \delta + \frac{\pi}{2}\right) = \tilde{\Psi}(\tilde{x}, \delta). \quad (6.100)$$

[29] J. M. Peterson, Phys. Rev. **125**, 955 (1962); K. W. McVoy, L. Heller, and M. Bolsterli, Rev. Mod. Phys. **39**, 245 (1967); K. W. McVoy, Ann. Phys. (N.Y.) **43**, 91 (1967).

[30] P. Walstra, Proc. Koninkl. Nederl. Akad. Wetensch. **B67**, 491 (1964).

Thus, $f_{\rm res}(\beta, 0)$, and consequently also the ripple, given by

$$\sigma_{\rm res} = \frac{4\pi a^2}{\beta} \operatorname{Im} f_{\rm res}(\beta, 0), \tag{6.101}$$

have the same quasiperiodicity in β as the intensity in the glory, with period given by (6.73)–(6.74).

For $N = 1.33$, the behavior of the cross section within one period is again determined by deviations from (6.94) at relatively low p. The type of deviation and the conditions for constructive interference are similar to those found for the back-scattered intensity. This explains the parallelism found by Bryant and Cox [feature (g), Sec. 5A].

Strictly speaking, the above results cannot be applied to the range $1 \leqslant \beta \leqslant 20$ for which most data on the ripple are available, since they are based upon asymptotic approximations that break down for such low β. However, we can try to employ them for a qualitative understanding of the behavior of the ripple within this range.

According to (6.49) and (6.94), the dominant contribution to the ripple for low β and $N = 1.33$ should arise from $p = 4$ (diffracted rays taking four shortcuts). It then follows from (6.91) and (6.101), again restricting ourselves to the contribution from the pole λ_1, that

$$\sigma_{\rm res} \sim A(\beta)\beta^{-\frac{2}{3}} \exp(-\tilde{\zeta}_4 \operatorname{Im} \lambda_1) \sin(4 \operatorname{Re} \delta + \chi), \tag{6.102}$$

where A is an amplitude factor, δ is given by (6.60), and χ is a constant phase.

As a function of β, (6.102) shows a sinusoidal behavior with variable amplitude. This agrees with the calculated curves up to $\beta \sim 10$.[30] As β increases, higher values of p start to contribute [cf. (6.49)] and deviations from the sinusoidal pattern should appear. Since the damping of the surface waves is not very strong for low β, interference with the contributions from values of p other than (6.94) and from poles other than λ_1 should also give rise to such deviations. This again agrees with the results of numerical calculations.[30]

The period of the oscillations, according to (6.102), is the same as that at 180°, given by (6.73). If we apply the approximation (6.74), neglecting the correction $\beta_0^{-\frac{2}{3}}$ in the denominator, we find

$$\Delta\beta \sim \frac{\pi}{4M + \zeta_2}, \tag{6.103}$$

if the dominant contribution arises from $p = 4$, as for $N = 1.33$. In general, for other values of N, (6.103) must be replaced by

$$\Delta\beta \sim \frac{2\pi}{2Mp + \tilde{\zeta}_p}, \tag{6.104}$$

where p is the lowest term that contributes. These results should not be very accurate at low β, since they are based upon the high-frequency approximation (6.74).

The expression (6.104) for the period was derived by Van de Hulst (Ref. 7, p. 377) on the basis of a model in which only the lowest p verifying (6.93) contributes. It was compared with the period observed in numerical calculations for $\beta \leqslant 20$ and several values of N, by Walstra.[30] It was found that (6.104) is in very good agreement with the data, although it predicts values systematically in excess of the observed ones.

This is exactly what should be expected. In fact, (6.104) should be replaced by a more accurate expression, corresponding to (6.73), and we have

$$d \operatorname{Re} \lambda_1/d\beta > 1. \tag{6.105}$$

Physically, this corresponds to the fact that the phase velocity of the surface waves is slightly smaller than that in free space (they are delayed due to the curvature of the surface). This was not taken into account by Van de Hulst in his computation of the optical path difference.

No ripple is observed in the total cross section for $N < 1$,[30] and, indeed, none should be expected, as the diffracted rays cannot take any shortcuts through the sphere in this case (cf. Sec. 6F).

The present theory also leads us to predict that the ripple must be damped for an absorbing sphere (complex refractive index), and that the attenuation must increase with the absorption. This follows from the fact that each shortcut is then accompanied by absorption, i.e., $\operatorname{Im} \delta$ in (6.60) has an additional component due to absorption. This attenuation of the ripple has indeed been observed in numerical computations for complex N.[31]

For sufficiently small β ($\beta \leqslant 4$), the peaks in the ripple may be attributed to resonances in successively higher partial waves.[30] However, as β increases, more than one partial wave may be near resonance, and we finally come to the surface-wave model of the ripple. As we have seen in connection with the glory (Sec. 6D), the two pictures actually merge together, each effect in one description corresponding to a collective effect produced by several terms in the other one.

[31] D. Deirmendjian, R. Clasen, and W. Viezee, J. Opt. Soc. Am. **51**, 620 (1961).

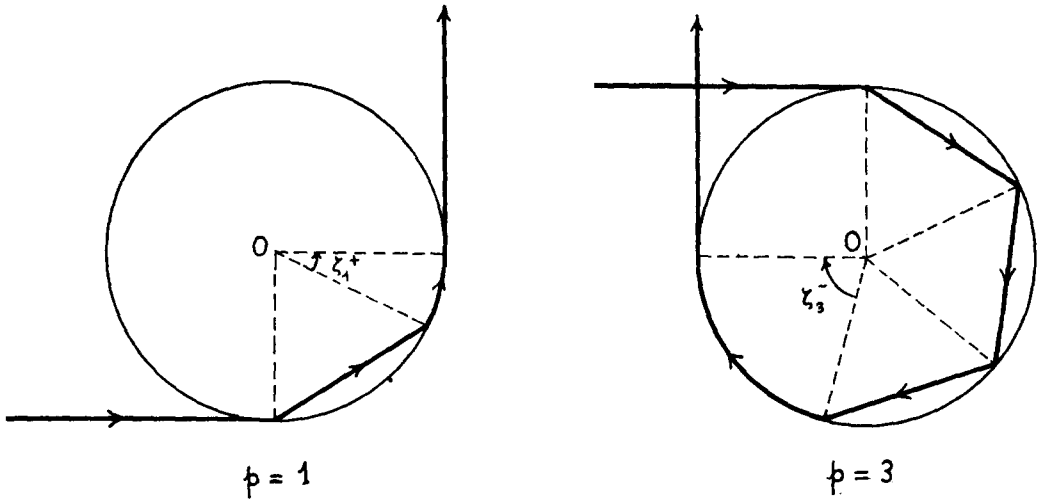

FIG. 13. The lowest-order residue-series contributions to the intensity at $\theta = 90°$.

Heretofore, we have restricted our discussion of higher-order surface-wave effects to the forward and backward directions. However, it is clear from (6.30) that similar ripple effects should also be observed in any other direction. For $\theta = 90°$, they have actually been found in Bryant and Cox's calculations, and the corresponding period is *twice* that found for $\theta = 0°$ and 180° (Ref. 8, Fig. 2).

The reason for this is indicated in Fig. 13, which shows the lowest-order contributions at 90° for $N = 1.33$: They correspond to $f^+_{1,\text{res}}$ and $f^-_{3,\text{res}}$ in (6.30). Instead of (6.53) and (6.94), the dominant contributions at 90° arise from $p = 2n + 1$ $(n = 0, 1, 2, \cdots)$, and the relative phase shift between successive contributions is $\frac{1}{2}$ Re δ, where δ is still given by (6.60). Thus, the period is $2\Delta\beta$, with $\Delta\beta$ given by (6.73). This completes the explanation of feature (g) for the glory (Sec. 5A).

We have seen that the amplitude of the ripple component relative to the remaining contributions to the scattering amplitude is at most of order $\beta^{-\frac{2}{3}}$ at $\theta = 0°$ [cf. (6.102)] and at most of order $\beta^{\frac{1}{3}}$ at $\theta = 180°$ [cf. (6.77)], where the ripple is the dominant term (glory). In other directions, far away from forward and backward, it follows from (6.30) [cf. also I, (5.32) and I (5.45)] that the relative amplitude of the ripple is of order $\beta^{-\frac{1}{6}}$. [This is related to the focusing factor $\beta^{\frac{1}{2}}$ in (6.32).]

Thus, *the relative amplitude of the ripple far away from the forward and backward directions is the geometric mean of the values found in these directions.* This is in good agreement with the estimates made by Penndorf.[10] From numerical calculations ranging up to $\beta \sim 400$, he found that the ripple is present in all directions (curves for $\theta = 10°$, 20°, and 40° are given), with increasing relative amplitude as θ increases from 0° to 180°, and he estimated the average amplitude as roughly 0.1 at 0°, 5 at 90°, and 500 at 180°.

We conclude, therefore, that the ripple is a very general phenomenon, that affects the intensity in any direction, but only becomes dominant near the backward direction, where it gives rise to the glory. It is a general manifestation of the resonance phenomena for diffracted rays discussed in Sec. 6D. A practical implication of this result for numerical calculations is that very closely spaced points in β are required for an accurate interpolation for the intensity in any direction.

F. Higher-Order Residue-Series Contributions to $f(\beta, \pi)$ for $N < 1$

Finally, let us consider the residue-series contributions to $f(\beta, \theta)$ for $N < 1$, e.g., at $\theta = \pi$. According to I, (5.8) and to (3.13), the contribution to $f_p(\beta, \pi)$ from the residue series at the poles $-\lambda'_n$ is of the form

$$f'_{p,\text{res}}(\beta, \pi) = -\frac{2\pi i}{\beta}\sum_{m=0}^{\infty}(-1)^m \times \sum_n \text{residue}\,\{\lambda U(\rho e^{2i\pi\lambda})^{p-1} \times \exp[i(2m+1)\pi\lambda]\}_{-\lambda_n'}. \quad (6.106)$$

Taking into account (2.2) and restricting ourselves to $m = 0$, this becomes

$$f'_{p,\text{res}}(\beta, \pi) \approx -\frac{2\pi i}{\beta}\sum_n \text{residue}\,(\lambda e^{-i\pi\lambda} U \rho^{p-1})_{\lambda_n'}. \quad (6.107)$$

Substituting U and ρ by their explicit expressions [cf. (3.20)], we find

$$f'_{p,\text{res}}(\beta, \pi) \approx (-1)^{p+1} i\,\frac{32}{\pi\beta^3}\sum_n r'_{n,p}, \quad (6.108)$$

where

$$r'_{n,p} = \text{residue}\left\{\frac{c'_p(\lambda, \beta)}{[d(\lambda, \beta)]^{p+1}}\right\}_{\lambda_n'}, \tag{6.109}$$

$$c'_p(\lambda, \beta) = \frac{\lambda e^{-i\pi\lambda}[H_\lambda^{(1)}(\alpha)]^{p-1}}{[H_\lambda^{(1)}(\beta)]^2[H_\lambda^{(2)}(\alpha)]^{p+1}}([1\ \beta] - N[1\ \alpha])^{p-1}, \tag{6.110}$$

and $d(\lambda, \beta)$ is given by (3.19).

The evaluation of the dominant term in $r'_{n,p}$ is performed in Appendix D. Substituting the result, given by (D18), in (6.108), we finally get

$$f'_{p,\text{res}}(\beta, \pi) \approx 4i\pi \frac{N^2}{M'} \times \exp(-2iM'\beta) \sum_n \frac{1}{p!}[\mathfrak{D}_n(\pi - \theta)]^p \times \exp[-i\lambda'_n(\pi - \theta_t)][1 + \mathcal{O}(\gamma^2)], \tag{6.111}$$

where, as in I, (4.76) and I, (5.67),

$$\theta_t = 2\cos^{-1} N, \tag{6.112}$$

$$\mathfrak{D}_n = \frac{e^{-i\pi/3}}{2\pi a_n'^2 \gamma'}, \quad \gamma' = (2/\alpha)^{\frac{1}{3}}. \tag{6.113}$$

In particular, for $p = 1$, the result agrees with I, (5.64), and for $p = 2$ it agrees with the analytic continuation of (3.33) (extended to $\theta = \pi$) to $N < 1$. Actually, as is readily verified, (6.111) reduces to the residue series in I, (4.85), for $p = 0$, so that it can be employed even in that case.

The physical interpretation of (6.111) is a generalization of that given in I, Sec. 5E for $p = 1$. It is illustrated in Fig. 14 for $p = 3$. Since no shortcuts through the sphere are possible for $N < 1$, the only possible "elementary interaction" of the surface waves at any point of the surface, as they travel along on the inner side, is a kind of "internal diffraction," described by the internal diffraction coefficient $\mathfrak{D}_n$, each time they shed a ray to the outside region.

Since the shadow boundary S_1S_1' is the same for all terms in the Debye expansion, all surface waves describe the same total angle $\pi - \theta_t$ before emerging in the backward direction; in between, however, they can undergo any number of internal diffractions, and $f'_{p,\text{res}}$ corresponds to a term with p internal diffractions.

For instance, for $p = 3$ (Fig. 14), the corresponding contribution is proportional to

$$\mathfrak{D}_n^3 \int_0^{\pi-\theta_t} d\varphi_1 \int_0^{\pi-\theta_t-\varphi_1} d\varphi_2 \times \int_0^{\pi-\theta_t-\varphi_1-\varphi_2} d\varphi_3 = \mathfrak{D}_n^3 \frac{(\pi - \theta_t)^3}{3!},$$

and for the general case this gives rise to the factor $[\mathfrak{D}_n(\pi - \theta_t)]^p/p!$ in (6.111). The physical interpretation of the remaining factors has already been given in I, Sec. 4E.

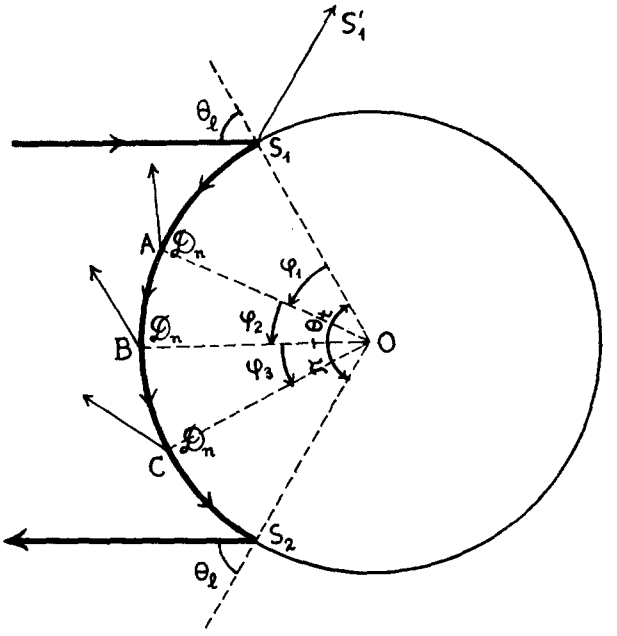

FIG. 14. Physical interpretation of (6.111) for $p = 3$. The only possible surface interaction of the diffracted rays as they travel along the surface on the inner side is "internal diffraction," described by the coefficient $\mathfrak{D}_n$, that can occur any number of times.

Since (6.111) is valid also for $p = 0$, the total (dominant) contribution to $f(\beta, \pi)$ from the residue series at the poles λ'_n is

$$f'_{\text{res}}(\beta, \pi) = \sum_{p=0}^{\infty} f'_{p,\text{res}}(\beta, \pi) \approx 4\pi i \frac{N^2}{M'} \exp(-2iM'\beta) \times \sum_n \exp[-i\lambda'_n(\pi - \theta_t)] \times \sum_{p=0}^{\infty} \frac{[\mathfrak{D}_n(\pi - \theta_t)]^p}{p!}[1 + \mathcal{O}(\gamma^2)], \tag{6.114}$$

which can be rewritten as

$$f'_{\text{res}}(\beta, \pi) \approx 4\pi i \frac{N^2}{M'} \exp(-2iM'\beta) \times \sum_n \exp[-i\lambda''_n(\pi - \theta_t)][1 + \mathcal{O}(\gamma^2)], \tag{6.115}$$

where

$$\lambda''_n = \lambda'_n + i\mathfrak{D}_n. \tag{6.116}$$

Thus, the total (dominant) effect of all residue-series contributions is equivalent to that from $p = 0$ [cf. I, (4.85)], but now evaluated with poles at shifted positions, given by (6.116). We can also say that the effect of higher-order contributions is to "renormalize" the phase velocities and damping constants of the surface waves.

In the approximation I, (3.35), for the poles,

$$\lambda_n' \approx \alpha + e^{-i\pi/3}\frac{x_n}{\gamma'} + i\frac{N}{M'}, \qquad (6.117)$$

the pole shift (6.116) corresponds to the replacement [cf. (6.113)]

$$x_n \to x_n + (i/2\pi a_n'^2). \qquad (6.118)$$

For large n, the correction term in (6.118) is $\mathcal{O}(n^{-\frac{1}{3}})$ [N, (D8)], but it has an appreciable effect for the lowest values of n, which are responsible for the dominant contribution.

In conclusion, we see that the behavior of the scattering amplitude for $N < 1$ is simpler in several respects than that for $N > 1$. The surface waves excited by the critically incident ray have the same shadow boundary for all terms in the Debye expansion, and they cannot make any shortcuts through the sphere. Their resultant effect, at least for the dominant term, can easily be summed (without the simplifying assumptions employed for $N > 1$), and leads simply to a renormalization of the propagation constants. There are no resonance effects, and, consequently, no ripple: the intensity in any direction, as well as the total cross section, have a much smoother behavior than for $N > 1$. In the quantum-mechanical interpretation we can say that a repulsive interaction leads to a simpler structure than an attractive one.

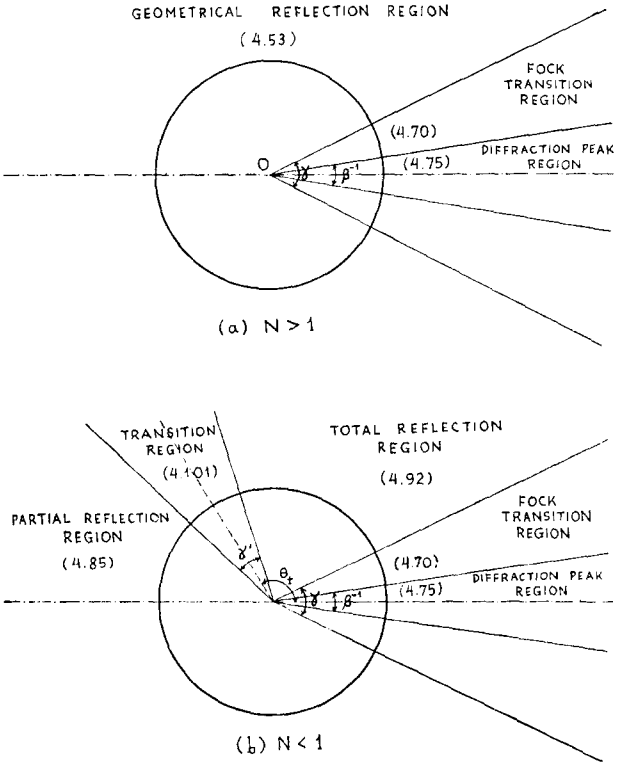

FIG. 15. Basic formulas applicable in each region for the first term $f_0(\beta, \theta)$ of the Debye expansion: (a) for $N > 1$; (b) for $N < 1$. All equation numbers refer to Paper I.

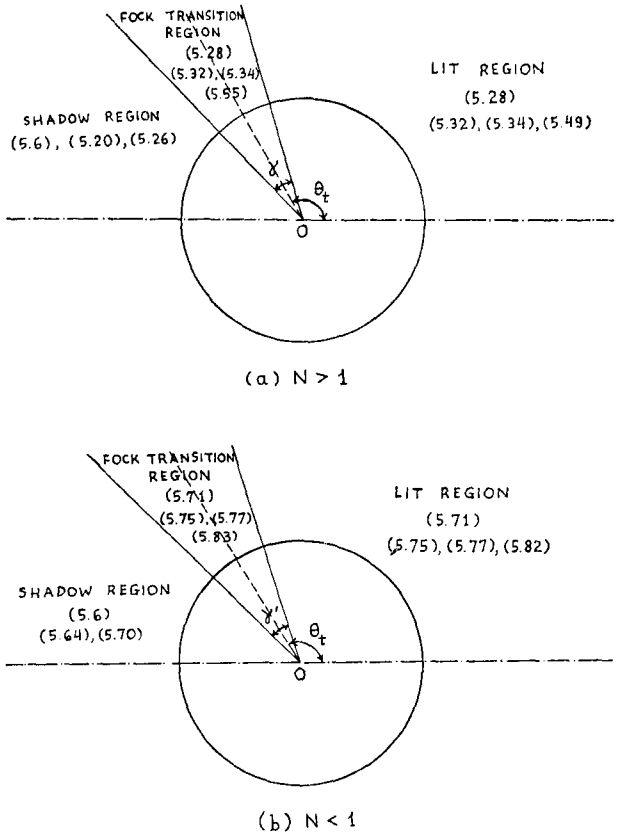

FIG. 16. Basic formulas applicable in each region for the second term $f_1(\beta, \theta)$ of the Debye expansion: (a) for $N > 1$; (b) for $N < 1$ All equation numbers refer to Paper I.

On the other hand, as remarked at the end of I, Sec. 5E, the structure of the transition region around the shadow boundary $\theta = \theta_t$ is quite complicated, because contributions from all terms in the Debye expansion must be taken into account.

7. CONCLUSION

The main conclusion that may be drawn from the present work is that the modified Watson transformation enables us to extract from the partial-wave expansion the complete asymptotic behavior of the scattering amplitude in any direction in the high-frequency domain I, (1.1). This is the purpose for which the Watson transformation was originally introduced.

To facilitate practical application of the results, it is convenient to list the basic formulas that should be applied within each angular region, for each term of the Debye expansion treated in Papers I and II. This is done in Figs. 15 to 17, which provide a graphical summary of the main results. The equations listed in Figs. 15 and 16 refer to Paper I; those in Fig. 17 to

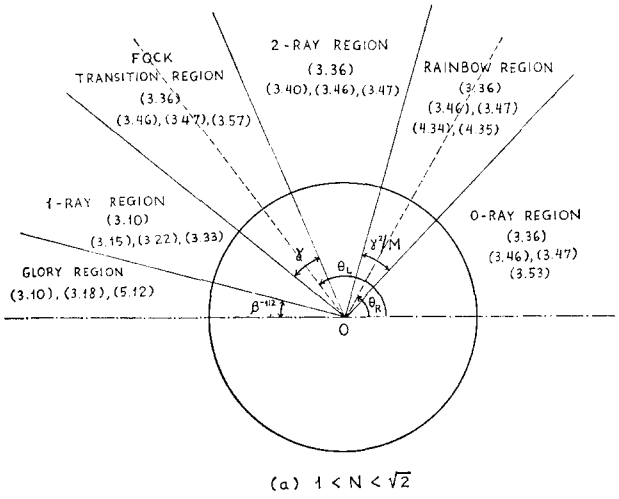

(b) HIGHER-ORDER RESIDUE-SERIES CONTRIBUTIONS

$N > 1$	$\theta = \pi -$	(6.50), (6.59), (6.64)
	$\theta = 0 -$	(6.95), (6.96), (6.99)
$N < 1$	$\theta = \pi -$	(6.115)

FIG. 17. Basic formulas applicable in each region: (a) for the third term $f_2(\beta, \theta)$ of the Debye expansion, for $1 < N < \sqrt{2}$; (b) for the effect of higher-order residue-series contributions. All equation numbers refer to Paper II.

Paper II. The angular width of the transition regions is greatly exaggerated in these figures. Only the main formulas are listed, without including the simplified versions given in the text for special ranges of values of the parameters within each region. The total scattering amplitude in any direction is obtained by summing the corresponding contributions from the first three terms of the Debye expansion and taking into account higher-order correction terms.

The subdivision into angular regions for each term of the Debye expansion corresponds to that predicted by geometrical optics for the associated class of rays, together with transition regions.

In lit regions, the dominant term is usually (not always!) given by the geometrical-optic contribution. Although these contributions were known, their precise domain of validity had not been established. The first correction term, representing the second-order WKB approximation, has been evaluated in each case; the first neglected term is $\mathcal{O}(\beta^{-2})$.

In shadow regions, the behavior is usually dominated by surface-wave contributions. The most convenient language for the description and physical interpretation of the results is provided by the geometrical theory of diffraction, although it must be used with due care.

For $N > 1$, the surface waves are excited by tangentially incident rays, just like those found for an impenetrable sphere. However, penetration into the sphere leads to several new effects. The diffracted rays can have two types of elementary interactions at the surface, as illustrated in Fig. 11. The combination of these two types leads to a series of diagrams characterized by the number of interactions or, equivalently, by the number of shortcuts taken through the sphere.

For $N < 1$, we have found a new class of surface waves excited by critically incident rays. They are related to Schmidt head waves, but their sense of propagation disagrees with that predicted by the geometrical theory of diffraction. The physical requirement is that surface waves always propagate from the shadow boundary into the shadow. The formulation of the geometrical theory of diffraction should be modified to take this requirement into account. It implies that the local behavior of a ray at the surface is determined not only by the tangent plane, but also by the distinction between shadow and lit sides.

Some of the most interesting phenomena appear in the transition regions. We have found essentially four different types of transition regions: (a) normal (Fock-type) transitions; (b) the region around the shadow boundary for $N < 1$; (c) the rainbow; (d) the glory.

Transition regions of type (a) are similar to those found for an impenetrable sphere. Their angular width is usually of order γ. The amplitude within these regions can be described in terms of generalized Fock functions. They include the region around the forward diffraction peak (I, Sec. 4D).

The transition region (b) has a more complicated structure, because it is a common transition region for all terms in the Debye expansion, and the transition is of a different nature for different terms (I, Secs. 4E and 5E).

The rainbow (c) is associated with the transformation of a pair of real rays into complex rays. The Chester–Friedman–Ursell method allows us to treat this situation. It leads to a uniform asymptotic expansion, which contains the Airy theory as a particular case, but represents a considerable extension beyond the domain of validity of this theory.

The glory (d) represents an impressive example of "Regge-pole dominance" of the scattering amplitude in near-backward directions. Van de Hulst's conjecture that the glory is due to surface waves is confirmed, although his model, corresponding to two shortcuts, must be supplemented by taking into account higher-order surface-wave contributions.

The present theory enables us to explain all the features of the glory listed in Sec. 5A, except, of course, the polarization. These features arise from a competition between four different effects: (1) the exponential damping of the surface waves as they travel along the surface of the sphere; (2) the focusing of diffracted rays along the axis, which enhances the back-scattered contribution; (3) the high internal reflectivity of diffracted rays at the surface, implying that a large number of internal reflections must be taken into account (At the same time, the deviation of the reflection coefficient from unity eventually leads to exponential damping of the surface-wave contributions.); (4) The resonance effects associated with nearly-closed circuits after four successive shortcuts (Fig. 12).

Although an accurate evaluation of the higher-order residue-series contributions would require techniques similar to those discussed in Sec. 5D, we have been able to estimate their resultant effect and to discuss its qualitative behavior, with the help of several simplifying assumptions. The technique is essentially equivalent to finding a generating function for an infinite class of diagrams and then employing it for their summation.

The resonance effects found for the diffracted rays lead to rapid quasiperiodic intensity fluctuations, which are present in all directions, but only become dominant near the backward direction, where they lead to the large intensity variations that appear in the glory. The ripple in the total cross section is a manifestation of the same effect, with greatly reduced amplitude. The relative amplitude of the surface-wave contributions also decreases as β increases (due to the exponential damping), and eventually, for large enough β, geometrical-optic terms again become dominant.

We have also established a link between diffracted-ray resonances and collective effects due to resonances in individual partial waves contained in the edge domain. This corresponds to the relation between the Debye expansion and the physical interpretation of Regge poles given in I, Sec. 2. In both descriptions, a large number of terms have to be taken into account. In fact, interference between many contributions is clearly required to explain the complicated structure of the curves for the back-scattered intensity obtained by Bryant and Cox.[8] However, the surface-wave picture is physically more appealing and it leads naturally to an explanation of all observed effects.

From the mathematical point of view, several problems have received only cursory treatment (if any) in the present work: (a) We have given only a heuristic discussion of the convergence of the Debye expansion for the residue-series contributions (Sec. 6D). It would be desirable to show that a more accurate evaluation of the residues leads to the same result. (b) The detailed shape of steepest-descent contours far away from the saddle points has not been discussed. (c) A more careful derivation of the residue-series contributions, by taking a sequence of contours passing between the poles, is required.[32]

From the point of view of numerical computation, an extensive program should be carried out for a detailed comparison between the present results and those obtained by numerical summation of the partial-wave expansion. The ripple effects require close spacing between calculated points for accurate interpolation. The knowledge of the behavior of the solution provided by the present results should be of considerable help for performing the interpolation. The irregular fluctuations due to the ripple may also be washed out by suitable averaging. If only average results are required, as is the case in many applications, the present approximations may already be adequate. A more ambitious program would be to substitute tables of partial waves or scattered intensities by tables of coefficients of WKB-expansion and residue-series contributions.

Finally, from the physical point of view, several applications and extensions of the present work can be envisaged:

(i) For the third term of the Debye expansion, only the range $1 < N < \sqrt{2}$ has been treated. Several interesting effects appear in other ranges, particularly in the neighborhood of transition points between different ranges (Fig. 3). For instance, one can have a confluence of saddle points near $\theta = \pi$, leading to a mixture of rainbow and glory effects. The neighborhood of these transition points should be investigated both theoretically and experimentally.

In the range $\sqrt{2} < N < 2$, where the neighborhood of the backward direction is a 3-ray region (Fig. 3), anomalously large back-scattering (e.g., from ice spheres) has already been found[33] and discussed by means of surface waves.[34] In this context, back-scattered rays corresponding to noncentral incident rays are sometimes called "glory rays," but this phenomenon is clearly quite different from that discussed in the present work, although the one discussed here can be regarded as a virtual continuation of the other one.

[32] R. F. Goodrich and N. D. Kazarinoff, Proc. Cambridge Phil. Soc. **59**, 167 (1963).

[33] D. Atlas and K. M. Glover, in *Electromagnetic Scattering*, M. Kerker, Ed. (The Macmillan Co., New York, 1963), p 213.

[34] J. R. Probert-Jones, in *Electromagnetic Scattering*, M. Kerker, Ed. (The Macmillan Co., New York, 1963), p. 237.

(ii) In Van de Hulst's chart of the $N - \beta$ domain (Ref. 7, Fig. 20, p. 132), we have treated the right-hand side of the square, excluding a neighborhood of the corners. It would be of interest to discuss also the transition to neighboring regions, such as the anomalous-diffraction and Rayleigh–Gans regions (where N is so close to 1 that the positions of the poles are strongly affected), and the region $N \gg 1$ (where the Debye expansion converges more slowly, but direct reflection is dominant). The relation with the resonance region has already appeared in the discussion of surface-wave resonances and the transition to low values of β (Sec. 6E).

(iii) Only the scattering amplitude has been treated. The behavior of the wavefunction in the near region should also be discussed, along similar lines to the discussion given in N for an impenetrable sphere. In particular, this would allow us to determine the behavior within the sphere, which is of interest near resonance. Instead of plane-wave scattering, one can also investigate Green's function. This may provide a useful model for focusing effects in the presence of a point source.

(iv) The extension to a complex refractive index, to represent an absorptive sphere, should not be difficult. Actually, the convergence of the Debye expansion would be improved in this case, in view of the increased damping due to absorption. The propagation of radio waves around the earth is an example.[35]

(v) The extension to complex N would be of particular interest for applications to nuclear physics, in connection with the optical model. Applications to atomic physics, including rainbow effects, have already been discussed.[36] The application to giant resonances in neutron scattering[29] has already been mentioned (Sec. 6E).

Although the nuclear surface does not seem to be very sharp, some evidence for nuclear glory scattering has been given by Bryant and Jarmie.[37] They have obtained a good fit to near-backward alpha-scattering from spinless nuclei at energies between 18 and 50 MeV with an angular distribution of the type (5.20), where a is the nuclear radius. As discussed in Sec. 5C, this indicates that high partial waves, with impact parameters close to the nuclear surface, play an important role. However, a model for the excitations near the nuclear surface that might be involved has not been given.

(vi) The treatment should be extended to bodies of different shapes, and the effect of the geometry on the propagation of surface waves should be discussed. Extension to inhomogeneous bodies should also be considered. In quantum mechanics, this corresponds to a discussion of the classical limit of quantum scattering for more general potentials.

(vii) Finally, in order to account for polarization effects, the scattering of an electromagnetic field should be considered. As will be shown in a forthcoming paper,[11] the present treatment can readily be extended to the electromagnetic case, allowing us to discuss the scattering of light by a transparent sphere.

ACKNOWLEDGMENTS

The research described in this paper was started during the author's stay at the Institute for Advanced Study, in 1964/65. The author is indebted to the late Professor J. R. Oppenheimer for his hospitality and encouragement. He also wishes to thank Professor E. Wolf for his hospitality at the University of Rochester and Mark Samuel for his help in numerical computations. This work was partially supported by grants from the National Science Foundation, the Air Force Office of Scientific Research, and the Air Force Cambridge Research Laboratories.

APPENDIX A: DETERMINATION OF THE SADDLE POINTS FOR $1 < N < \sqrt{2}$

According to (2.47) and (2.20), the saddle points of (2.43) are given by (2.48), where

$$2\theta_2 - \theta_1 = (\pi - \theta)/2, \quad \sin\theta_1 = N \sin\theta_2. \quad \text{(A1)}$$

It follows from (A1) that

$$\cos\frac{\theta}{2} = \frac{2\sin\theta_1}{N^2}\left\{[(1-\sin^2\theta_1)(N^2-\sin^2\theta_1)]^{\frac{1}{2}} - \frac{N^2}{2} + \sin^2\theta_1\right\}, \quad \text{(A2)}$$

where the positive square root is taken, because, for the real saddle points, we must have $0 \leq \theta_1 \leq \pi/2$, $0 \leq \theta_2 \leq \pi/2$.

Introducing

$$z = \sin\theta_1 = \bar{\lambda}/\beta, \quad d = 2\cos(\theta/2), \quad m = N^2/4, \quad \text{(A3)}$$

we find that (A2) becomes

$$z\{[(1-z^2)(4m-z^2)]^{\frac{1}{2}} + z^2 - 2m\} - md = 0. \quad \text{(A4)}$$

Transposing the square root to the other side and squaring, we find

$$z^4 - 2m\,d\,z^3 - 4m(1-m)z^2 + 4m^2\,d\,z + m^2\,d^2 = 0. \quad \text{(A5)}$$

[35] H. Bremmer, *Terrestrial Radio Waves* (Elsevier Publ. Co., Amsterdam, 1949).

[36] K. W. Ford and J. A. Wheeler, Ann. Phys. (N.Y.) 7, 259, 287 (1959).

[37] H. C. Bryant and N. Jarmie, Ann. Phys. (N.Y.) (to be published).

The roots of this fourth-degree equation include, in addition to those of (A4), spurious roots, which verify (A4) with opposite sign for the square root.

The standard procedure for solving an algebraic equation of the fourth degree[38] is to reduce it to a pair of quadratic equations, the coefficients of which are obtained by solving an auxiliary third-degree equation, the resolvent equation. One must first choose the appropriate root of the resolvent; in the present range of values for N, where at least two of the roots are spurious [cf. Fig. 3(b)], one must also choose the appropriate quadratic equation, such that its roots verify (A4).

This can be done by identifying first a particular solution, corresponding to specific value of d (i.e., θ), and then following it by continuity as d changes. A suitable choice for θ is the rainbow angle θ_R; according to (2.35)–(2.36), we must then have

$$d = d_R = \frac{4}{m}\left(\frac{1-m}{3}\right)^{\frac{3}{2}} \Rightarrow z = z_R = 2\left(\frac{1-m}{3}\right)^{\frac{1}{2}}, \tag{A6}$$

and this must be a double root [cf. Fig. 3(b)].

Applying the procedure indicated above, we find that the correct roots are given by

$$z' = b + (b^2 - c)^{\frac{1}{2}}, \quad z'' = b - (b^2 - c)^{\frac{1}{2}}, \tag{A7}$$

where

$$b = \tfrac{1}{2}(md + e), \tag{A8}$$

$$c = \frac{1}{2}\left[u + \frac{md}{e}(u + 4m)\right], \tag{A9}$$

$$e = [u + 4m(1-m) + m^2d^2]^{\frac{1}{2}} \quad \text{(positive square root)}, \tag{A10}$$

and u, the solution of the cubic resolvent equation, is given by

$$u = s_1 + s_2 - \tfrac{4}{3}m(1-m), \tag{A11}$$

$$s_{1,2} = [r \pm (\Delta)^{\frac{1}{2}}]^{\frac{1}{3}}, \tag{A12}$$

where

$$r = \tfrac{4}{3}m^3\{-\tfrac{16}{9}(1-m)^3 + 4[(1-m)^2 + \tfrac{3}{2}m]d^2 + \tfrac{3}{2}md^4\}, \tag{A13}$$

and Δ is the discriminant, given by

$$\Delta = \tfrac{64}{27}m^6d^2\{-16(1-m)^3 + [8(1-m)^3 + 27m^2]d^2 - \tfrac{1}{2}[2(1-m)^3 + 27m^2]d^4 + \tfrac{27}{16}m^2d^6\}. \tag{A14}$$

The condition for a double root is $\Delta = 0$. This indeed happens for $d = d_R$, leading to the solution (A6). For $d < d_R$, i.e., $\theta < \theta_R$, corresponding to the 0-ray region in Fig. 3(b), we have $\Delta > 0$, and the positive cube root is to be taken in (A12). In this region, (A7) gives a pair of complex-conjugate solutions which leave the real axis at right angles (cf. Fig. 4).

For $d < d_R$, i.e., $\theta > \theta_R$, we have $\Delta < 0$ and (A12) becomes

$$s_{1,2} = [r \pm i(|\Delta|)^{\frac{1}{2}}]^{\frac{1}{3}} = \rho^{\frac{1}{3}} \exp(\pm i\phi/3), \tag{A15}$$

where the phase ϕ must be so chosen that

$$0 < \phi < \pi \tag{A16}$$

and ϕ increases as d decreases. The roots z', z'' are now real and they move away from the point z_R, in opposite directions, as d decreases. The smaller root z'' tends to the origin as $d \to 0$ ($\theta \to \pi$). The larger root z' tends first to the point $z = 1$ ($\theta_1 = \pi/2$), which is reached for $\theta = \theta_L$, the 1-ray/2-ray shadow boundary given by (2.30), corresponding to

$$d = d_L = m^{-1} - 2. \tag{A17}$$

Thus, in the domain $d_L < d < d_R$, we have two real roots, corresponding to the 2-ray region in Fig. 3(b).

As d decreases from d_L to 0, the larger root z' decreases from 1 to $2[m(1-m)]^{\frac{1}{2}}$. However, it is now a spurious root, verifying (A4) with opposite sign for the square root. Thus, only the smaller root z'' is acceptable. This corresponds to the 1-ray region in Fig. 3(b).

To determine the behavior of the roots in the neighborhood of $\theta = \theta_R$, it is simpler to go back to (A1) and to expand θ in a Taylor series around $\theta_1 = \theta_{1R}$, making use of (2.34)–(2.36), as well as of the relation

$$d\theta_2/d\theta_1 = \cos\theta_1/(N\cos\theta_2). \tag{A18}$$

This leads to

$$\epsilon = \frac{3s}{4c}\delta^2 + \frac{(3+c^2)}{16c^2}\delta^3 + \frac{s(17c^2+3)}{256c^3}\delta^4 + \frac{(25c^4+6c^2-15)}{1024c^4}\delta^5 + \frac{s(721c^4-1770c^2-855)}{122\,880}\delta^6 + \mathcal{O}(\delta^7), \tag{A19}$$

where

$$\epsilon = \theta - \theta_R, \quad \delta = \theta_1 - \theta_{1R}, \tag{A20}$$

and s and c are given by (2.35).

Inverting (A19), we find the two solutions

$$\begin{Bmatrix}\delta' \\ \delta''\end{Bmatrix} = \pm p\epsilon^{\frac{1}{2}} - q\epsilon \pm \frac{1}{2p}\left[5q^2 - \frac{(17c^2+3)}{108s^2}\right]\epsilon^{\frac{3}{2}} - \left[8\frac{q^3}{p^2} + \frac{(c^4-6c^2+3)}{108s^3c}\right]\epsilon^2 + \mathcal{O}(\epsilon^{\frac{5}{2}}), \tag{A21}$$

[38] J. V. Uspensky, *Theory of Equations* (McGraw-Hill Book Co., Inc., New York, 1948), p. 94.

where

$$p = \left(\frac{4c}{3s}\right)^{\frac{1}{2}}, \quad q = \frac{3 + c^2}{18s^2}. \tag{A22}$$

The corresponding roots z', z'', according to (A3) and (A20), are

$$\begin{Bmatrix} z' \\ z'' \end{Bmatrix} = s \pm cp\epsilon^{\frac{1}{2}} - \left(cq + \frac{s}{2}p^2\right)\epsilon \pm \left[\frac{5}{2}c\frac{q^2}{p} - \frac{c(17c^2+3)}{216s^2p} + spq - \frac{c}{6}p^3\right]\epsilon^{\frac{3}{2}} + \mathcal{O}(\epsilon^2), \tag{A23}$$

where upper signs correspond to z' and lower ones to z''.

For $\epsilon > 0$, (A23) gives the two real saddle points around the rainbow angle. For $\epsilon < 0$, we must substitute

$$\epsilon^{\frac{1}{2}} \to -i\,|\epsilon|^{\frac{1}{2}} = -i(\theta_R - \theta)^{\frac{1}{2}} \quad (\theta < \theta_R), \tag{A24}$$

and (A23) then gives the two complex-conjugate saddle points shown in Fig. 4, where we have arbitrarily associated the root z' with the lower saddle point and z'' with the upper one.

The corresponding values of $\cos\theta_1$ and $N\cos\theta_2$ are

$$\begin{Bmatrix} \cos\theta_1' \\ \cos\theta_1'' \end{Bmatrix} = c \mp sp\epsilon^{\frac{1}{2}} + \left(sq - \frac{c}{2}p^2\right)\epsilon \mp \left\{\frac{s}{2p}\left[5q^2 - \frac{(17c^2+3)}{108s^2}\right] - cpq - \frac{s}{6}p^3\right\}\epsilon^{\frac{3}{2}} + \mathcal{O}(\epsilon^2), \tag{A25}$$

$$\begin{Bmatrix} N\cos\theta_2' \\ N\cos\theta_2'' \end{Bmatrix} = 2c \mp \frac{sp}{2}\epsilon^{\frac{1}{2}} + \left[\frac{sq}{2} + \frac{p^2}{16c}(3 - 7c^2)\right]\epsilon \mp \left\{\frac{s}{4p}\left[5q^2 - \frac{(17c^2+3)}{108s^2}\right] + \frac{pq}{8c}(3 - 7c^2) - \frac{sp^3}{192c^3}(43c^2 + 9)\right\}\epsilon^{\frac{3}{2}} + \mathcal{O}(\epsilon^2). \tag{A26}$$

The expansion of $N\cos\theta_2 - \frac{1}{2}\cos\theta_1$ will also be required. It is given by

$$\begin{Bmatrix} N\cos\theta_2' - \frac{1}{2}\cos\theta_1' \\ N\cos\theta_2'' - \frac{1}{2}\cos\theta_1'' \end{Bmatrix} = \frac{3c}{2} + \frac{s}{4}\epsilon \pm \frac{cp}{6}\epsilon^{\frac{3}{2}} + \frac{c(11c^2 - 15)}{144s^2}\epsilon^2 \pm \frac{p}{34\,560c^2s^3} \times (875c^6 - 1257c^4 + 657c^2 + 45)\epsilon^{\frac{5}{2}} + \mathcal{O}(\epsilon^3). \tag{A27}$$

APPENDIX B: THE METHOD OF CHESTER, FRIEDMAN, AND URSELL

Let us consider the integral

$$F(\kappa, \epsilon) = \int g(w)\exp\left[\kappa f(w, \epsilon)\right] dw, \tag{B1}$$

where κ is a large positive parameter and g and f are sufficiently regular functions of their arguments (cf. Refs. 3, 4).

We assume that, for some range of values of the parameter ϵ, the integrand has two saddle points, $w'(\epsilon)$ and $w''(\epsilon)$, and that, for some value of ϵ, e.g., $\epsilon = 0$, the two saddle points coincide. For fixed $\epsilon \neq 0$, the ordinary method of steepest descents may be applied, provided that κ is sufficiently large, $\kappa > \kappa_0(\epsilon)$. However, $\kappa_0(\epsilon) \to \infty$ as $\epsilon \to 0$, so that the corresponding asymptotic expansions are not uniform. In order to obtain a uniform asymptotic expansion in a region containing $\epsilon = 0$, the following procedure is applied.

A new variable μ is introduced by

$$f(w, \epsilon) = \tfrac{1}{3}\mu^3 - \zeta(\epsilon)\mu + A(\epsilon). \tag{B2}$$

The two saddle points w', w'' must correspond, respectively, to $\pm\zeta^{\frac{1}{2}}$, i.e.,

$$w = w' \to \mu = -\zeta^{\frac{1}{2}}(\epsilon); \quad w = w'' \to \mu = \zeta^{\frac{1}{2}}(\epsilon). \tag{B3}$$

This allows us to determine $\zeta(\epsilon)$ and $A(\epsilon)$, by solving the equations

$$\begin{aligned} f(w', \epsilon) &= \tfrac{2}{3}\zeta^{\frac{3}{2}}(\epsilon) + A(\epsilon); \\ f(w'', \epsilon) &= -\tfrac{2}{3}\zeta^{\frac{3}{2}}(\epsilon) + A(\epsilon). \end{aligned} \tag{B4}$$

The transformation $w \leftrightarrow \mu$ has one branch that is uniformly regular and one-to-one near $\mu = 0$. This branch is characterized by the fact that (B3) holds on it. On this branch, for small μ and ϵ, we can expand

$$G(w, \epsilon) = g(w)\frac{dw}{d\mu} = \sum_m p_m(\epsilon)(\mu^2 - \zeta)^m + \sum_m q_m(\epsilon)\mu(\mu^2 - \zeta)^m, \tag{B5}$$

where the coefficients $p_m(\epsilon)$, $q_m(\epsilon)$ can be determined by repeatedly differentiating (B5) and setting $w = w'$, $\mu = -\zeta^{\frac{1}{2}}$ and $w = w''$, $\mu = \zeta^{\frac{1}{2}}$.

It follows that

$$F(\kappa, \epsilon) \approx 2\pi i \exp\left[\kappa A(\epsilon)\right]\left\{\sum_m p_m(\epsilon)F_m(\zeta, \kappa, C) + \sum_m q_m(\epsilon)G_m(\zeta, \kappa, C)\right\}, \tag{B6}$$

where

$$F_m(\zeta, \kappa, C) = \frac{1}{2\pi i}\int_C (\mu^2 - \zeta)^m \exp\left[\kappa(\tfrac{1}{3}\mu^3 - \zeta\mu)\right] d\mu, \tag{B7}$$

$$G_m(\zeta, \kappa, C) = \frac{1}{2\pi i}\int_C \mu(\mu^2 - \zeta)^m \exp\left[\kappa(\tfrac{1}{3}\mu^3 - \zeta\mu)\right] d\mu, \tag{B8}$$

and C is the transformed contour of integration, where the limits of integration are formally extended to infinity.

The functions F_m and G_m can be expressed in terms of the Airy function and its derivative. In particular, if C is the contour C_1 defined by

$$\int_{C_1} = \int_{e^{-i\pi/3}\infty}^{e^{i\pi/3}\infty}, \tag{B9}$$

we have

$$\begin{aligned} F_0(\zeta, \kappa, C_1) &= \kappa^{-\frac{1}{3}} \operatorname{Ai}(\kappa^{\frac{2}{3}}\zeta), \\ G_0(\zeta, \kappa, C_1) &= -\kappa^{-\frac{2}{3}} \operatorname{Ai}'(\kappa^{\frac{2}{3}}\zeta), \\ F_1(\zeta, \kappa, C_1) &= 0, \\ G_1(\zeta, \kappa, C_1) &= -\kappa^{-\frac{4}{3}} \operatorname{Ai}(\kappa^{\frac{2}{3}}\zeta), \end{aligned} \tag{B10}$$

and higher-order functions are determined by the recurrence relations

$$\begin{aligned} F_m(\zeta, \kappa, C_1) &= -\frac{2}{\kappa}(m-1)G_{m-2}(\zeta, \kappa, C_1), \\ G_m(\zeta, \kappa, C_1) &= -\frac{1}{\kappa}[(2m-1)F_{m-1}(\zeta, \kappa, C_1) \\ &\quad + 2(m-1)\zeta F_{m-2}(\zeta, \kappa, C_1)]. \end{aligned} \tag{B11}$$

Substituting these results in (B6), we are led to an asymptotic expansion of the type

$$\begin{aligned} F(\kappa, \epsilon) = \exp[\kappa A(\epsilon)] &\times \left\{ \frac{\operatorname{Ai}(\kappa^{\frac{2}{3}}\zeta)}{\kappa^{\frac{1}{3}}} \left[\sum_{s=0}^{M} \frac{a_s(\epsilon)}{\kappa^s} + \mathcal{O}\left(\frac{1}{\kappa^{M+1}}\right) \right] \right. \\ &\left. + \frac{\operatorname{Ai}'(\kappa^{\frac{2}{3}}\zeta)}{\kappa^{\frac{2}{3}}} \left[\sum_{s=0}^{M} \frac{b_s(\epsilon)}{\kappa^s} + \mathcal{O}\left(\frac{1}{\kappa^{M+1}}\right) \right] \right\}, \end{aligned} \tag{B12}$$

where the coefficient functions $a_s(\epsilon)$ and $b_s(\epsilon)$ are regular for small ϵ and the error terms are uniform in ϵ for small ϵ. Thus, (B12) is valid in a region $|\epsilon| \leq R_\epsilon$, independently of κ.

If appropriate regularity conditions are satisfied,[4] the domain of validity of the uniform asymptotic expansion (B12) can be extended to a larger region by matching it with the steepest-descent expansion, with which it has a common domain of validity.

For this purpose, one makes use of the asymptotic expansions of the Airy function and its derivative[39]:

$$\operatorname{Ai}(z) \approx \frac{z^{-\frac{1}{4}}}{2(\pi)^{\frac{1}{2}}} \exp(-\eta)\left[1 - \frac{5}{72\eta} + \mathcal{O}(\eta^{-2})\right] \quad (|\arg z| < \pi), \tag{B13}$$

$$\operatorname{Ai}'(z) \approx -\frac{z^{\frac{1}{4}}}{2(\pi)^{\frac{1}{2}}} \exp(-\eta)\left[1 - \frac{7}{72\eta} + \mathcal{O}(\eta^{-2})\right] \quad (|\arg z| < \pi), \tag{B14}$$

[39] *Handbook of Mathematical Functions*, M. Abramowitz and I. A. Stegun, Eds. (National Bureau of Standards, Washington, 1964), p. 448.

$$\operatorname{Ai}(-z) \approx \frac{z^{-\frac{1}{4}}}{(\pi)^{\frac{1}{2}}}\left\{[1 + \mathcal{O}(\eta^{-2})]\sin\left(\eta + \frac{\pi}{4}\right) - \frac{5}{72\eta}[1 + \mathcal{O}(\eta^{-2})]\cos\left(\eta + \frac{\pi}{4}\right)\right\} \quad (|\arg z| < \tfrac{2}{3}\pi), \tag{B15}$$

$$\operatorname{Ai}'(-z) \approx -\frac{z^{\frac{1}{4}}}{(\pi)^{\frac{1}{2}}}\left\{[1 + \mathcal{O}(\eta^{-2})]\cos\left(\eta + \frac{\pi}{4}\right) - \frac{7}{72\eta}[1 + \mathcal{O}(\eta^{-2})]\sin\left(\eta + \frac{\pi}{4}\right)\right\} \quad (|\arg z| < \tfrac{2}{3}\pi), \tag{B16}$$

where

$$\eta = \tfrac{2}{3}z^{\frac{3}{2}}. \tag{B17}$$

APPENDIX C: EVALUATION OF $r_{n,p}$

According to (6.24), we have

$$r_{n,p} = \frac{1}{p!}\frac{d^p}{d\epsilon^p}\left\{\epsilon^{p+1}\frac{c_p(\lambda, \beta)}{[d(\lambda, \beta)]^{p+1}}\right\}_{\epsilon=0}, \tag{C1}$$

where

$$\epsilon = \lambda - \lambda_n. \tag{C2}$$

Only the behavior of $d(\lambda, \beta)$ near $\epsilon = 0$ is relevant for the evaluation of the residue. Thus, we can employ the Taylor series expansion

$$d(\lambda, \beta) = d(\lambda_n, \beta)\sum_{k=1}^{\infty}\frac{d^{(k)}(\lambda_n, \beta)}{d(\lambda_n, \beta)}\frac{\epsilon^k}{k!}, \tag{C3}$$

where $d^{(k)}$ denotes the kth derivative with respect to λ and $d^{(1)} = \dot{d}$.

It follows from I, (A11)–(A18), that

$$\dot{H}^{(1)}_{\lambda_n}(\beta)/H^{(1)}_{\lambda_n}(\beta) = iM + \mathcal{O}(\gamma^2), \tag{C4}$$

where $M = (N^2 - 1)^{\frac{1}{2}}$, as in (2.38), whereas all other ratios that appear in I, (A25)–(A27), such as $\dot{H}'^{(1)}_{\lambda_n}(\beta)/H^{(1)}_{\lambda_n}(\beta)$, $\ddot{H}^{(1)}_{\lambda_n}(\beta)/H^{(1)}_{\lambda_n}(\beta), \cdots$ are at least $\mathcal{O}(\gamma^2)$. Similarly, by I, (A23), the derivatives of $[1\ \alpha]$ are at least $\mathcal{O}(\gamma^3)$. Therefore, it follows from I, (A22) and I, (A25) that

$$\begin{aligned} d(\lambda_n, \beta) &= -[1\ \beta]\dot{H}^{(1)}_{\lambda_n}(\beta)/H^{(1)}_{\lambda_n}(\beta) + \mathcal{O}(\gamma^2) \\ &= -M^2 + \mathcal{O}(\gamma^2). \end{aligned} \tag{C5}$$

Similarly, by complete induction, one can show that

$$d^{(k+1)}(\lambda_n, \beta) = -(k+1)\,d^{(k)}(\lambda_n, \beta) \times \dot{H}^{(1)}_{\lambda_n}(\beta)/H^{(1)}_{\lambda_n}(\beta) + \mathcal{O}(\gamma^2), \tag{C6}$$

so that, by (C4) and (C5),

$$d^{(k)}(\lambda_n, \beta)/d(\lambda_n, \beta) = k!\,(-iM)^{k-1} + \mathcal{O}(\gamma^2). \tag{C7}$$

Substituting this result in (C3), we find

$$d(\lambda, \beta) = d(\lambda_n, \beta) \epsilon \sum_{k=0}^{\infty} (-iM\epsilon)^k + \mathcal{O}(\gamma^2)$$
$$= -\frac{M^2\epsilon}{1 + iM\epsilon} + \mathcal{O}(\gamma^2). \quad \text{(C8)}$$

On the other hand, according to I, (3.6),

$$[2\,\alpha] - [1\,\alpha] = -\frac{4i}{\pi\alpha H_\lambda^{(1)}(\alpha) H_\lambda^{(2)}(\alpha)}, \quad \text{(C9)}$$

so that

$$[1\,\beta] - N[1\,\alpha] = d(\lambda, \beta) - \frac{4i}{\pi\beta H_\lambda^{(1)}(\alpha) H_\lambda^{(2)}(\alpha)}. \quad \text{(C10)}$$

Near $\lambda = \lambda_n$, N, (A16) and I, (A6) give

$$H_\lambda^{(1,2)}(\alpha) = \left(\frac{2}{\pi M\beta}\right)^{\frac{1}{2}} \times \exp\left[\pm i\left(\beta M - \lambda \cos^{-1}\frac{1}{N} - \frac{\pi}{4}\right)\right] \times [1 + \mathcal{O}(\gamma^2)], \quad \text{(C11)}$$

so that (C10) becomes, with the help of (C8),

$$[1\,\beta] - N[1\,\alpha] \approx d(\lambda, \beta) - 2iM = \frac{M^2\epsilon - 2iM}{1 + iM\epsilon} + \mathcal{O}(\gamma^2). \quad \text{(C12)}$$

Similarly, let

$$u(\lambda, \beta) = [H_\lambda^{(1)}(\beta)]^{-2}. \quad \text{(C13)}$$

Then, just as for (C6), one can prove by complete induction that

$$u^{(k)}(\lambda_n, \beta) = (-1)^k (k+1)!\, u(\lambda_n, \beta) \times \left[\frac{\dot{H}_{\lambda_n}^{(1)}(\beta)}{H_{\lambda_n}^{(1)}(\beta)}\right]^k [1 + \mathcal{O}(\gamma^2)], \quad \text{(C14)}$$

i.e., with the help of (C4),

$$u^{(k)}(\lambda_n, \beta)/u(\lambda_n, \beta) = (k+1)!\,(-iM)^k[1 + \mathcal{O}(\gamma^2)]. \quad \text{(C15)}$$

Thus, near $\lambda = \lambda_n$, neglecting $\mathcal{O}(\gamma^2)$,

$$u(\lambda, \beta) = u(\lambda_n, \beta) \sum_{k=0}^{\infty} \frac{u^{(k)}(\lambda_n, \beta)}{u(\lambda_n, \beta)} \frac{\epsilon^k}{k!}$$
$$= \sum_{k=0}^{\infty} (k+1)(-iM\epsilon)^k = \frac{1}{(1 + iM\epsilon)^2}. \quad \text{(C16)}$$

Taking into account I, (A11), I, (A19), I, (A8), this becomes

$$\frac{1}{[H_\lambda^{(1)}(\beta)]^2} = \frac{M^2 e^{i\pi/3}}{4a_n'^2\gamma^4} \cdot \frac{[1 + \mathcal{O}(\gamma^2)]}{(1 + iM\epsilon)^2}. \quad \text{(C17)}$$

Substituting (C11), (C12), and (C17) in (6.25), we finally get, near $\lambda = \lambda_n$,

$$c_p(\lambda, \beta) = (-i)^p e^{i\pi/3} \frac{\pi\beta^3}{16} \frac{M^3}{a_n'^2\gamma} \times \exp(2ipM\beta + i\lambda_n\zeta_p) \frac{(-2iM + M^2\epsilon)^{p-1}}{(1 + iM\epsilon)^{p+1}} \times \exp(i\epsilon\zeta_p)[1 + \mathcal{O}(\gamma^2)], \quad \text{(C18)}$$

where [cf. I, (5.21)]:

$$\zeta_p = s\pi - 2p\cos^{-1}\frac{1}{N} = s\pi - p\theta_t. \quad \text{(C19)}$$

Taking into account (C8) and (C18), we find that (C1) becomes

$$r_{n,p} = -i^p \frac{e^{i\pi/3}}{\gamma} \frac{\pi\beta^3}{16} \frac{e^{2ipM\beta}}{M^{2p-1}} \times \frac{\exp(i\lambda_n\zeta_p)}{a_n'^2} \mathcal{F}_p(M, \zeta_p)[1 + \mathcal{O}(\gamma^2)], \quad \text{(C20)}$$

where

$$\mathcal{F}_p(M, \zeta_p) = \frac{1}{p!}\frac{d^p}{d\epsilon^p}[(-2iM + M^2\epsilon)^{p-1} \exp(i\epsilon\zeta_p)]_{\epsilon=0}. \quad \text{(C21)}$$

With the change of variable

$$-2iM + M^2\epsilon = \frac{M^2}{i\zeta_p} x, \quad \text{(C22)}$$

we finally get

$$\mathcal{F}_p(M, \zeta_p) = \frac{i}{2} M^{2p-1} L_p^{(-1)}(-2\zeta_p/M), \quad \text{(C23)}$$

where

$$L_p^{(-1)}(-x) = \frac{xe^{-x}}{p!}\frac{d^p}{dx^p}(x^{p-1}e^x) = \sum_{m=1}^{p}\binom{p-1}{m-1}\frac{x^m}{m!} = \frac{x}{p} L_{p-1}^{(1)}(-x) = L_p(-x) - L_{p-1}(-x) \quad (p \geq 1) \quad \text{(C24)}$$

is a generalized Laguerre polynomial (Ref. 26, p. 239). We define

$$L_0^{(-1)}(-x) = 1. \quad \text{(C25)}$$

From (C20) and (C23) we obtain the final result

$$r_{n,p} = -i^{p+1} \frac{e^{i\pi/3}}{\gamma} \frac{\pi\beta^3}{32} \exp(2ipM\beta) L_p^{(-1)}(-2\zeta_p/M)(a_n')^{-2} \times \exp(i\lambda_n\zeta_p)[1 + \mathcal{O}(\gamma^2)]. \quad \text{(C26)}$$

APPENDIX D: EVALUATION OF $r'_{n,p}$

From (6.109), we get

$$r'_{n,p} = \frac{1}{p!}\frac{d^p}{d\epsilon^p}\left\{\epsilon^{p+1}\frac{c_p'(\lambda, \beta)}{[d(\lambda, \beta)]^{p+1}}\right\}_{\epsilon=0}, \quad \text{(D1)}$$

where

$$\epsilon = \lambda - \lambda_n'. \quad \text{(D2)}$$

Again, only the behavior of $d(\lambda, \beta)$ near $\epsilon = 0$ is relevant, so that, as in (C3), we expand

$$d(\lambda, \beta) = d(\lambda'_n, \beta) \sum_{k=1}^{\infty} \frac{d^{(k)}(\lambda'_n, \beta)}{d(\lambda'_n, \beta)} \frac{\epsilon^k}{k!}. \tag{D3}$$

From I, (A11)–(A18), we find that,

$$\dot{H}^{(2)}_{\lambda_n'}(\alpha)/H^{(2)}_{\lambda_n'}(\alpha) = -iM'/N + \mathcal{O}(\gamma^2), \tag{D4}$$

where $M' = (1 - N^2)^{\frac{1}{2}}$, as in I, (3.31), whereas all other ratios that appear in the analogs of I, (A25)–(A27) for $[2\ \alpha]$ are at least $\mathcal{O}(\gamma^2)$. Similarly, by I, (2.39), the derivatives of $[1\ \beta]$ are at least $\mathcal{O}(\gamma^3)$. Thus, we find

$$d(\lambda'_n, \beta) = [1\dot{\beta}] - N[2\dot{\alpha}] = N \frac{\dot{H}^{(2)}_{\lambda_n'}(\alpha)}{H^{(2)}_{\lambda_n'}(\alpha)} [2\ \alpha] + \mathcal{O}(\gamma^2)$$

$$= \frac{M^2}{N'} + \mathcal{O}(\gamma^2). \tag{D5}$$

One can show by complete induction that

$$d^{(k+1)}(\lambda'_n, \beta) = -(k+1) \frac{\dot{H}^{(2)}_{\lambda_n'}(\alpha)}{H^{(2)}_{\lambda_n'}(\alpha)} d^{(k)}(\lambda'_n, \beta) + \mathcal{O}(\gamma^2), \tag{D6}$$

so that

$$\frac{d^{(k)}(\lambda'_n, \beta)}{d(\lambda'_n, \beta)} = k! \left(i \frac{M'}{N}\right)^{k-1} + \mathcal{O}(\gamma^2). \tag{D7}$$

Substituting this result in (D3) and (D5), we find

$$d(\lambda, \beta) = \epsilon d(\lambda'_n, \beta) \sum_{k=0}^{\infty} (iM'\epsilon/N)^k + \mathcal{O}(\gamma^2)$$

$$= \frac{M'^2 \epsilon}{N - iM'\epsilon} + \mathcal{O}(\gamma^2). \tag{D8}$$

On the other hand, we have [cf. (3.31)]

$$H^{(1)}_{\lambda}(\alpha) \approx 2 \frac{e^{-i\pi/3}}{\gamma'} \operatorname{Ai}(e^{i\pi/3} x), \tag{D9}$$

where

$$x = e^{i\pi/3}(\lambda - \alpha)/\gamma', \quad \gamma' = (2/\alpha)^{\frac{1}{3}}, \tag{D10}$$

and, by (3.32),

$$H^{(1)}_{\lambda}(\alpha) \approx H^{(1)}_{\lambda_n'}(\alpha) \approx -\frac{e^{-i\pi/6}}{\pi a'_n \gamma'}. \tag{D11}$$

Similarly, from (D9),

$$[1\ \alpha] = \mathcal{O}(\gamma'), \quad [1\dot{\alpha}] = \mathcal{O}(\gamma'^2), \tag{D12}$$

so that, near λ'_n,

$$[1\ \beta] - N[1\ \alpha] \approx [1\ \beta]_{\lambda_n'} = iM', \tag{D13}$$

with the help of I, (2.39). To the present order of accuracy, (D11) and (D13) may be directly substituted in (6.110). Similarly, we may replace $H^{(1)}_{\lambda}(\beta)$ by [cf. (C11)]

$$H^{(1)}_{\lambda}(\beta) \approx \left(\frac{2}{\pi M'\beta}\right)^{\frac{1}{2}} \exp\left(iM'\beta - i\lambda \frac{\theta_t}{2} - i\frac{\pi}{4}\right), \tag{D14}$$

where θ_t is given by I, (4.76).

On the other hand, by I, (A1), and by (D10),

$$H^{(2)}_{\lambda}(\alpha) \approx 2e^{i\pi/3} \operatorname{Ai}(-x)/\gamma', \tag{D15}$$

and, with the help of (D4), we find

$$H^{(2)}_{\lambda}(\alpha) \approx H^{(2)}_{\lambda_n'}(\alpha) + \epsilon \dot{H}^{(2)}_{\lambda_n'}(\alpha) \approx H^{(2)}_{\lambda_n'}(\alpha)\left(1 - i\frac{M'}{N}\epsilon\right)$$

$$= 2e^{i\pi/6} \frac{N}{M'} \gamma'^2 a'_n \left(1 - i\frac{M'}{N}\epsilon\right), \tag{D16}$$

with all higher derivatives yielding higher-order contributions.

Substituting (D11)–(D16) in (6.110), we finally get, near $\lambda = \lambda'_n$,

$$c'_p(\lambda, \beta)$$

$$= -\frac{\pi^2 M' N \beta^3}{8} \exp\left[-2iM'\beta - i\lambda'_n(\pi - \theta_t)\right]$$

$$\times \left(-\frac{e^{i\pi/6} M'^2}{2\pi N a'^2_n \gamma'}\right)^p \frac{\exp\left[-i\epsilon(\pi - \theta_t)\right]}{\left(1 - i\frac{M'}{N}\epsilon\right)^{p+1}} [1 + \mathcal{O}(\gamma^2)]. \tag{D17}$$

Replacing (D8) and (D17) in (D1), we find

$$r'_{n,p} = -\frac{\pi^2 N^2 \beta^3}{8M'}$$

$$\times \exp\left[-2iM'\beta - i\lambda'_n(\pi - \theta_t)\right]\left(-\frac{e^{i\pi/6}}{2\pi a'^2_n \gamma'}\right)^p$$

$$\times \frac{1}{p!}\left\{\frac{d^p}{d\epsilon^p}\left[e^{-i\epsilon(\pi - \theta_t)}\right]\right\}_{\epsilon=0} [1 + \mathcal{O}(\gamma^2)],$$

so that, finally,

$$r'_{n,p} = -\frac{\pi^2 N^2 \beta^3}{8M'} \exp\left[-2iM'\beta - i\lambda'_n(\pi - \theta_t)\right]$$

$$\times \frac{1}{p!}\left[-\frac{e^{-i\pi/3}(\pi - \theta_t)}{2\pi a'^2_n \gamma'}\right]^p [1 + \mathcal{O}(\gamma^2)]. \tag{D18}$$